R. & M. No. 3477

MINISTRY OF TECHNOLOGY

AERONAUTICAL RESEARCH COUNCIL
REPORTS AND MEMORANDA

The Design-Point Performance of Model Internal-Expansion Propelling Nozzles with Area Ratios up to 4

By M. V. HERBERT, D. L. MARTLEW and R. A. PINKER

LONDON: HER MAJESTY'S STATIONERY OFFICE
1967
PRICE £2 1*s.* 0*d.* NET

AERONAUTICAL RESEARCH COUNCIL

Reports and Memoranda No. 3477

CORRECTION

Page 45 (centre): amend to read

$$\delta^* = \frac{D_g}{4}\left\{\frac{\int dA}{A_i} - \frac{\int \rho v dA}{\rho_i v_i A_i}\right\}$$

$$= \frac{D_g}{4}\left(\frac{1}{C_D} - 1\right).$$

Page 46 (bottom): amend to read

$$\beta \,.\, \tilde{F}_e = \int_{A_g}^{A_e} P_w \, dA - \int_{A_g}^{A'_e} P'_w \, dA - P_e \,(A_e - A'_e)$$

Page 56 (top): amend to read

$$\beta = G_1 \,(M_e) \int_1^{M_e} (1 - \eta_f)\, G_2 \,(M)\, dM.$$

Ministry of Technology, July 1967

LONDON: HER MAJESTY'S STATIONERY OFFICE

The Design-Point Performance of Model Internal-Expansion Propelling Nozzles with Area Ratios up to 4

By M. V. HERBERT, D. L. MARTLEW and R. A. PINKER

(Appendices III, IV and V by M. V. Herbert)

COMMUNICATED BY THE DEPUTY CONTROLLER OF AIRCRAFT (RESEARCH AND DEVELOPMENT), MINISTRY OF AVIATION

Reports and Memoranda No. 3477*
December, 1963

Summary.

The construction of a new dry air thrust rig is described, for testing model propelling nozzles in quiescent air, and its pretensions to accuracy are examined. Use has been made of certain types of convergent nozzle as a means of checking the absolute level of air mass flow measurement.

Experimental results have been obtained for the performance of a family of conically divergent nozzles running correctly expanded, and compared with theoretical estimates of the contributory losses. Other basic shapes of internal-expansion nozzle, both axisymmetric and two-dimensional, have also been tested.

LIST OF CONTENTS

*Replaces N.G.T.E. R.258—A.R.C. 26 495.

PART II

LIST OF APPENDICES

LIST OF ILLUSTRATIONS

---

1. *Introduction.*

A flight vehicle designed for sustained cruise requires a propelling nozzle which during that phase is capable of converting pressure to velocity energy in the exhaust stream at very high efficiency. This is especially so as flight speed increases, since the net propulsive force is the difference between two quantities which approach each other in magnitude. If, as is typical of medium supersonic speed (Mach number between 2 and 3), the air inlet momentum is between 70 and 80 per cent of the outlet momentum, any loss in the latter arising from inefficiency of nozzle energy conversion will have a greatly magnified effect on aircraft cruise performance.

Nozzle efficiencies therefore have to be, and fortunately are, high. Design-point values around 97 to 99 per cent can be expected, and the odd $\frac{1}{2}$ per cent one way or the other is of considerable importance. This imposes a need for accuracy of measurement perhaps greater than for any other engine component, and certainly on the limit of what can in practice be achieved with normal equipment. For an efficiency in terms of air specific thrust to be obtained to $\pm\frac{1}{4}$ per cent accuracy, as the project engineer requires, both air mass flow and thrust must be individually accurate to $\pm\frac{1}{8}$ per cent; and only those who have tried can really appreciate how difficult a problem this poses.

Now it may be thought that tests of small-scale model nozzles fed with cold air are but a poor simulation of full-scale hot gas conditions. Possibly so, but sufficient accuracy of measurement even for comparative purposes would be extremely difficult to achieve under engine operating conditions, and a programme of work covering a wide range of nozzle types would be prohibitively costly and slow. Small-scale models with high quality manufacturing finish yield figures which can be regarded as the upper limit of practical possibility. In justification for their extensive use it must be pointed out that, of the losses taking place in a nozzle running full, only friction is dependent on the level of Reynolds number; this is generally a small part of the total loss, and in the usual range of Reynolds number the sensitivity is quite slight. Furthermore, the effects of size and temperature are largely self-cancelling. Hence such tests as are reported herein can be expected to give substantially correct answers for the design-point performance, under uniform supply conditions – i.e. ignoring such further losses as may be introduced by temperature stratification in the gas stream at entry to the nozzle, which are in any case a function of the particular engine system.

Previous tests at N.G.T.E.[1] with models on this scale (throat diameter generally 2 in.) were carried out on a rig fed with cold compressed air very near saturation point. Plant of sufficient capacity was not available to permit operation with dry air. For this reason, and because of ineradicable limitations to the accuracy of thrust and air mass flow measurement on the existing rig, construction of a new one was undertaken. The intention was to obtain a tool which could measure design-point efficiencies to a high standard of absolute, rather than just comparative, accuracy. No consideration was given to the provision of an external flow around the model, which would greatly complicate the system and jeopardise the required accuracy of thrust measurement. For an exercise in the investigation of design-point performance of internal-expansion nozzles, it is only necessary to ensure that each nozzle is run completely expanded, and this can more satisfactorily and more cheaply be done on a quiescent air rig.

The first models to be tested on the new rig were all simple shapes, with no attempt being made to produce an arrangement covering any particular aircraft requirement. All nozzles had wholly internal-expansion surfaces, and most were axisymmetric. These types may be regarded as 'standards' by which the performance of more sophisticated designs can be judged. Data on them provide target figures for use in aircraft project work, and show, for instance, the inherent penalty associated with such geometric variables as outlet divergence and cross-sectional shape.

PART I

2. *The Test Rig.*

2.1. *Rig Design.*

The general layout of the rig (Fig. 1) was governed by prejudice both in the choice of suspension system and in the use of dead weights to balance it. A sufficiently delicate form of suspension in which the nozzle feed pipe is carried by a parallelogram system compounded of strips, links or joints, can suffer serious trouble due to the geometry of the system not remaining constant with variation of temperature, air pressure loads, and model weight. Air bearings fitted round the pipe offer an alternative which is ideal in almost every respect.

Any method of force balancing other than dead weights requires initial, and generally regular, calibration, for which purposes one turns back to weights. In order to eliminate an intermediate sub-standard, the rig was made vertical and so arranged that weights take up all but the last 2 lb of out-of-balance force.

Capacity of dry air plant imposed a limit on nozzle air mass flow, and this in turn dictated atmospheric pressure at entry to the rig and the use of suction equipment at outlet. Available suction plant was capable of handling the design nozzle flow through a pressure ratio of about 6. In order to achieve substantially higher pressure ratios across the model, a nozzle exhaust diffuser was required.

It would naturally be preferable from the stand-point of thrust measurement to allow the nozzle to discharge into a relatively large plenum chamber, so that the nozzle and moving pipe assembly are not surrounded by violent flow recirculations created by the exhaust jet. The necessity for a recovery pipe to be fitted downstream of the nozzle led to the use of a baffle plate across the depression box in the

outlet plane of the nozzle, with about $\frac{1}{8}$ in. radial clearance around the body of the nozzle; this serves to shield the nozzle mounting pipe and flanges from the region of intense shear at entry to the mixing tube. Such a system has been proved satisfactory for wholly internal-expansion nozzles; with nozzles incorporating some external-expansion surface, there is a danger that this may be influenced by the surrounding pressure field in the mixing zone.

The heart of the rig is a pipe of $3\frac{1}{2}$ in. bore held in a vertical position by two air bearings which allow frictionless vertical movement limited to about $\frac{1}{4}$ in. Air from the drying plant at substantially atmospheric pressure and temperature is fed through twin ducts to a plenum chamber containing a cylindrical gauze and radial inlet guide vanes, the latter designed to ensure that air enters the pipe with zero momentum in the axial direction. It is then turned upwards by means of a flare, from which is suspended by four aerofoil section tie-rods a flat back-plate attached to the force-balancing system.

Immediately above – i.e. downstream of – the flare, provision was made for the mounting of straighteners and gauzes for control of flow distribution. None of these were found to be needed in service.

Further up the pipe is the airflow measuring section. Four plugs are fitted in the pipe walls; one carries a traversing mechanism moving a pitot probe, the stem of which passes through the opposite plug. The remaining plugs carry fixed static probes. All the plugs are interchangeable, so that traverses may be made across two mutually perpendicular diameters. The top of the pipe terminates in a flange on which are mounted a series of optional packing rings, followed by a further measuring section with four wall statics, which is always placed immediately ahead of the test nozzle. The number of packing rings is arranged to locate the outlet plane of the nozzle in correct relation to the recovery system.

The latter consists of a parallel mixing tube in which shock compression takes place, followed by a conical subsonic diffuser. This discharges into a suction manifold at ceiling height, with in-bleed valves which are used to control the pressure ratio across the nozzle under test. Suction is applied to the manifold by means of two fixed volume flow exhauster pumps and an ejector driven from a compressor at 90 p.s.i.g. These may be used separately or together as required.

2.2. *Instrumentation.*

The instrumentation system is shown diagrammatically in Fig. 2. Reference to the key gives the quantities normally measured. Plenum pressure and quantities associated with the mass flow are measured on water *U*-tubes, and nozzle base pressures are measured against depression chamber pressure on tetralin *U*-tubes. Depression chamber pressure is a quantity required to high accuracy and, when greater than 2 in. Hg, is measured on a Kew pattern barometer. In the lower range depression chamber pressure is measured on two *U*-tubes, one containing vacuum oil and the other dibutylphthalate, both opposed by vacuum maintained by a pump. This reference vacuum is measured on a Pirani gauge.

The system described above is in operation during all normal tests for thrust efficiency. When required in particular cases, nozzle internal wall pressures can be conveyed from the depression chamber to separate mercury manometers. Further provision is made for metering and passing a relatively small supply of secondary air into the depression chamber when testing two-stream nozzles. For examining the flow pattern on external-expansion nozzles a shadowgraph system is installed, and arranged for photographic recording.

2.3. *Measurement of Out-of-Balance Forces.*

It is necessary at this point to consider the arrangement of forces acting on the moving pipe assembly, reference being made to Fig. 3. The thrust of the nozzle (X), which is the quantity ultimately required, acts downwards. Opposed to and exceeding it in magnitude is a force (Y) acting across the system of seals by which the moving pipe passes from the plenum chamber to the depression box. The composition of this force will be described more fully in Section 3.2.1 dealing with rig calibration. A further small upward force (Z) arises due to the pressure difference across the baffle plate through which the nozzle body protrudes.

The net effect of these three aerodynamic forces is upwards. Tending to restore balance is the gravitational force composed of a fixed weight of pipe assembly (W_p) and a weight of nozzle and packing rings (W_n) which varies from one test to another. The greater part of any remaining out-of-balance force is then removed by hanging weights (W_w) from the bottom of the pipe. The rig is finally brought into balance by means of a spring balance of special construction working up to 4 lb and capable of reading 0·01 lb. The force exerted (W_s) acts in an upward direction. This spring system also serves to stabilise the moving pipe assembly in a position of equilibrium within its $\frac{1}{4}$ in. of available travel.

Fig. 4 shows the arrangement of the balancing equipment, which is situated below the floor level of the rig. The spring balance itself consists of a high quality spring whose movement is followed by a travelling microscope. A dial gauge indicates the position of the microscope and hence gives the extension of the spring, whose rate is adjustable and can be calibrated *in situ*. It is normally set to move $\frac{1}{10}$ in. per lb loading. The position of the moving pipe system is indicated by a second dial gauge, and the standard operating position is reached by adjustment of a turnbuckle attached between the spring and the yoke frame.

A small oil-filled dash-pot with variable by-pass is fitted to apply sufficient damping for readings to be taken in cases when a nozzle runs very roughly.

Omitting small force terms introduced by the resistance of the second dial gauge and the dash-pot, the force balance equation can be written:

$$X = Y+Z+W_s-W_p-W_n-W_w$$

3. *Calibration.*

3.1. *Air Mass Flow.*

The scale of model for which the rig was designed has a throat area of π sq in. and passes approximately 1 lb/sec at atmospheric pressure and temperature. This quantity of flow is nearly constant (normally within ± 5 per cent) at all times, and thus conditions in the pipe metering section vary only within very narrow limits. There is a distinct advantage in this, as it means that once the flow has been explored in detail at the design condition, some reference quantity can be selected as an indicator of flow for all tests.

Air is delivered from the drying plant by a low pressure fan, and is thus not perfectly free from pressure pulsations. It was found, however, that provision of a blow-off ahead of the feed ducts to the plenum chamber enables this to run at a sufficiently steady pressure in the range $\frac{1}{4}$ to $\frac{1}{2}$ in. water. As the throat of the model nozzle is normally run choked, so that any unsteadiness in the exhaust system cannot feed back upstream, it was hoped that the flow in the measuring sections, coming from a steady source, would then be substantially smooth.

Some initial trouble was experienced with asymmetry of flow distribution within the pipe. Investigation showed that this was not associated with the flare profile or back-plate shape. Provision existed for the insertion of gauzes and straighteners in the pipe immediately after the flare, and a variety of combinations of number and mesh of gauzes and types of straightener were tried in turn. In general it was found that any forced re-distribution of flow to give a flat velocity profile was accompanied by the onset of pressure fluctuations of a magnitude and frequency which prevented accurate reading of manometers. Further investigation led to some change of the inlet guide vane system which eliminated much of the asymmetry, and all internal obstructions were then dispensed with.

The critical readings for mass-flow measurement are the total and static pressures in the traversing plane. At the design flow of 1 lb/sec the pipe Mach number is 0·2, and the dynamic head only 12 in. water. This calls for high accuracy in the reading of total and static pressures. It was found that inclined manometers were less satisfactory than a well-designed vertical pattern, while the Betz type of projection manometer is unsuitable for use with probes of $\frac{1}{2}$ mm bore hypodermic tubing, as its large air capacity requires an excessively long settling time.

In the early days a combined pitot-static instrument head 2 mm in diameter was fitted to the traversing gear. This showed uniformity of static pressure across the pipe except where the proximity of the walls introduced errors in the probe reading. Thereafter static pressure was measured by two fixed probes of 1 mm diameter placed at approximately half-radius either side of the line of traverse. Traversing is possible to within 0·05 in. of each wall.

The results of a set of pitot traverses on four quadrants are shown in Fig. 5. The procedure adopted for calculating mass flow was as follows. Values of P_t at each measured point were divided by a constant P_s taken from the fixed probe readings, and the compressible flow function $Q\sqrt{T_t}/AP_s$ corresponding to each value of P_t/P_s was obtained from tables. Then, for any one quadrant, the total mass flow Q is given by:

$$Q = \frac{P_s}{\sqrt{T_t}} \int \left(\frac{Q\sqrt{T_t}}{AP_s}\right)_{\text{local}} dA$$

Hence

$$\frac{Q\sqrt{T_t}}{AP_s} = \frac{2}{R^2} \int_0^R \left(\frac{Q\sqrt{T_t}}{AP_s}\right)_{\text{local}} r.dr$$

This integral was evaluated arithmetically for each of the four quadrants separately, and a mean obtained of the four resulting values of $Q\sqrt{T_t}/AP_s$, which was then taken to apply to the whole pipe flow. This gives average values of P_t/P_s and hence of P_t. Dividing the average P_t by the centreline value we get the 'form factor' (κ), which, for a constant supply total pressure, is then dependent only on the level of mass flow. The value of κ corresponding to the traverses of Fig. 5 (mass flow approximately 1 lb/sec for a nozzle of throat diameter 2 in.) is 0·99602, a figure which was repeated several times within very close limits.

The ability to traverse the pipe along only two diameters makes the success of the device as an air meter conditional upon fair uniformity of circumferential flow distribution. It is interesting to note how the results for each quadrant compare, when converted into an effective discharge coefficient for the pipe and nozzle assembly downstream of the metering section.

TABLE 1

Values of C_D for Pipe and Nozzle

Quadrant	Test No. 1	Test No. 2	Average of Tests 1 and 2
1	0·9831	0·9859	0·9845
2	0·9889	0·9871	0·9880
3	0·9861	0·9833	0·9847
4	0·9832	0·9829	0·9830
Average of quadrants	0·9853	0·9848	0·98505

It can be seen from Table 1 that variation between individual quadrants is from +0·295 per cent to −0·205 per cent about the mean. Repeatability of the separate quadrants is 0·28 per cent or better, and that of their average is down to 0·05 per cent. This is considered satisfactory.

A limited amount of calibration work was also done at different mass flow levels. The variation in form factor was found to be linear with dynamic head, i.e. with the square of the mass flow as shown in Fig. 6.

There are certain potential sources of error in the total and static probe readings which may be considered at this point. They are three in number; one accidental and two fundamental.

(i) Pitot and static measuring planes are different. In order to reduce the indeterminate errors associated with short static tubes, the replacement fixed static probes were positioned with the holes approximately 0·75 in. upstream of the plane in which the tip of the pitot tube is traversed. There is a loss due to friction in this short length of pipe which, on the proven basis of a uniform static traverse, can be calculated. Using an incompressible friction factor of 0·0144, the observed static must be multiplied by $(1-0{\cdot}00011x)$, where x is the distance in inches, hence the ratio P_t/P_s multiplied by $(1+0{\cdot}00011x)$, and the mass flow in consequence by $(1+0{\cdot}00193x)$. The effect is thus to under-estimate mass flow by 0·15 per cent.

(ii) Total head position error. The presence of the tube has the effect of deflecting flow towards the wall, so that the tube reads the pressure of a streamline originally nearer the centre of the pipe. This displacement could be around 0·008 in. in our case. Making allowance for this in the integration process shows that the flow would have been over-estimated by 0·26 per cent.

(iii) Static hole error. A static hole of finite size, however accurately made, has an error associated with the formation of an eddy within the hole. For holes of large length/diameter ratio, the effect is to produce a spuriously high reading. But where a shallow hole connects with a relatively large plenum chamber, as in a static probe, it is possible to suppose errors in the opposite sense. Detailed discussion of the general problem is given in Reference 2. In the present case, both the sense and quantity of the error are unknown, but it could amount to $\frac{1}{4}$ per cent in mass flow.

Summing up, we have two known errors which are partly self-cancelling, and one quite unknown. The general level of certainty can thus not be given as better than $\pm\frac{1}{4}$ per cent, despite every care in manufacture and operation. It is thought unlikely that any system of direct mass flow measurement can hope to achieve substantially better accuracy than this.

Fortunately, in an exercise involving thrust, there is available a reliable 'second opinion'. Certain types of convergent nozzle, when run choked, can define the mass flow within more precise limits than any system relying critically upon measurement of static pressure. This technique is considered in a later Section.

3.1.1. *Nozzle discharge.*

The presence of a length of some five to ten pipe diameters between the air metering section and the test nozzle, depending on its own length, introduces an appreciable loss of pressure from friction. In consequence, a further pressure measuring station is always included immediately upstream of the nozzle. A total-head rake at this point was not suitable, as a sufficient number of tubes to register the non-uniform profile would introduce further drag losses, and could cause interference with the flow entering the nozzle. Despite their inherent limitations, recourse was therefore made to wall static tappings. A measuring section of the same diameter as the main pipe (3·500 in.), and about $1\frac{1}{2}$ diameters in length, carries a symmetrical arrangement of four static holes in the same cross-sectional plane. Very careful attention was given to the production of accurate holes, and the readings of each are in good agreement.

In this application, some error in pressure measurement can be tolerated. At the air meter itself mass flow is derived, via the function $Q\sqrt{T_t}/AP_s$, from measurement of P_t/P_s. A certain percentage change in the latter at this pipe Mach number produces a 17-fold change in the flow function, so that the whole system is highly critical to accuracy of pressure measurement – a basic weakness on which we have already commented. In the case of the nozzle entry measuring section, however, one is only concerned with determining a correction to the flow function, on which static pressure reacts linearly.

The usual procedure is to obtain a corrected flow function by multiplying that from the air meter by the ratio of air meter static to average entry wall static, thus:

$$\left(\frac{Q\sqrt{T_t}}{AP_s}\right)_{\text{entry}} = \left(\frac{Q\sqrt{T_t}}{AP_s}\right)_{\text{meter}} \times \frac{P_{s,\ \text{meter}}}{P_{s,\ \text{entry}}}$$

A value of A/A^* corresponding to the entry flow function is obtained from tables, which then gives us A^*, the isentropic nozzle throat area required for the mass flow being passed. The discharge coefficient is defined as:

$$C_D = \frac{A^*}{A_g}$$

where A_g is the physical area of the nozzle at its minimum section.

Typical values of $P_{s,\,\text{meter}}/P_{s,\,\text{entry}}$ lie between 1·0025 and 1·0055, and it is of interest to try and analyse this loss. It may be divided into three components:

(i) drag of the total head traversing probe (a stem 2 mm wide spanning the pipe),

(ii) friction in the 14·5 in. of really smooth permanent pipe,

(iii) friction in the assembly of spacing rings and make-up sections, whose length varies with that of the nozzle.

Putting C_d = Drag coefficient of probe stem = 1

A_s = Projected area of probe stem = 0·280 in^2

A_p = Internal cross-sectional area of pipe = 9·621 in^2

l_0 = Length of smooth permanent pipe = 14·5 in.

Δl = Total length of spacers

$\frac{\rho v^2}{2g}$ = 0·4 p.s.i.

P_{s1} = 14·5 p.s.i.

C_f = Friction factor for smooth pipe = 0·0144
at Re = $3{\cdot}5 \times 10^5$

C_f' = Effective friction factor for spacers

we can write

$$P_{s1} - P_{s2} = \Delta P_s = \frac{\rho v^2}{2g}\left\{C_d\frac{A_s}{A_p} + C_f\frac{l_0}{D_e} + C_f'\frac{\Delta l}{D_e}\right\}$$

where D_e = hydraulic mean diameter of pipe.

Hence
$$\frac{\Delta P_s}{\rho v^2/2g} = 0{\cdot}0887 + 0{\cdot}286\ C_f'\cdot\Delta l$$

Now
$$\frac{P_{s1}}{P_{s2}} \simeq 1 + \frac{\Delta P_s}{P_{s1}}$$

$$= 1{\cdot}00245 + 0{\cdot}00789\ C_f'\cdot\Delta l$$

Fig. 7 shows a plot of P_{s1}/P_{s2} against Δl for a wide range of nozzles tested during the present cycle of work. The intercept calculated above (1·00245) almost exactly coincides with the experimental results when $\Delta l = 0$. For an average fit to the other points, the value of C_f' would be around 0·0184, which seems quite reasonable for the minor surface discontinuities which exist within the spacers.

3.2. *Thrust.*

As already indicated (Section 2.3), the nozzle thrust is derived from a system of six main force components, shown in Fig. 3. Approximate values of each are given in Table 2, illustrating their magnitudes relative to the thrust force X. It can be seen that by far the greatest difficulty arises over the aerodynamic force Y. Unlike a gravitational force, it cannot be measured directly, and, being some four times the size of the nozzle thrust, the whole system is critically dependent on the accuracy of its determination.

TABLE 2

Typical Values of Force Components (see Fig. 3)

Force	High Pressure ratio	Low Pressure ratio
X = Nozzle thrust	63	34
Y = Pipe seal force	240	125
Z = Nozzle base force	0	1
W_p = Weight of basic pipe assembly	50	50
W_s = Spring balance load	2	2
W_n = Weight of nozzle and spacers	25	25
W_w = Dead weights to balance	100	15
	Figures in pounds	

Let us first dispose of the components which are easy to deal with. The spring balance force W_s is inherently capable of measurement to 0·01 lb. The dead weight terms W_w and W_n involve only accurate weighing equipment, and by courtesy of Inspection Department, R.A.E., the weight of each piece of metal is obtained to 0·001 lb.

The weight of permanent moving parts of the rig (W_p) could be similarly treated, but this is not in fact very useful. A few minor force terms are known to exist when the rig is 'live', which do not appear in the simple balance drawn up in Table 2. These include the spring loading of a dial gauge registering pipe position, and the buoyancy force exerted by the dash-pot. It is thus more satisfactory to obtain an effective value of W_p which embraces all such effects, by including it as a variable in the calibration procedure.

3.2.1. *Pipe seal force.*

This calibration is primarily needed to determine the effective value of A_0, the 'piston' area of the moving pipe. There are strictly two forces; the first arises where the pipe emerges from the plenum chamber, and the second where it enters the depression box. The pressure difference in the former is, however, a very great deal smaller than that in the latter ($\frac{1}{2}$ in. water, as against a minimum of $\frac{1}{2}$ atm with the nozzle choked). Furthermore, the pipe diameter at each point is the same within very close limits, having been hard-chrome plated and ground for the sake of the air bearings. It is thus expedient to treat the two seal forces together as one term, $A_0(P_{pl}-P_c)$. An annular clearance amounting to 0·004 in. on radius exists between the pipe and the inner diameter of a 6-stage labyrinth gland at the base of the depression box. Through this gap leakage air is induced, and the drag force associated with it is distributed between the moving pipe and the stationary labyrinth. As a result the effective area A_0 will lie somewhere between that of the pipe and that of the inner extremities of the labyrinth. The possibility exists that this effective area may vary with the pressure difference across the seal.

Once the seal system is choked, the leakage from atmosphere is constant, as must therefore be the drag force. Under those conditions, it could well be incorporated in the term W_p, and the geometric pipe area used in place of A_0, leaving only a single variable. But, although all nozzles were run choked, so that the pressure ratio across the seal in any test always exceeded the critical value, it is unfortunately true that a labyrinth of this type will not choke until a very much higher value. Hence the calibration must treat both W_p and A_0 as variables.

It should perhaps be mentioned that the air bearings do not themselves contribute any force on the pipe. The air from each bearing is discharged symmetrically, and they are separated from the seal passages by chambers vented to atmosphere.

Calibration was carried out by fitting a blanking plate across the top of the nozzle entry pipe, and exhausting the depression box. The usual system of spring balance and dead weights was used to balance the rig. As there was no flow through the pipe, no air was fed to the plenum chamber, and $P_{pl} = P_a$. Values of pressure difference $(P_a - P_c)$ between 5·7 and 25·3 in. Hg could be obtained, limited respectively by the minimum rig weight ($W_w = 0$) and by the available plant suction.

The depression pressure (P_c) is clearly the quantity which controls the whole level of thrust accuracy, as indeed it does during nozzle tests. During the calibration this pressure was outside the range of the 72 in. dibutylphthalate-vacuum manometer system, and all readings were taken on the Kew barometer. This is an instrument which, after allowing for various forms of correction, can register pressure to a comparative accuracy of 0·002 and a probable absolute accuracy of 0·005 in. Hg – always provided that the pressure is steady enough to allow reading of the vernier scale to better than these figures. It usually is not.

In addition to simple 'jumpiness' of the depression chamber pressure, a movement small in amplitude but at a frequency high enough to confuse visual observation of the barometer, there is often the further problem of 'drift' – a gentle movement of greater amplitude at a frequency of two or three cycles per minute. The effect of this on the Y term upsets the balance of the rig, which has to be continually restored by means of the spring balance following the movements of pressure. A technique is therefore used, both for calibration and nozzle testing, in which two operators take simultaneous readings of the depression pressure and spring position. Four or more sets of such readings are taken and averaged at each test condition.

It should be mentioned that the dash-pot is only brought into full effectiveness in cases of very rough nozzle running, such as when greatly over-expanding the flow, and in all normal service the by-pass valve is open.

Since the Z term is zero during calibration, the force balance equation can now be written:

$$A_z(P_a - P_c) + W_s - W_w = W_p - D$$

where

A_z = external cross-sectional area of pipe ($< A_0$)

D = leakage air drag

W_w = dead weights + blanking plate

The left-hand side of this equation is composed of measured quantities, and was used as the ordinate of a graph with $(P_a - P_c)$ as abscissa. This plot showed unmistakably the form of a straight line with slight negative slope, implying a relation of the form:

$$W_p - D = -m(P_a - P_c) + c$$

Now clearly, $D = 0$ when $(P_a - P_c) = 0$, so that the intercept $c = W_p$. We are thus left with the relation $D = m(P_a - P_c)$, when it is convenient to re-introduce the effective area A_0, defined as $A_0 = A_z + m$. The actual values of both W_p and A_0 for use in the nozzle tests were determined from a computer programme, which applied the method of least squares to a series of calibration runs totalling some ninety sets of readings.

The persistent linearity of the graph described above implies that the labyrinth was not choked throughout the range of calibrating conditions (corresponding to nozzle applied pressure ratios between 1·23 and 6·4). It may, however, be remarked that some nozzles have been tested at values of applied pressure ratio around 40, when the labyrinth could hardly fail to be choked. To cover this range in calibration would have required an extension of the value of $(P_a - P_c)$ from 25·3 to 29 in. Hg, for which suction plant was not available. Some uncertainty therefore exists as to the form of relation to be assumed over this interval. One could either 'freeze' $(W_p - D)$ at its value at 25·3 in. depression, or take it as continuing to follow the straight line relation. The maximum error from this uncertainty could be 0·06 lb at applied pressure ratio 40, equal to about 0·1 per cent thrust.† It was found more convenient to assume a continuation of the linear calibration, implying a constant value of A_0 for all pressure ratios.

3.2.2. *Nozzle base force.*

This term, Z, is in effect another 'piston' force of the same type as Y, and arises in just the same way. Part of the moving assembly (in this case the nozzle itself) protrudes from a region at depression pressure into one at a pressure normally lower, separated by the baffle plate. This is located close to the outlet plane of the nozzle. The lower pressure in the downstream compartment is associated with entrainment of flow by the nozzle exhausting into the recovery system, and the baffle plate prevents air in the rest of the depression box from taking part in the general exhaust flow recirculation. Tests without a baffle plate in position demonstrated appreciable differences of pressure acting across the flanges and other changes of outside section which occur on the nozzle and entry pipe. A fairly generous clearance exists between the nozzle and baffle plate, and some flow is induced through the gap. The effective 'piston' area is, therefore, once again uncertain. Partly for this reason, the force cannot be estimated with great precision, but in view of its low magnitude this is not serious.

The other uncertain factor is the pressure acting on the downstream side. Measurement of nozzle base pressure is made by incorporating six tappings equally spaced around the rearward facing rim of each nozzle, normally 0·10 in. in annular thickness. Some circumferential variation of base pressure can exist, presumably associated with asymmetry of the flow induced over the extreme end of the nozzle afterbody, where it passes through the baffle plate. This arrangement of nozzle exhaust can virtually be regarded as imposing a slight external flow, characterised by the pressure difference across the baffle plate. In amount this is trivial, normally not exceeding 4 in. water, and almost disappearing when a nozzle reaches its design condition.

Thus the force Z is a small one (*see* Table 2). Treating the area as the physical one of the nozzle afterbody $(A_e + A_b)$ as in Fig. 3, and the downstream pressure as that at the nearest possible measuring position (P_b), a reasonable range of uncertainty could be up to 10 per cent of the force itself. For a high pressure ratio design of nozzle, this might amount to a possible error of 0·05 per cent of thrust when correctly expanded, and perhaps 0·5 per cent of thrust when just choked.

PART II

4. *Convergent Nozzles.*

At the end of the exercise on direct air mass flow calibration (Section 3.1), we were left with the conclusion that the air meter readings provide a quite high degree of consistency, but that they could not be regarded as having a basis of absolute accuracy within $\frac{1}{4}$ per cent or more either way, due to inherent uncertainties as to the bias of static pressure measurement. Once a correction factor can be fixed by independent means, then the air meter becomes a satisfactory device for all tests within the same range of mass flow. Certain types of convergent nozzle when choked can be used for this purpose, and tests on a set of such nozzles formed an important part of the rig calibration process prior to the main test programme on convergent-divergent nozzles.

---

†This quantity is within the general scatter band of the calibration data, which embraces a spread unfortunately as wide at $\pm 0{\cdot}08$ lb. The best that could be done was to seek safety in the number of points taken, and the position of the resulting mean line can scarcely be in doubt to more than $\pm 0{\cdot}02$ lb at any point (*see* also Section 4.2).

Now the one-dimensional gauge thrust of an isentropic convergent nozzle exhausting to P_∞ is given by:

$$F^* = \frac{Qv^*}{g} + A^*(P_s^* - P_\infty)$$

The counterpart of this nozzle in real life passes the same flow Q, and has a discharge coefficient or flow efficiency defined as

$$C_D = \frac{A^*}{A_g}$$

where A_g is the geometric outlet area.

Hence

$$F^* = C_D A_g P_t \left\{ \frac{Q\sqrt{T_t}}{A^* P_t} \cdot \frac{v^*}{g\sqrt{T_t}} + \frac{P_s^*}{P_t} - \frac{P_\infty}{P_t} \right\}.$$

When $\gamma = 1{\cdot}4$ this reduces to

$$F^* = C_D A_g P_t \left(1{\cdot}26789 - \frac{P_\infty}{P_t}\right).$$

Now by definition

$$\eta_{F,\,\mathrm{conv}} = \frac{\text{measured gauge thrust}}{F^*}$$

wherefore

$$C_D \cdot \eta_{F,\,\mathrm{conv}} = \frac{\text{measured gauge thrust}}{A_g P_t \left(1{\cdot}26789 - \frac{P_\infty}{P_t}\right)} \tag{1}$$

Thus the product $C_D \cdot \eta_{F,\,\mathrm{conv}}$ at any test condition can be obtained to whatever accuracy the thrust system is capable of without reference to the air meter. Any opinion on C_D which the latter may contribute automatically carries with it a corresponding value for $\eta_{F,\mathrm{conv}}$; and conversely, if $\eta_{F,\mathrm{conv}}$ can be specified, then the air meter must be corrected to give the appropriate C_D.

Experimental results for three convergent nozzles shaped as shown in Fig. 8 are given in Figs. 9 to 11, taking the air meter readings at their face value. The so-called 'standard' nozzle has the same contracting profile as the convergent-divergent nozzles of Reference 1 and many of those tested later in the present work.

The second form of thrust efficiency used in presenting these results is based on vacuum as opposed to gauge thrust, the isentropic vacuum thrust being given by:

$$S^* = \frac{Qv^*}{g} + A^* P_s^* = F^* + A^* P_\infty$$

$$= 1{\cdot}26789\, C_D A_g P_t \text{ when } \gamma = 1{\cdot}4$$

and we define

$$\eta_{S,\mathrm{conv}} = \frac{\text{measured vacuum thrust}}{S^*}.$$

Now measured vacuum thrust exceeds gauge thrust by the term $A_g P_\infty$, so that

$$C_D.\eta_{S,\text{conv}} = \frac{1}{1{\cdot}26789}\left(\frac{\text{measured gauge thrust}}{A_g P_t} + \frac{P_\infty}{P_t}\right) . \tag{2}$$

At any test condition, therefore, the product $C_D.\eta_{S,\text{conv}}$ is also dependent only on the thrust measuring system.

Writing $P_{s,g}$ for some average static pressure in the outlet plane of the real nozzle, and defining a velocity efficiency η_v such that the average actual velocity in the outlet plane is equal to $\eta_v.v^*$, we can say

$$\eta_{F,\text{conv}} = \frac{\eta_v.\dfrac{Qv^*}{g} + \dfrac{A^*}{C_D}(P_{s,g} - P_\infty)}{\dfrac{Qv^*}{g} + A^*(P_s^* - P_\infty)}$$

and

$$\eta_{S,\text{conv}} = \frac{\eta_v.\dfrac{Qv^*}{g} + \dfrac{A^*}{C_D}.P_{s,g}}{\dfrac{Qv^*}{g} + A^* P_s^*}$$

Now it is reasonable to suppose that, once C_D is constant for any nozzle, the whole flow field in the neighbourhood of the throat is 'frozen', and to expect both $P_{s,g}$ and η_v to be constant also. If one were to idealise the situation further by assuming $P_{s,g} = P_s^*$, one could produce relations of the following form:

$$\eta_{F,\text{conv}} = \frac{\eta_v + \dfrac{K}{C_D}}{1+K}$$

$$\eta_{S,\text{conv}} = \frac{\eta_v + \dfrac{0{\cdot}71429}{C_D}}{1{\cdot}71429}$$

where K is a function increasing from 0 at the critical value $P_t/P_\infty = 1{\cdot}893$ to 0·71429 at $P_t/P_\infty = \infty$. Now C_D is necessarily < 1, and is also $< \eta_v$ (*see* Section 4.3). It then follows by inspection that under the assumed conditions $\eta_{S,\text{conv}}$ is a constant greater than unity, while $\eta_{F,\text{conv}}$ must increase with pressure ratio from η_v (i.e. < 1) at $P_t/P_\infty = 1{\cdot}893$ to equal $\eta_{S,\text{conv}}$ (i.e. > 1) at $P_t/P_\infty = \infty$.

In practice there is no ready means of obtaining either η_v or $P_{s,g}$, and the true flow conditions at outlet are too complex to be adequately represented by a superficial treatment based on assumed values. But the above relations do provide us with a useful indication of the form which these two types of thrust efficiency can be expected to take, and no surprise need be occasioned at finding $\eta_{F,\text{conv}}$ rising above unity with increase of pressure ratio, as for instance in Fig. 11. Let it be said here that no question exists of the thrust ever exceeding what is possible in an isentropic fully-expanded system. Were the form of gauge thrust efficiency η_F to be used, it would be found to be always and progressively below unity for all convergent nozzles.

4.1. *Outlet Flow Conditions.*

C_D is not necessarily constant for a convergent nozzle above a pressure ratio of 1·893, the critical value for isentropic one-dimensional flow. The nozzles of Fig. 8 exhibit curves of C_D which level off at values ranging from 2·4 to 3·9. It is necessary to regard the point at which the discharge characteristic becomes flat as the true 'choking' condition for a nozzle, beyond which the sonic flow field is frozen[†].

[†] *See* second footnote to page 16.

A difference between the critical and choking pressure ratios is associated with the mixed flow regime at outlet from a convergent nozzle, which was investigated by Stanton[4] as early as 1926. He traversed both a sharp-edged orifice and a convergent-divergent nozzle in the planes where they reached sonic conditions on the centreline , and showed that the outer boundary of flow was in each case supersonic. This effect was attributed to local curvature of the flow approaching the throat. In the case of the sharp-edged orifice the plane of traverse was outside the walls, as the main core of the jet was found to be still subsonic in the outlet plane. The centreline of the jet did not become sonic until appreciably further downstream than the outlet plane even when choked. A gradual upstream movement of the centreline sonic point took place as pressure ratio was increased, the movement ceasing at a condition which tallied closely with the levelling of the discharge curve†. Similar behaviour was observed for a convergent nozzle with smooth contour resembling Fig. 8a, although the effect was less pronounced.

These measurements were only made at pressure ratios above the critical, although a convergent-divergent nozzle can, as Stanton himself recognised, choke at a pressure ratio below critical. The actual choking value is, of course, related to the amount of divergence and its performance as a subsonic diffuser.

The position of the sonic point at the boundary was not examined by Stanton, and some interesting measurements have been made during the present investigation to supplement the picture given above. Wall pressure tappings were fitted just inside both the 'standard' and 'rapid approach' nozzles, at distances of approximately 0·02 throat diameters from the outlet planes. In addition, static probes were placed on the centreline of each nozzle with their holes in the outlet plane. Results in terms of Mach number are shown in Figs. 13 and 15.

Let us look first at the 'standard' nozzle. This has the convex curvature typical of most convergent-divergent nozzles with smooth continuous throat profiles. Curvature in this sense can be expected to produce high velocities near the walls and low ones near the axis, as G. I. Taylor[5] predicted in 1930, which results in a displacement of the boundary sonic point upstream of the geometric throat. Fig. 13 shows that the flow is indeed supersonic around the throat boundary, and subsonic on the axis. The boundary Mach number increases with the discharge coefficient, and then levels off at a value of 1·214 at a point which corresponds well with the choking pressure ratio of 2·4 obtained from Fig. 9‡. If, as seems likely, the position of the boundary sonic point and the distribution of wall pressure ahead of the geometric throat are unaffected by the presence or otherwise of subsequent divergence, once the nozzle is truly choked, then the above result would indicate an equivalent Prandtl-Meyer turn of 4 deg. before the minimum area section in many of the convergent-divergent nozzles discussed later.

At the centreline the Mach number increases more gradually to 0·849 at choking, which is in accord with the movement of the sonic point observed by Stanton on a kindred shape of nozzle. The flow pattern at outlet from a nozzle of this type will thus be much as depicted in Fig. 12.

On turning to the 'rapid approach' nozzle, we find an appreciably different situation. Here the curvature is in the opposite sense, i.e. concave, and in consequence the boundary flow conditions are also inverted. This time the Mach number near the lip is down to 0·735 at conditions above choking (Fig. 15), and changes little at lower pressure ratios. On the centreline, however, the flow at outlet is once again subsonic, as might be expected from Stanton's work, with the Mach number rising to 0·707 at the choking pressure ratio of 3·9.

---

†It may be mentioned in passing that a sharp-edged orifice made to B.S.1042 was tested on the rig already described. When blown from the reverse or chamferred side, it was found to choke at a pressure ratio of 5 ($C_D = 0{\cdot}925$). When turned the conventional way round, it produced an ill-defined choking condition around pressure ratio $7\frac{1}{2}$ ($C_D = 0{\cdot}883$).

‡It is of interest to note that the pressure ratio at which the nozzle is observed to choke is that corresponding to the maximum Mach number achieved in the outlet plane–i.e. for $M = 1{\cdot}214$ at the wall the pressure ratio is 2·47. It may be argued that, at any lower pressure ratio, the boundary Mach number cannot be as high, so that the flow field at outlet is not fully developed and the discharge characteristic will be that of a system not yet choked.

It is interesting to consider the behaviour of flow around the nozzle lip in this case, and an attempt to portray the pattern is given in Fig. 14. The whole expansion field associated with the applied pressure ratio must be concentrated at the sharp lip, as substantially ambient pressures have been measured at all radii on a narrow annular base surrounding the nozzle outlet plane. It seems, therefore, that the first Mach line generated from the lip will initially run perpendicular to the nozzle outlet wall angle of 30 deg. This would necessitate the sonic line taking on a shape such as is indicated in Fig. 14, with a region of supersonic flow formed towards the outside of the jet as it emerges from the nozzle. Despite basic differences of internal pressure distribution between these two nozzles of opposite curvature, a broad similarity may after all exist in the types of mixed outlet flow to which the curvature gives rise. This could be of some importance when analysing the effects of curvature on stream thrust.

4.2. *Nozzles for Calibration.*

Coming now to the question of using a convergent nozzle as a calibration device, a compromise must be reached between the effects of friction and throat curvature. The less curvature there is the greater the friction, and vice versa. Both properties result in a reduction of C_D, and attempts have been made at quantitative estimation of the component losses (e.g. References 3 and 17). These authors concur in recommending a shallow convex curvature (radius of curvature r_c approximately twice the throat diameter D_g) for calibration purposes despite the relatively large frictional loss, on the grounds that a knowledge of C_D based entirely on calculation will then have the best hope of reliability. Where, however, one is concerned with a method involving measurement of thrust, there is a distinct advantage in choosing a shape to give the highest value of the product $C_D.\eta_{F,\text{conv}}$ in equation (1). This will allow of the smallest error in an analysis of the combined losses, such as is attempted in the following pages. The nozzles of Figs. 8a and 8b both have values of $r_c = \frac{1}{2}D_g$, the wall profile becoming parallel to the axis in the outlet plane.

At the other end of the scale comes a sharp-edged orifice, from which our 'rapid approach' nozzle is not far removed. There the friction component is negligible and the effects of curvature (now concave) are a maximum. Neither flow nor thrust can be accurately predicted, and the product $C_D.\eta_{F,\text{conv}}$ is very low (Fig. 11), so that no use can be made of this nozzle as a calibrating device. It does, however, serve some purpose in the present exercise as affording experimental evidence of curvature effects on stream thrust in the absence of noticeable friction. This is referred to again in the analysis of losses.

All three convergent nozzles tested comprehensively (Figs. 9 to 11) exhibit a scatter of around $\pm 0{\cdot}15$ per cent in C_D, this being evidently the limit of repeatability of the air metering system, although throughout any one test almost perfect consistency is maintained. Computation of thrust efficiencies from equation (1) must reflect any variation in C_D, on top of which is added errors introduced from the thrust measurement, so that the result is likely to be a scatter if anything wider than that in C_D. Best results were achieved on the 'faired entry' nozzle with only $\pm 0{\cdot}15$ per cent, the others showing generally around $\pm 0{\cdot}20$ per cent.

A point deserving note here is that the product $C_D.\eta_{F,\text{conv}}$ only contains the scatter from thrust measurement. Just as, from equation (1), this product is independent of the absolute accuracy of the air meter, so it is of the scatter in C_D. Thus the ensuing analysis of losses, from which the air meter correction factor is derived, revolves about a quantity concerning which very little doubt can be entertained.

It will be observed from Figs. 9 and 10 that the two calibrating nozzles have quite similar flow characteristics, choking at a pressure ratio around 2·4 as already noted. In the range of pressure ratio 2 to $2\frac{1}{2}$, and again above 8, the values of $\eta_{F,\text{conv}}$ are also similar. No explanation can be given for the individual patterns occurring in the interval. From choking to the highest pressure ratio tested a net rise of 0·4 per cent in $\eta_{F,\text{conv}}$ takes place in both cases, while the curves of $\eta_{S,\text{conv}}$ end at pretty well the same level as they start. As already shown, $\eta_{S,\text{conv}}$ would be expected to be constant above choking; points below choking have been omitted†.

† The trend of $\eta_{S,\text{conv}}$ below choking pressure ratio is shown in Fig. 11 for the 'rapid approach' nozzle.

The analysis of losses will be performed at the condition where the nozzles are just choked, pressure ratio 2·4, taking average values from Figs. 9 and 10 as follows:

TABLE 3

Nozzle	'Standard'	'Faired entry'	Average
C_D	0·989	0·990	0·9895
$\eta_{F,\text{conv}}$	0·999	0·999	0·999
$\eta_{S,\text{conv}}$	1·003	1·003	1·003
$C_D.\eta_{F,\text{conv}}$	0·98801	0·98901	0·98851
$C_D.\eta_{S,\text{conv}}$	0·99197	0·99297	0·99247

4.3. *Analysis of Losses.*

The effects of friction and throat curvature will first be discussed in isolation.

(i) *Friction.*

This is quite a small quantity in convergent nozzles with rather abrupt contraction and fed through a duct with only a partially developed boundary layer, as is typical both of these tests and of aircraft propelling nozzle practice. Its effect is to reduce both C_D and η_v below unity. Using suffix f to denote the defects due to friction, we can say from Appendix IV (Section 1) that, for the thin boundary layers existing in these nozzles,

$$\begin{cases} 1-C_{D,f} = \dfrac{4}{D_g}.\delta^* \\ 1-\eta_{v,f} = \dfrac{4}{D_g}.\theta \end{cases}$$

whence

$$H = \frac{\delta^*}{\theta} = \frac{1-C_{D,f}}{1-\eta_{v,f}}. \tag{3}$$

Now at $M = 1$, approximate values of H are

$$\begin{cases} 1{\cdot}8 \text{ for turbulent flow (Reference 6)} \\ 3{\cdot}3 \text{ for laminar flow (Reference 7).} \end{cases}$$

The actual Mach number at the wall is in fact known to be at least 1·214 at outlet as a result of curvature, for which the values of H would be rather higher. But in treating friction in the absence of curvature it is appropriate to consider average conditions through the flow, and take values corresponding to $M = 1$. In any case the effect on H of variation in M is small by comparison with the change from turbulent to laminar state.

Evidence to be cited later, on the separation characteristics of convergent-divergent nozzles with this same shape of throat section, leaves little doubt that the conditions produced in this rig are in fact laminar in the absence of any deliberate attempt to promote transition in the boundary layer entering the nozzle. A figure for Re^*, the Reynolds number based on nozzle throat diameter and sonic velocity, of $0{\cdot}75 \times 10^6$ applies to all nozzles and all conditions in these tests. Nevertheless, the analysis has been done with both the above values of H, in order to establish the sensitivity to variation of this quantity.

Unfortunately one cannot obtain η_v from experimental measurements. But, in treating friction alone with no distortion of the sonic line, one is quite justified in taking $P_{s,g} = P_s{}^*$, so that we have:

$$\eta_{S,\mathrm{conv},f} = \frac{\eta_{v,f}\dfrac{Qv^*}{g} + \dfrac{A^*}{C_{D,f}} \cdot P_s{}^*}{\dfrac{Qv^*}{g} + A^* P_s{}^*}$$

$$= \frac{\eta_{v,f} + \dfrac{0{\cdot}71429}{C_{D,f}}}{1{\cdot}71429},$$

all variables being independent of pressure ratio. Substitution from equation (3) then gives:

$$\eta_{S,\mathrm{conv},f} = \frac{1 - \dfrac{1}{H}(1 - C_{D,f}) + \dfrac{0{\cdot}71429}{C_{D,f}}}{1{\cdot}71429}$$

$$= G_1[C_{D,f}]. \tag{4}$$

This quantity is always above unity.

(ii) *Curvature of the sonic line.*

We are now concerned with non-uniformity of pressure, flow direction and velocity across the outlet plane. The resulting flow defect is written as $1 - C_{D,c}$ and we define the relation

$$\lambda = \frac{\eta_{S,\mathrm{conv},c} - 1}{1 - C_{D,c}},$$

it being understood that $\eta_{S,\mathrm{conv},c} > 1$. This merely reflects the shape of the curve of vacuum stream thrust against Mach number, which is a minimum when $M = 1$. For any mixed flow, therefore, comprising a region in which $M > 1$ and another where $M < 1$, it follows that

$$\sum AP_s(1 + \gamma M^2) > A^* P_s{}^* (1 + \gamma),$$

while

$$\sum A = \frac{A^*}{C_D}.$$

Some quantitative estimate may be formed of the behaviour of λ by considering the relation between an element of isentropic flow at any condition ($M \neq 1$) and the same quantity of flow at $M = 1$. For this treatment it will at present be assumed that the flow direction is always axial. Then, for any such

element, one can obtain expressions for the 'local' flow and thrust efficiencies, which are dependent only on M and γ. Writing these 'local' quantities as

$$\begin{cases} \bar{C}_D & \text{representing } C_{D,c} \\ \bar{\eta}_S & \text{representing } \eta_{S,\text{conv},c} \end{cases}$$

and

$$\bar{\lambda} = \frac{\bar{\eta}_S - 1}{1 - \bar{C}_D}$$

we know by definition that

$$\bar{C}_D = \frac{A^*}{A} \text{ and } \bar{\eta}_S = \frac{S}{S^*}.$$

Now $S = Q\sqrt{T_t/Y}$, where Y is a function of M and γ. In this comparison both Q and T_t are constant, so that

$$\bar{\eta}_S = \frac{Y^*}{Y} \text{ and } \bar{\lambda} = \frac{Y^*/Y - 1}{1 - A^*/A}$$

When $\gamma = 1{\cdot}4$, this becomes

$$\bar{\lambda} = \frac{\dfrac{1+1{\cdot}4M^2}{2{\cdot}4M}\sqrt{\left(\dfrac{1{\cdot}2}{1+0{\cdot}2M^2}\right)} - 1}{1 - M\left(\dfrac{1{\cdot}2}{1+0{\cdot}2M^2}\right)^3}.$$

The form of this relation is shown in Fig. 16.

In any practical case of mixed flow, the overall value of λ will be some average of the values of $\bar{\lambda}$ for the individual elements. Those of our nozzles with convex curvature have been seen to produce a flow distribution at outlet varying from $M = 0{\cdot}849$ on the axis to at least $M = 1{\cdot}214$ at the wall. If all the flow be assumed to be axial, Fig. 16 gives a corresponding range of $\bar{\lambda}$ between 0·48 and 0·36, and a reasonable average for λ should lie around 0·43. Although the wall is parallel to the axis in the outlet plane, the approach curvature will in fact give rise to some slight inclination of the flow. To what the effect of this may amount is uncertain, but a realistic answer for λ is probably around 0·4.

Since the thrust and flow defects of the 'rapid approach' nozzle result almost completely from curvature, it can provide us with an experimental estimate of λ for rather sharp concave curvature. In Fig. 17 are shown values derived from the mean curves of Fig. 11, and it is apparent that once the nozzle has become choked λ remains close to 0·3. The reason for a value so low by comparison with Fig. 16 is no doubt associated with the pronounced inclination of much of the flow. At the wall, as has been seen, this approaches the outlet plane at $M = 0{\cdot}735$ in a direction making 30 deg. to the axis. Variation of the above analysis for $\bar{\lambda}$ to take account of flow inclination is not quantitatively useful, but the general trend is a reduction in $\bar{\lambda}$ with increase of flow angle. Alternative values of 0·3 and 0·4 for λ have been used in the analysis in order to discover its sensitivity to this factor.

Then

$$\eta_{S,\text{conv},c} = 1 + \lambda(1 - C_{D,c})$$

$$= G_2[C_{D,c}]. \tag{5}$$

This also exceeds unity.

Adding the above components of loss, we get:

$$1-C_D = (1-C_{D,f})+(1-C_{D,c})$$

therefore
$$C_D = C_{D,f}+C_{D,c}-1 \tag{6a}$$

$$1-\eta_{F,\text{conv}} = (1-\eta_{F,\text{conv},f})+(1-\eta_{F,\text{conv},c})$$

therefore
$$\eta_{F,\text{conv}} = \eta_{F,\text{conv},f}+\eta_{F,\text{conv},c}-1 \tag{6b}$$

$$\eta_{S,\text{conv}}-1 = (\eta_{S,\text{conv},f}-1)+(\eta_{S,\text{conv},c}-1)$$

therefore
$$\eta_{S,\text{conv}} = \eta_{S,\text{conv},f}+\eta_{S,\text{conv},c}-1 \tag{6c}$$

The three quantities C_D, $\eta_{F,\text{conv}}$ and $\eta_{S,\text{conv}}$ are related by the expression

$$\eta_{F,\text{conv}} = \frac{\eta_{S,\text{conv}}.S^* - \dfrac{A^*P_\infty}{C_D}}{S^*-A^*P_\infty}$$

At pressure ratio 2·4 and with $\gamma = 1{\cdot}4$ this reduces to

$$C_D.\eta_{F,\text{conv}} = 1{\cdot}48950\, C_D.\eta_{S,\text{conv}} - 0{\cdot}48950 \tag{7}$$

For this condition Table 3 gives average values of the products $C_D.\eta_{F,\text{conv}}$ and $C_D.\eta_{S,\text{conv}}$ which satisfy equation (7) within 0·00028. This is considered good enough to proceed without any adjustment. Hence the framework within which the rig results must fit is given by the relation

$$(C_{D,f}+C_{D,c}-1)\left\{G_1\left[C_{D,f}\right]+G_2\left[C_{D,c}\right]-1\right\} = 0{\cdot}99247 \tag{8}$$

It is clear that the possible variation of either $C_{D,f}$ or $C_{D,c}$ is restricted to the range between unity and some lower values yet to be determined, so that extreme limits to the true C_D are set by the two conditions $C_{D,f} = 1$ and $C_{D,c} = 1$. Solutions to equation (8) have been obtained for four conditions, viz:

(*a*) $H = 1{\cdot}8$; $\lambda = 0{\cdot}3$

(*b*) $H = 1{\cdot}8$; $\lambda = 0{\cdot}4$

(*c*) $H = 3{\cdot}3$; $\lambda = 0{\cdot}3$

(*d*) $H = 3{\cdot}3$; $\lambda = 0{\cdot}4$

and the results are shown in Figs. 18a to d. It can be seen that in all cases the C_D as calculated above changes very little between one limit and the other, and lies close to the value given by the air meter.

In deciding exactly where to place the true level of C_D within this quite narrow range, we may note that Fig. 8 of Reference 3 suggests a value of $C_{D,f} = 0{\cdot}997$ for our throat Reynolds number ($Re^* = 0{\cdot}75 \times 10^6$), it being independent at this condition of whether the boundary layer is turbulent or laminar. Application of this value to our Fig. 18 would require air meter correction factors in the above four cases of:

(*a*) 1·0006 (*c*) 1·0000

(*b*) 0·9995 (*d*) 0·9987

and would yield the following values of $C_{D,c}$:

(*a*) 0·9931 (*c*) 0·9925

(*b*) 0·9920 (*d*) 0·9912

All four of the latter lie around a level which seems to be on the upper limit of probability for this curvature, and little room is left for adjustment of $C_{D,f}$. It seems reasonable to conclude that these values for the breakdown of losses can be accepted to $\pm 0{\cdot}10$ per cent – a range of uncertainty in the positioning of C_D which is not serious.

Thus there is no great difference resulting from changes in the values assumed for the quantities H and λ. Case (*d*) above, for laminar conditions and $\lambda = 0{\cdot}4$, is probably the most realistic, and it is evident that the air meter is giving answers very close to the truth. Electing for convenience to ignore the small correction, we arrive at an approximate breakdown of losses (i.e. rounded to the nearest 0·05 per cent) as follows:

TABLE 4

$C_D = 0{\cdot}9895$	$C_{D,f} = 0{\cdot}997$	$C_{D,c} = 0{\cdot}9925$
$\eta_{F,\mathrm{conv}} = 0{\cdot}999$	$\eta_{F,\mathrm{conv},f} = 0{\cdot}999$	$\eta_{F,\mathrm{conv},c} = 1{\cdot}000$
$\eta_{S,\mathrm{conv}} = 1{\cdot}003$	$\eta_{S,\mathrm{conv},f} = 1{\cdot}0005$	$\eta_{S,\mathrm{conv},c} = 1{\cdot}0025$

4.4. *Effective curvature.*

The level of $C_{D,c}$ given above affords a subject for some speculation. Theoretical attempts to predict this quantity emerge with values for our curvature considerably lower than are compatible with the experimental results, analysed as above. A treatment which is thought to be exact is given by Hall[16], but his solution is unfortunately in the form of a series which becomes divergent around $r_c \leqslant 0{\cdot}8\, D_g$. A suggested extrapolation[3] of his results to sharper curvatures yields a figure for $C_{D,c}$ in the neighbourhood of 0·982 at our condition of $r_c = 0{\cdot}5\, D_g$, as compared with about 0·992 from experiment. This discrepancy would seem to imply around 100 per cent inaccuracy in the best theory available. One should therefore consider whether it is possible that the effective curvature of these nozzles can be substantially different to the nominal. An examination has been made of the variation of boundary-layer displacement thickness ahead of the throat, based on an estimate of boundary-layer height at the end of the parallel approach pipe and a measured wall pressure distribution along the contraction. It is interesting to note that the resulting boundary-layer thickness in the outlet plane agrees very well with that derived from the thrust efficiency *via* equation (A2). Regarding the effective local radius of curvature as that of the displacement boundary, calculations then suggest that this can reach a value much greater than the nominal $0{\cdot}5\, D_g$ in the immediate neighbourhood of the outlet plane. Fig. 19 illustrates the computed trend. It is difficult to assess over what final length of wall contour the local curvature really governs the flow, but Fig. 19 suggests that a mean effective value could be as high as $r_c = 0{\cdot}8\, D_g$. This would correspond to a level of $C_{D,c}$ as given by Hall[16] of around 0·991, which is in close agreement with the experimental. It seems, therefore, that the presence of a boundary layer which, as a result of the variation of Mach number in the vicinity of the nozzle throat, reaches a minimum displacement thickness slightly ahead of the outlet plane (Fig. 19), can produce an effective wall curvature significantly shallower than the nominal. Were it not for this factor, the product $C_D \cdot \eta_{S,\mathrm{conv}}$ would apparently be much lower for our nozzles; and their advantage of near-optimum balance of friction and curvature seems to rest upon the diminished effect of curvature caused by the boundary layer.

It should be noted that the C_D of the 'standard' convergent nozzle above choking is effectively the same as in obtained with the addition of a divergent portion (*see* Section 6, describing the nozzles of design pressure ratios 5, 10, 15 and 25 with 10 deg. conical half-angle, and design pressure ratios 15, 25 and 35 with 15 deg. angle, all having nominally the same throat shape). Hence there is justification for saying that the vacuum efficiency $\eta_{S,\mathrm{conv}}$ given in Table 4 should be applicable to the stream thrust in the throat of a convergent-divergent nozzle with a similar approach. Use can be made of this relationship

in obtaining thrust efficiencies from a plot of pressure distribution down the divergent portion of a nozzle only (*see* Appendix V).

4.5. *Accuracy.*

In formulating the final claim to a particular level of accuracy in mass flow measurement, we find that the foregoing analysis yields a determination within very close limits, around $\pm 0{\cdot}10$ per cent, and is subject only to the possible errors in measured thrust governing the product $C_D.\eta_{S,\text{conv}}$. In previous Sections, we have seen that these may arise in two ways, to wit:

(i) Uncertainty in the values obtained for W_p and A_0 (Section 3.2.1). Selection of a mean line through the rather wide scatter in calibration data was done mathematically, using the method of least squares, and a sufficient quantity of data was obtained to ensure a fairly reliable answer. The test data are in fact concentrated, as mentioned previously, in the range of seal pressure difference $(P_a - P_c)$ between 5·7 and 25·3 in. Hg. Doubt arises mainly over the slope of the selected mean line through the spread of points (giving A_0), and hence in the intercept obtained by extrapolation of this line to zero pressure difference (equal to W_p).

It is important to note here that errors in A_0 and W_p caused by taking the wrong slope are mutually opposing. Suppose, for instance, that a clockwise rotation of the mean line through the calibration data be considered: then both A_0 and W_p are increased. But the force terms Y and W_p act in opposite sense, so that the net change can be small. Over the range of pressure ratio through which the convergent nozzles were tested, it is considered unlikely that more than 0·02 lb aggregate error in thrust could arise, corresponding to $\pm 0{\cdot}05$ per cent.

(ii) Possible error in estimation of the force term Z. This has already been discussed in Section 3.2.2, and for convergent nozzles the level of confidence is again about $\pm 0{\cdot}05$ per cent.

These two constituents give a total uncertainty of $\pm 0{\cdot}10$ per cent in the level of measured thrust, and hence in the product $C_D.\eta_{S,\text{conv}}$. Adding the further $\pm 0{\cdot}10$ per cent for the breakdown of this product *via* the analysis of friction and curvature effects as discussed above, we arrive at a final figure of $\pm 0{\cdot}20$ per cent certainty of mass flow measurement.

A useful by-product of this exercise in air meter calibration is fairly accurate knowledge of the discharge characteristics of certain types of convergent nozzle. Replicas of the 'standard' and 'faired entry' nozzles could now be used elsewhere as a means of air mass flow measurement, provided that they are run choked (i.e. at pressure ratios in excess of 2·4). At different values of Reynolds number, and then depending slightly on whether conditions are turbulent or laminar, there will be some change in the friction component $C_{D,f}$, but this is likely to affect the result by less than 0·1 per cent in the range of practical interest.

However, differences of C_D for nozzles with nominally identical profiles approaching the throat have been observed. As shown in Section 6, the family of seven convergent-divergent nozzles based on the 'standard' convergent shape of throat exhibits a spread from 0·9875 to 0·9915 (0·4 per cent) in the average values of C_D. No reason other than manufacturing idiosyncrasies can be adduced for this behaviour, and one is forced to conclude that minor inexactitudes of wall profile local to the throat can cause variation within these limits†. This should be borne in mind when considering the use of nozzles nominally similar to our models for air flow measurement elsewhere.

---

†The exercise on correlating effective curvature with the displacement boundary in the vicinity of the nozzle throat, of which mention has already been made, indicates that the flow is likely to be very critical to the precise wall profile over a short length of contour in the minimum area region. Although care is taken during manufacture to ensure a fairly accurate and uniform curvature over the surface taken as a whole, the available methods of machining do not permit a faithful reproduction of the desired curvature to be guaranteed in this critical locality. It is unfortunately most probable that variations in exact throat profile can be expected to occur from one nozzle to another even when made from the same template, and with this will go some difference in the effective curvature. The observed spread of C_D values corresponds to an approximate range of r_c/D_g between 0·75 and 0·95 which, if taken over a length of 0·2 in., would require the local profile to be flattened by only 0·0007 inch.

5. *Convergent-divergent nozzle performance quantities.*

5.1. *Nozzle discharge pressure.*

Throughout these tests, on both convergent and convergent-divergent nozzles, the base pressure[‡] P_b was treated as the pressure to which the nozzle was expanding, so that the applied pressure ratio (A.P.R.) is given by P_t/P_b. This quantity is convenient in a rig arrangement of this type, in which the nozzle exhausts into a depression chamber, since

(i) the nozzle base is the nearest point at which a measurement can be taken representative of the environment produced around the nozzle jet as it discharges into the exhaust recovery system.

(ii) the only feasible competitor is the pressure in the upstream compartment of the depression box, which in fact differs from P_b only by the very small pressure drop existing across the baffle plate.

There is in addition, however, a fundamental reason for using base pressure as a reference quantity for the performance of wholly internal-expansion nozzles under all conditions. Where P_b differs from P_∞, as it generally does in the presence of an external flow, the internal pressure distribution and hence the nozzle gross thrust is governed uniquely by the base pressure – i.e. that part of the outer world with which the expanding flow first comes in contact. One can therefore say that P_∞, which is related to P_b in any particular case by the arrangement of afterbody geometry and the external flow velocity, is in general quite irrelevant in determining the nozzle internal-expansion conditions. The separation of internal flow resulting from shock-boundary-layer interaction within the nozzle is, for instance, correlated with or without external flow by the same criterion of pressure ratio from separation point to base, and, so long as P_t/P_b is the same, the nozzle demonstrates the same internal pressure distribution[12].

The ratio P_t/P_∞ is, of course, the quantity with which the project engineer or aircraft designer is concerned, since it is the exhaust pressure ratio (E.P.R.) supplied by the gas generator. He will be interested in knowing what is the best thrust efficiency which is attainable at a particular combination of E.P.R. and flight condition. But to link internal nozzle performance with E.P.R. it is necessary to obtain, either by calculation or from tunnel tests, the relation between P_b and P_∞ for any given geometry of nozzle and afterbody. Once this relation is known, the efficiency of an internal-expansion nozzle can be read across from measurements of thrust on a quiescent air rig operating at the required value of A.P.R. It is thus clear that in general the results of static tests of internal-expansion nozzles should be presented in terms of A.P.R.

An exception must be made in the case of mixed-expansion nozzles, i.e. those with partially external expansion. The free jet boundary then formed around the external-expansion field, which determines the effective area ratio of expansion, is governed mainly by P_∞, rather than by whatever base pressure may exist at the end of the shroud. The influence of P_b is then restricted to the internal-expansion region within the confines of the shroud, the internal-expansion pressure ratio being controlled by P_b. It therefore follows that no very useful purpose may be served by testing a system with external expansion on a quiescent air rig other than at the design-point.

5.2. *Nozzle Efficiencies.*

Many forms of internal thrust efficiency can be found in general use, depending whether one elects:

(*a*) to work in terms of gauge or vacuum thrust,

(*b*) to relate measured thrust to a reference based on the same mass flow or the same throat area,

(*c*) to consider the reference nozzle as having fixed or variable geometry.

All our results are presented as gauge thrust per unit mass flow, but it is convenient with internal-expansion nozzles to give two alternative efficiencies for the cases of fixed and variable geometry isentropic reference

---

[‡] Each nozzle tested was equipped with six base pressure tappings in the narrow annular face around the outlet plane of the nozzle.

nozzles. Definitions of these quantities will be found in Appendix I. The ideal gauge thrust from a fixed geometry nozzle is then

$$\frac{Qv_e'}{g}+A_e'(P_e'-P_b) \text{ or } [\tilde{F}]_{DPR}+A_e'(P_e'-P_b)$$

using definition (i) for D.P.R. [$= P_t/P_e'$ corresponding to A_e'/A^*: *see* Appendix V], and that from a variable geometry nozzle giving complete expansion is

$$[\tilde{F}]_{APR}.$$

Hence

$$\eta_F' = \frac{\dfrac{\text{measured gauge thrust}}{C_D A_g P_t}}{\left[\dfrac{\tilde{F}}{A^*P_t}\right]_{DPR}+\dfrac{A_e'}{A^*}\left(\dfrac{1}{D.P.R.}-\dfrac{1}{A.P.R.}\right)} \tag{9}$$

and

$$\eta_F = \frac{\dfrac{\text{measured gauge thrust}}{C_D A_g P_t}}{\left[\dfrac{\tilde{F}}{A^*P_t}\right]_{APR}} \tag{10}$$

A relation of interest, composed only of isentropic functions†, is obtained by combining equations (9) and (10) to give

$$\frac{\eta_F}{\eta_F'} = \frac{\left[\dfrac{\tilde{F}}{A^*P_t}\right]_{DPR}+\dfrac{A_e'}{A^*}\left(\dfrac{1}{D.P.R.}-\dfrac{1}{A.P.R.}\right)}{\left[\dfrac{\tilde{F}}{A^*P_t}\right]_{APR}}. \tag{11}$$

It should be noted that the fixed geometry efficiency (η_F') is only of significance for an internal-expansion nozzle running full. In the cases of nozzles with either external expansion or internal separation, equations (9) and (11) should not be used.

Now, if the losses in an internal-expansion nozzle are caused only by friction and outlet divergence, the measured gauge thrust may be written as

$$\eta_d\left\{\eta_f\frac{Qv_e'}{g}+A_e(P_e-P_b)\right\}$$

the divergence loss factor η_d applying to both momentum and pressure thrusts (Appendix III). In this expression it is to be understood that A_e is the geometric outlet area inclusive of allowance for divergence, so that as in Appendix V (page 56)

$$A_e = \frac{A_e'}{\left(1-\dfrac{4\delta^*}{D}\right)_e} = \frac{A_e'}{1-H_e(1-\eta_f)}$$

say $$= \zeta A_e', \text{ where } \zeta > 1.$$

---

† *See* Appendix VI.

In this particular case we may also take $P_e = P_e'$.[†] Then the measured gauge thrust becomes

$$\eta_d \left\{ \eta_f [\tilde{F}]_{DPR} + \zeta A_e' (P_e' - P_b) \right\}$$

or

$$\eta_f = \frac{\dfrac{\text{measured gauge thrust}}{\eta_d C_D A_g P_t} - \zeta \dfrac{A_e'}{A^*} \left(\dfrac{1}{D.P.R.} - \dfrac{1}{A.P.R.} \right)}{\left[\dfrac{\tilde{F}}{A^* P_t} \right]_{DPR}}. \tag{12}$$

Using the estimates of η_f obtained from Appendix IV, the quantity η_d may be evaluated and compared with the relations given in Appendix III.

Considerable similarity exists between the terms in equations (9) and (12), and one can, for the special case just considered, combine the two to give an expression dependent only on calculable quantities:

$$\eta_F' = \eta_d \cdot \frac{\eta_f \left[\dfrac{\tilde{F}}{A^* P_t} \right]_{DPR} + \zeta \dfrac{A_e'}{A^*} \left(\dfrac{1}{D.P.R.} - \dfrac{1}{A.P.R.} \right)}{\left[\dfrac{\tilde{F}}{A^* P_t} \right]_{DPR} + \dfrac{A_e'}{A^*} \left(\dfrac{1}{D.P.R.} - \dfrac{1}{A.P.R.} \right)}. \tag{13}$$

Simple convergent-divergent nozzles exhibit curves of fixed and variable geometry efficiency against A.P.R. whose characteristic shapes can be determined from examination of equations (11) and (13). For a nozzle with only friction and divergence losses, our three definitions of D.P.R. are very close together. At the design-point, A.P.R. = D.P.R. and it is obvious that

$$\eta_{F,\,\max} = \eta_F' = \eta_d \eta_f.$$

At values of A.P.R. on either side of the design-point, equation (13) shows that the factor η_d acts on the whole thrust, and η_f on the momentum term only. The ratio of the latter to the total thrust depends on the degree of over- or under-expansion; for D.P.R. > 10, over the range $0{\cdot}5 < \dfrac{\text{A.P.R.}}{\text{D.P.R.}} < 2$, this ratio is confined between 1·18 and 0·93, the band narrowing with increase of D.P.R. Thus ζ acts on a proportion less than 20 per cent of the total thrust. Furthermore, for nozzles having values of D.P.R. and divergence angle within the current range of interest, friction effects in general form a minor part of the whole loss. Hence it is approximately true at any A.P.R. where the nozzle is running full to say

$$\eta_F' \doteq \eta_d \eta_f = \text{constant}.$$

On this basis equation (11) allows the variation of η_F with A.P.R. to be calculated from no knowledge other than the design-point value ($\eta_{F,\max}$), again within the range in which the nozzle runs full. Conversely, if a test at D.P.R. is not possible, design-point performance can be obtained from test data at any other pressure ratio where the nozzle is still running full.

One may at this point consider the instance of a nozzle with some constant internal expansion defect, such as a discontinuity in profile, or secondary flow effects in a rectangular nozzle[≠]. Suppose that this loss amounts to a proportion q of the completely-expanded design-point thrust, then the momentum thrust at any other pressure ratio at which the nozzle runs full will be reduced by the same proportion q.

[†] No losses besides friction and divergence (*see* Appendix V).

[≠] In this category would also come any additional loss from outlet divergence over and above that given in Appendix III, as in the case of a very short conical nozzle (*see* Section 6.1).

In effect, this form of loss can be likened to a reduction in the factor η_f. It is then unlikely that we can any longer regard η_F' as constant, or η_F as following a curve given by the right-hand side of equation (11). Expressing the loss now as a proportion of total thrust, instead of momentum thrust, we shall get a value for this proportion smaller than q when A.P.R. < D.P.R. and higher than q when A.P.R. > D.P.R. This produces a tendency for η_F' to increase with A.P.R.

Let us now see what happens when a nozzle ceases to run full, that is, when separation takes place internally. The resultant pressure rise within the nozzle increases its thrust above that which it would give if continuing to run full. It is therefore evident that the quantity η_F' obtained from equation (9) will start to rise above the nearly constant value which it has been seen to have elsewhere (and it eventually reaches values well in excess of unity at very low A.P.R.). So likewise will η_f when derived from equation (12). The value of A.P.R. at which the curve of η_F' turns upwards with decreasing A.P.R. is traditionally termed the 'kink point'[1], and corresponds to the condition at which the exit shock first enters the nozzle. Here the curve of variable geometry efficiency η_F may exhibit a change of slope in its downward course.

Illustrations of these shapes will be found in the graphs accompanying the next Section.

Finally, looking once more at equations (9) and (10), we see that for a given nozzle at a given A.P.R. they have the form

$$\eta \propto \frac{\text{measured gauge thrust}}{C_D A_g P_t}$$

or

$$\propto \frac{\text{measured gauge thrust}}{Q\sqrt{T_t}}$$

This relation implies, just as for convergent nozzles, that a small error of measurement in the quantity A_g does of course result in an incorrect value of C_D, but does not affect η. However, any error in measurement of mass flow leads to a proportional error in the opposite sense in thrust efficiency.

6. *Conical Nozzles.*

The nozzles discussed in this Section are those of which details are tabulated below, reference being made to Fig. 20 which shows the two geometrical arrangements of approach section. All but one of the models conform to type (a), this being based on the 'standard' convergent nozzle shape (Fig. 8a). The nominal throat curvature is the same for both types (a) and (b).

TABLE 5

Conical Nozzles

(*see* Fig. 20)

Approach section	αdeg.	$\frac{A_e}{A_g}$	Nominal D.P.R.	C_D
a	10	1·351	5	0·9880 ± 0·0015 (7) †
a	10	1·930	10	0·9875 ± 0·0010 (6)
a	10	2·438	15	0·9905 ± 0·0010 (5)
a	15	2·436	15	0·9910 ± 0·0010 (2)
b	10	2·906	20	0·9920 ± 0·0010 (7)
a	10	3·317	25	0·9890 ± 0·0010 (7)
a	15	3·326	25	0·9890 ± 0·0010 (4)
a	15	4·109	35	0·9915 ± 0·0005 (3)

†Number of runs

The lowest value of applied pressure ratio tested was 2, and at this condition all the nozzles were choked, so that no variation of C_D was experienced with A.P.R. Table 5 shows a spread in mean C_D level from 0·9875 to 0·9915, i.e. 0·4 per cent, for nominally identical throat sections[†]. That of the 'standard' convergent nozzle (Fig. 9) is 0·9890, which is fairly near the middle of the range.

6.1. *Design-Point Performance.*

In Fig. 21 is shown the design-point performance of these nozzles. The value of $\eta_{F,\max}$ is actually taken not from the peak of a curve of η_F, which may depend on the accuracy of a single experimental point, but from the average level of the quantity η_F' (as in Section 5.2) over a wide range of A.P.R. and during repeated runs. It is an unfortunate law of nature that the amount of scatter in test results increases with the number of experiments made, and the widest scatter bands in Fig. 21 occur with two of the nozzles most comprehensively tested.

By adding to $\eta_{F,\max}$ the momentum loss from friction (η_f) as calculated in Appendix IV, one can arrive at the divergence loss factor η_d, considering there to be no other source of loss in this type of nozzle. Values for η_f have been obtained for $Re^* = 0{\cdot}75 \times 10^6$ and a laminar boundary layer. Fig. 22 presents on this basis the points from Fig. 21, and also marked on it are the theoretical values of η_d according to Appendix III.

A marked discrepancy exists in Fig. 22 for the case of the 10 deg. nozzle with D.P.R. = 5. The reason is disclosed by an examination of wall pressures within a nozzle having this cone angle and blown so as to run full. Fig. 23 illustrates the distribution as far as area ratio 2, the value of pressure in the geometric throat (area ratio 1) being taken from Fig. 13 for a choked convergent nozzle of the same approach shape. The transition from circular arc contour to straight taper (Fig. 20) occurs at an area ratio of 1·031, and it is apparent that the flow has by then undergone a total supersonic expansion equivalent to a turn of 11·0 deg. This happens to correspond quite closely with the geometric angle of 10 deg. by which the wall direction has changed after the minimum area section, but it should be remembered from Section 4.1 that nearly 4 deg. of expansion had in fact taken place by the time the flow had reached the geometric throat plane[≠].

As a result of this initial over-expansion in the neighbourhood of the throat, the wall pressure is locally considerably below the one-dimensional isentropic value corresponding to the area ratio (Fig. 23). Gradual recovery takes place, the measured and one-dimensional pressure curves converging to cross at area ratio 1·26. So long as the measured curve remains thereafter above the one-dimensional, so the process of recovery continues, and any premature ending of the nozzle will introduce a loss over and above that which the assumption of point-source flow (Appendix III) suggests as being the minimum loss from outlet divergence for a nozzle of this cone angle.

It is interesting to compute from Fig. 23 the effective value of η_d for 10 deg. conical nozzles of varying area ratio, i.e. cut off at different lengths. This may be done by evaluating the difference in $\int P_w dA$ between the measured and one-dimensional curves. In doing this one has to make allowance for the friction inherent in a plot of measured wall pressure. The subject is discussed in detail in Appendix IV, and it is the 'displacement loss' (β) therein described[≠] which must be added to any difference of $\int P_w dA$

[†] The probable reason for this variation is discussed in Section 4.5.

[≠] Some tests were also made on a nozzle with a sharp throat, consisting of the junction between two conical sections each of 10 deg. semi-angle. Thus an abrupt change of direction of 20 deg. occurred at the wall. Wall pressure measured immediately after this discontinuity showed approximately 18 deg. of supersonic expansion.

[≠] This additional term amounts to the shaded area in Fig. 42, in relation to which β is defined on page 46.

to give the quantity we require. Thus

$$1-\eta_d = \frac{\left[\int_1^{A_e/A_g} \frac{P_w}{P_t} d\left(\frac{A}{A_g}\right)\right]_{\text{isentropic}}}{C_D \left[\frac{\tilde{F}}{A^* P_t}\right]_{DPR}} - \left\{ \frac{\left[\int_1^{A_e/A_g} \frac{P_w}{P_t} d\left(\frac{A}{A_g}\right)\right]_{\text{measured}}}{C_D \left[\frac{\tilde{F}}{A^* P_t}\right]_{DPR}} - \beta \right\}$$

$$= \frac{\left[\int_1^{A_e/A_g} \frac{P_w}{P_t} d\left(\frac{A}{A_g}\right)\right]_{\text{isentropic}} - \left[\int_1^{A_e/A_g} \frac{P_w}{P_t} d\left(\frac{A}{A_g}\right)\right]_{\text{measured}}}{C_D \left[\frac{\tilde{F}}{A^* P_t}\right]_{DPR}} + \beta .$$

Values of η_d obtained according to this relation are presented in Fig. 25†, β being a function of D.P.R., again computed for a laminar boundary layer at $Re^* = 0{\cdot}75 \times 10^6$. A minimum is reached at D.P.R. close to 4, after which the curve climbs steadily to level off around D.P.R. 10 at a value of η_d in quite good agreement with the expression $(1+\cos\alpha)/2$. Shown also on this Figure are experimental points taken from Fig. 22.

A similar plot of wall pressure distribution is given in Fig. 24 for the 15 deg. nozzles. The circular arc wall contour ends in this case at area ratio 1·070, where the flow has achieved a total turn of 16·8 deg. from sonic. Application of the foregoing relation for η_d produces the curve shown in Fig. 25 for this cone angle, which serves to explain why the measured thrust efficiency of the nozzle with D.P.R. 15 is lower than that for D.P.R. 25.

Also shown on Fig. 25 are values obtained in similar manner for nozzles of 5 deg. cone angle, and the same nominal throat curvature ($r_c = \frac{1}{2}D_g$). These results may be summarised as follows:

TABLE 6

Divergence Losses in Conical Nozzles

α deg.	Flow turn on curved surface (degrees)	$\frac{1-\cos\alpha}{2}$	$(1-\eta_{d,\min})$	A.P.R. for $\eta_{d,\min}$	$\frac{1-\eta_{d,\min}}{\frac{1}{2}(1-\cos\alpha)}$
5	5·9	0·0019	0·0058	3·0	3·05
10	11·0	0·0076	0·0155	4·2	2·04
15	16·8	0·0170	0·0290	6·3	1·70

We see, therefore, that the 'divergence loss' increases by anything up to a factor of 3 as the nozzle is shortened below a critical length, depending on cone angle. As a corollary to this follows the necessity for reducing the angle of nozzles with short divergent sections. In such cases the true picture departs from that shown in Figs. 51 to 53, in which the minimum divergence loss is assumed throughout (as given by Fig. 39).

† Using definition (i) for D.P.R. as given in Appendix V. It should be noted that the nozzle outlet pressure is in general not the same as that corresponding in one-dimensional theory to the area ratio, and the flow leaving the nozzle when operated at this D.P.R. may be either under- or over-expanded.

6.2. *Separation.*

The general pattern of behaviour at other values of A.P.R. at which the nozzle runs full has already been considered in Section 5.2. As an example, results for the D.P.R. 20 nozzle are shown in Figs. 26 and 27. It can be seen from Fig. 27 that the curve of η_F' turns upwards quite close to the design pressure ratio and that the initial rise is very gentle, becoming progressively steeper with reduction of A.P.R. There is a marked contrast here with the data given by other investigators, e.g. Reference 1, which exhibit a form similar to the dotted line shown in the same Figure, the 'kink point' being quite well defined. The reason for this discrepancy is not far to seek, and may be found in the plot of pressure distributions appearing as Fig. 28. This confirms that internal separation is taking place at a value of A.P.R. as high as 16·7, and further shows that the pressure rise through the separation shock is then extremely small. For separation to occur with so low a pressure rise implies that the boundary layer in these tests is laminar.

It is of interest to check the value of Reynolds number based on boundary-layer momentum thickness. If we take separation as occurring near the outlet of this nozzle, we have

$$D = 3{\cdot}4 \text{ in.}$$

$$\frac{4\theta}{D} = 1 - \eta_f \simeq 0{\cdot}003$$

therefore

$$Re_\theta \simeq 760.$$

This is below the critical value of 1000 found by Liepmann[18], working at subsonic speed, for transition on flat or convex surfaces, so that the existence of a laminar boundary layer should perhaps cause no surprise. Denoting by the symbol k the ratio of pressure at incipient separation to that at outlet, we see that this lies close to 0·9 when A.P.R. > 10, which is a familiar value for laminar separation on flat plates. A comparable figure for turbulent flat-plate separation, and for observed separation in nozzles with Re_θ well above 1000, would be around 0·4.

The point is worth noting, although no firm explanation is at present forthcoming, that the value of k in Fig. 28 falls with A.P.R., that is as the separation shock moves further upstream, to a level of 0·5 at A.P.R. = 2. This is very close to the turbulent value for the same condition, although Re_θ can be no greater than about 300. Other manifestations of the same phenomenon have been experienced in another test rig[19], and some discussion appears in Reference 12.

6.3. *Effect of Humidity.*

In order to determine the result of operating a nozzle of this area ratio on undried air, opportunity was taken during conditions of fairly high summer humidity to draw from atmosphere air containing moisture up to 0·011 lb/lb. Fig. 29 illustrates the effect; for a given absolute humidity, the increase in thrust efficiency is effectively independent of A.P.R. at least down to 3. A theoretical treatment of condensation effects presents considerable difficulty, but some calculations have been made based on the simple and rather arbitrary model of a normal shock followed by saturation conditions at $M = 1$, and these suggest that for the conditions of Fig. 29 the onset of condensation will occur at a Mach number around 1·3. The corresponding one-dimensional area ratio is then 1·07, and Fig. 28 shows that the nozzle is still running full beyond that station at a value of A.P.R. as low as 2. Avoidance of a condensation shock and its associated thrust increase under conditions of high humidity seems therefore to demand that separation be complete almost to the throat of the nozzle.

6.4. *Boundary-Layer Transition.*

The existence of a laminar boundary layer in these models at the operating conditions of the rig, of which evidence has been given above, is in the nature of a rather severe handicap. Values of Re^* typical of full-scale flight conditions are around 4×10^6, at which, unfortunately from the performance point of view, the nozzle boundary layer cannot be other than turbulent[12]. This difference has but little significance at the nozzle design-point, since only the frictional momentum loss is affected and, as was shown in Section 5.2, this amounts in many cases to only a fairly small proportion of the total loss.

Furthermore, by comparing Figs. 48 to 50, it can be seen that the increase in Re^* from 0·75 to 4×10^6 tends to compensate for the higher friction in a turbulent system, so that one may be nearer the full-scale answer with a laminar boundary layer at $Re^* = 0{\cdot}75 \times 10^6$ than one would be if transition were brought about at the same Re^*. When, however, the nozzle is operating in a region where separation can take place, the marked difference in separation characteristics between the cases of laminar and turbulent flow imposes a serious limitation on the useful range of the rig unless boundary-layer transition can be promoted.

An attempt to do this was made by introducing, in the nozzle of D.P.R. 20, a region of artificial surface roughening ahead of the throat, following Cook[23]. Silicon carbide powder of No. 150 grade, on a paint base, was thinly spread in a band $\frac{1}{2}$ in. wide around the periphery, the downstream edge of the band being $\frac{1}{2}$ in. from the plane of minimum area. Tests of this method gave encouraging results, in that the object of the exercise appears to be achieved. In Fig. 30 is shown the wall pressure distribution, which may be compared with that of Fig. 28 for the same nozzle without surface roughening. There is not a great difference in the patterns at A.P.R. 2, but at higher A.P.R. it is clear that separation is now following the conventional turbulent pattern, with values of k in the range 0·42 to 0·50, giving a 'kink point' around A.P.R. 10.

In terms of thrust efficiency the result can be seen in Fig. 31. Measured design-point performance ($\eta_{F,\max}$) is now 0·9875, i.e. reduced by 0·25 per cent, as compared with 0·33 per cent difference in the calculated values of momentum loss η_f at $Re^* = 0{\cdot}75 \times 10^6$. At the same time the measurements showed an apparent fall of about 0·10 per cent in C_D. The form of η_F' now corresponds with the dotted curve shown in Fig. 27.

7. *Other Nozzles.*

In addition to the conical nozzles described in the previous Section, certain other types of wholly internal-expansion nozzle have been tested. These may be divided into three categories according to geometry:

(i) axisymmetric

(ii) square section throughout

(iii) rectangular with two parallel sides.

7.1. *Axisymmetric 'Tulip' Nozzles.*

The general form of these nozzles is conveyed by Fig. 32, from which it can be seen that an abrupt discontinuity of wall profile occurs at the throat, followed by a wholly concave divergent portion. In principle the sudden turn at the throat, into which is concentrated the expansion field normally spread over the initially convex divergence of a conventionally contoured nozzle, is limited in the simplest case of a two-dimensional system to half the total Prandtl-Meyer angle corresponding to the design pressure ratio. For an axisymmetric system, the corresponding theoretical limit is nearer one quarter of the total angle. It may, however, be possible to exceed these values somewhat in practice without introducing any very serious losses.

Normal designs of contoured nozzle, with divergence at first convex and subsequently concave, can of course eliminate outlet divergence loss by producing a completely axial flow discharge, but at the cost of excessive length which is reflected in both extra weight and friction loss. Nozzles of 'tulip' form have the potential advantage of also restoring axial flow at outlet with a shorter length than in the former case. Unfortunately the length saving, which is related to the amount of turning concentrated at the throat, is only of real significance when the nozzle D.P.R. is high. For example, the throat turn in an axisymmetric nozzle of D.P.R. 10 could, if limited to 25 per cent of the whole, be only $7\frac{1}{2}$ deg. It is therefore a matter of determining how far the theoretical limit can be exceeded before internal over-expansion losses assume such proportions as to outweigh the reduction in divergence loss. As a further compromise, it would seem desirable to terminate the concave surface of the 'tulip' somewhat prematurely, since the gain to be derived from removing the last few degrees of outlet divergence is insufficient to justify the

length involved. The arbitrary criterion of design adopted here was that the total divergent length should not exceed that of the optimum conical nozzle, taken to have 10 deg. half-angle for D.P.R. $\geqslant 10$, so that the mean divergent surface angle of the 'tulip' must also be around 10 deg. This consideration led to the choice of initial and final divergence angles of 16 deg. and 5 deg. respectively as shown in Fig. 32.

Two nozzle arrangements of nominal D.P.R. 10 and 20 have been tested, using a common throat and initial divergent section. Subsequent concave contours were suggested by Hall[15], consisting of parabolic curves smoothly joining the 16 deg. and 5 deg. portions of straight surface, the equations being as follows:

D.P.R. 10 nozzle.

(i) From $x = 0$, $y = 1$ (throat plane) to $x = 0{\cdot}75$, $y = 1{\cdot}2151$
$$y = 0{\cdot}28675\,x + 1$$

(ii) From $x = 0{\cdot}75$, $y = 1{\cdot}2151$ to $x = 1{\cdot}5$, $y = 1{\cdot}3555$
$$y = -0{\cdot}13283\,x^2 + 0{\cdot}4860\,x + 0{\cdot}92532$$

(iii) From $x = 1{\cdot}5$, $y = 1{\cdot}3555$ to $x = 1{\cdot}8834$, $y = 1{\cdot}3890$ (outlet plane)
$$y = 0{\cdot}0875\,x + 1{\cdot}2242$$

D.P.R. 20 nozzle.

(i) From $x = 0$, $y = 1$ (throat plane) to $x = 1$, $y = 1{\cdot}2868$
$$y = 0{\cdot}28675\,x + 1$$

(ii) From $x = 1$, $y = 1{\cdot}2868$ to $x = 3$, $y = 1{\cdot}6610$
$$y = -0{\cdot}04982\,x^2 + 0{\cdot}3864\,x + 0{\cdot}9502$$

(iii) From $x = 3$, $y = 1{\cdot}6610$ to $x = 3{\cdot}4773$, $y = 1{\cdot}7028$ (outlet plane)
$$y = 0{\cdot}0875\,x + 1{\cdot}3985$$

Table 7 gives the measured C_D and peak thrust efficiency of these nozzles. It appears that the D.P.R. 20 design (with only $5\frac{1}{2}$ deg. more initial expansion than the 25 per cent value) has a performance very similar to that of a 10 deg. conical nozzle (Fig. 21), while the D.P.R. 10 'tulip' nozzle (with $8\frac{1}{2}$ deg. excess turn at the throat) is about 1 per cent worse than its conical counterpart. This behaviour affords a further example of the situation noted in Section 6.1, whereby the adverse effect of a given initial over-expansion is progressively overcome as increased length is provided for recovery. Quite evidently, in the case of the D.P.R. 10 'tulip', the throat turn must be reduced in order to obtain adequate recovery. On the evidence of computer work based on the method of characteristics, Hall[15] has suggested that a reduction from 16 deg. even to 14 deg. may be sufficient to restore the performance to a level around 0·99. A rough guide may therefore be to limit the throat turn to 6 deg. more than the 25 per cent value.

Figs. 34 to 37 show the internal wall pressures down these two 'tulip' nozzles with and without surface roughening ahead of the throat, as described in Section 6.4. It is interesting to note that the pressure immediately after the throat corresponds to a turn of 19·6 deg. from sonic. The approach section of this arrangement has the same local throat curvature as the 'standard' convergent and conical nozzles already described, for which 4 deg. of supersonic expansion was observed to have taken place at the wall of the throat plane. If the same be assumed to occur in this case, the remaining turn of 15·6 deg. matches very closely the 16 deg. physical change of slope at the throat.

In the case of the D.P.R. 10 nozzle when running full, the wall pressure is not far from constant throughout, ending at $P_t/6{\cdot}8$ and thereby confirming that recovery from the initial severe over-expansion is substantially incomplete.

Several features of the separation pressure patterns are worth noting:

(i) There is little difference in the results obtained with and without roughening. The general level of k and the shape of the separation patterns exhibit greater similarity to conventional turbulent behaviour than to laminar. One must therefore consider the possibility that, even without roughening, boundary-layer transition can be promoted at this value of throat Reynolds number by the discontinuity in wall profile at the throat.

(ii) Although the value of C_D is constant for these nozzles down to A.P.R. 2, so that they can be regarded as choked at that condition, it is evident from the pressure plots that below A.P.R. 2·4 the flow pattern around the discontinuity at the throat is not fully established. Recompression apparently commences without the flow having completed the full 16 deg. of abrupt turn.

(iii) For both nozzles the trend is towards a rise of k with increase of A.P.R., contrary to that in conical nozzles with turbulent boundary layer[12]. However, the results at highest A.P.R. probably fall in a regime where the full separation pressure rise does not develop. The last internal tapping in the nozzle of D.P.R. 20 is less than one estimated boundary-layer thickness from the outlet, and in all nozzles with a shock at outlet some compression may be expected to feed up the boundary layer for a distance of this order. As the shock strengthens, the zone of compression or 'foot' of the shock will spread further up the nozzle until the boundary layer just starts to separate in the outlet plane.

(iv) Separation is taking place just inside the D.P.R. 10 nozzle at A.P.R. around 4, and remains near the outlet down to A.P.R. 2·8. At 2·65, however, the nozzle is running almost completely separated, implying a sudden and rapid movement of the shock down the divergent part of the nozzle. Clear reflection of this appears in the behaviour of η_F (Fig. 33). Although tests were only carried out with A.P.R. progressively increasing, it seems probable in the light of other experience that some hysteresis will occur here, the shock travel taking place at a rather lower value when A.P.R. is decreasing.

Comparison between 'tulip' and conical nozzle efficiency measurements must be reviewed in the light of item (i) above, namely that in the former case boundary-layer transition would seem to have occurred without any artificial promotion. Comparable values of $\eta_{F,\max}$ for D.P.R. 20 should therefore be:

10 deg. conical, 0·9875 (roughened, Section 6.4)

Tulip, 0·991 (Table 7)

From this it appears that the 'tulip' design has some small advantage to offer at this D.P.R.; at higher values the superiority should be more pronounced. Full-scale performance will tend to be better than the foregoing figures, as they relate to the worst case of a turbulent boundary layer at low Reynolds number.

TABLE 7

Design-Point Performance of Other Nozzles

Nozzle	C_D (choked)	$\frac{A_e}{A_g}$	Nominal D.P.R.	Outlet divergence angle (deg.)	$\eta_{F,\max}$ †
Axisymmetric 'tulip'	0·985	1·928	10	5	0·980
Axisymmetric 'tulip'	0·985	2·897	20	5	0·991
Square	0·990	1·932	10	10	0·983
Two-dimensional 'tulip'	0·994	3·991	33·5	14	0·989

† Without surface roughening.

7.2. *Two-Dimensional 'Tulip' Nozzle.*

This nozzle had two flat parallel sidewalls, enclosing two profiled walls of constant width. For a D.P.R. of 33·5 the corresponding overall turning angle is 48 deg., and an abrupt turn at the throat was made with the theoretical 50 per cent figure of 24 deg. Thereafter the concave wall contour was designed by the method of characteristics[†]. Further paper studies were carried out to find the optimum balance between friction and outlet divergence, the downstream portion of the contour being cut off in each case at a point of given slope and replaced by a straight line of that slope so as to retain the same outlet area. It was found, with the assumption of a turbulent boundary layer at $Re^* = 4 \times 10^6$, that the highest performance was obtained with a final slope of 6 deg. This geometry gave a computed value of $\eta_{F,\max} = 0{\cdot}994$, based on an integration of outlet flow across the characteristics. In such a nozzle the line-source relation for outlet divergence (Appendix III) is, of course, quite inapplicable.

A very short nozzle length could be achieved if the outlet angle were increased to 14 deg., for which a value of $\eta_{F,\max} = 0{\cdot}990$ was calculated. Rig tests were carried out with this latter geometry, and the results are given in Table 7. If the difference in boundary-layer conditions be allowed for, the computed performance would become 0·991, as against the measured figure of 0·989.

7.3. *Square Nozzle.*

A close relationship exists between this type of nozzle and the conical ones already discussed. Wall contour is the same as in Fig. 20a, but any section through the nozzle now shows a square passage instead of a round. All four walls diverge uniformly after the throat, their centrelines making angles of 10 deg. with the nozzle axis.

Of this family a single example was tested, with nominal D.P.R. 10. The measured value of C_D (Table 7) agrees very well with those obtained from the conical nozzles (Section 6 and Table 5). Peak thrust efficiency was found to be 0·983, without surface roughening. This figure is to be set against a theoretical estimate based on Figure 56 of 0·988, from which it appears that some $\frac{1}{2}$ per cent of thrust is being lost from causes in addition to friction and outlet divergence. To investigate this, wall pressures were examined on one of the four nozzle sides, with three rows of static tappings placed one on the centreline and one symmetrically either side of it fairly near the nozzle corners. Good agreement was obtained between the two corner rows, and the marked difference in centreline and corner behaviour is shown in Fig. 38. Only pressure curves for the nozzle running full were obtained with a laminar boundary layer, the separation patterns corresponding to turbulent state. As can be seen, the running-full characteristics have no similarity: the centreline pressure curve starts with a $9\frac{1}{2}$ deg. turn very like that in a 10 deg. conical nozzle (Table 6), and ends somewhat over-expanded at a pressure of $P_t/11{\cdot}5$; the curve of corner pressure starts with a severe over-expansion equivalent to 16 deg. turn, and ends up under-expanded at $P_t/8{\cdot}2$. Such lack of uniformity suggests that quite considerable cross-flow must be taking place throughout most of the nozzle length, and it may be presumed that what we will term the 'corner loss' arises from this defect.

In comparing a square nozzle with a conical one of the same nominal D.P.R., throat area and wall angle, it must be borne in mind that the square nozzle is shorter. Both have similar wetted surface areas, and hence friction losses, but the divergence loss of the square nozzle is greater (Fig. 39). Taking instead two nozzles of the same length, D.P.R. and throat area, the angle of the round nozzle will now be greater than that of the square, e.g. $11\frac{1}{4}$ deg. compared with 10 deg. Performance losses from friction and divergence combined are now almost identical. The square nozzle will, however, have some 'corner loss' in addition.

8. *Conclusions.*

It is a property of real convergent nozzles with curvature of flow approaching the throat plane that they can, when choked, produce thrust efficiencies based on isentropic convergent thrust which exceed unity. The vacuum thrust efficiency of such nozzles is always greater than unity, and independent of

[†]This design was the work of Dr. J. B. McGarry, 1958.

applied pressure ratio above choking; the gauge thrust efficiency increases from a value near unity at choking pressure ratio to approach the vacuum efficiency at high pressure ratio. This behaviour can occur with either convex or concave curvature of contraction; the effect is less marked in the former case with, as is usual for nozzles having subsequent divergence, a wall profile which becomes axial in the throat plane, but with concave curvature and a necessarily non-axial flow discharge the 'excess' thrust can be as high as 2 per cent. Under the conditions at which this occurs the highest convergent nozzle performance is, of course, still inferior to that obtainable by the use of divergent walls to expand the flow completely.

Nozzle thrust rigs can in general only give an absolute measurement of force, and this measured force is proportional to the product of nozzle discharge coefficient and thrust efficiency. In order to determine either quantity separately it is necessary to fix the other, and airflow calibration is notoriously difficult when high accuracy is required. Certain types of convergent nozzle when choked afford a ready and satisfactory means of calibrating the air meter in a nozzle thrust rig. For this purpose it is necessary to choose a nozzle having a very high value of the product 'discharge coefficient × thrust efficiency', which restricts the field to nozzles of convex curvature and zero wall slope at outlet. Fairly sharp curvature is desirable, and a value for the above product of 0·99 has been obtained using a nozzle with nominal radius of curvature equal to the throat radius. For comparison, the figure for the nozzle with concave curvature and high 'excess' thrust is only about 0·96.

A convergent nozzle with convex curvature such as that recommended above is found to choke, by which term it is meant that the flow field in the throat plane becomes 'frozen' and the discharge coefficient constant, at a value of applied pressure ratio which corresponds to the maximum Mach number achieved in the throat, this occurring at the wall. In the nozzle with radius of curvature equal to throat radius, a value of 1·21 was obtained for wall Mach number close to the outlet, with 0·85 on the centreline.

From an analysis of the losses deriving from friction and curvature in a choked convergent nozzle of suitable design, it is possible to isolate the four constituents in the measured product 'discharge coefficient × thrust efficiency': namely, the separate flow deflects from friction and curvature and (taking vacuum thrust) the corresponding thrust increments. This can be done by considering the extreme limits between which the discharge coefficient can move, corresponding to the two conditions of zero friction and zero curvature. It is found that these limits are in fact quite close, no further than 0·4 per cent apart in the examples taken. In consequence the certainty with which the discharge coefficient can be placed within these limits is as good as $\pm 0{\cdot}1$ per cent.

The nozzle thrust rig here described is thought to be capable of measuring the above product to an accuracy of $\pm 0{\cdot}1$ per cent; hence the overall accuracy in determination of either discharge coefficient or thrust efficiency individually should be around $\pm 0{\cdot}2$ per cent.

During the foregoing analysis of losses, it becomes clear that the flow defect from curvature is appreciably less than is given by certain theoretical predictions for this rather sharp nominal curvature. Examination of wall pressures in the neighbourhood of the throat enables the variation in boundary-layer displacement thickness to be calculated, and it appears that the curvature of the displacement boundary is considerably less sharp than that of the physical wall. Regarding this larger radius of curvature as being the effective value for the bulk of the flow, the corresponding theoretically predicted flow defect is found to be in much better agreement with that derived from the experimental data.

Operating conditions in this rig produce a value of nozzle throat Reynolds number $= 0{\cdot}75 \times 10^6$, at which level the nozzle boundary layer is normally found to be laminar. Boundary-layer transition can be promoted by the addition of some surface roughening upstream of the nozzle throat.

Experimental figures for the design-point performance of a series of conical convergent-divergent nozzles agree well with estimates based on the calculation of losses arising from friction and outlet divergence, so long as the divergent portion of any nozzle is above a certain length. This minimum length varies with cone angle and probably throat curvature, and is associated with the initial rapid and local over-expansion taking place on the wall as the flow turns through the half-cone angle after the throat. Recovery from this over-expansion is gradual, and, if the nozzle divergent walls end before the recovery process is complete, there will be a loss in thrust on those walls which exceeds the minimum loss appropriate to the particular cone angle. For example, with 10 deg. half-angle this recovery is not substantially

complete in a nozzle of design pressure ratio less than 10, and in the case of 15 deg. half-angle the corresponding figure is as high as 20. In nozzles of design pressure ratio lower than these values, it is found that the 'divergence loss' obtained from wall pressure distribution can reach a maximum which is 2 to 3 times the loss calculated according to the simple model of point-source flow.

When estimating thrust from a curve of divergent wall pressure distribution, allowance for friction must be made. The amount of this correction exceeds the loss from friction experienced on a rig measuring convergent-divergent nozzle thrust directly. In the latter case only the 'momentum loss' is involved, whereas an additional quantity, the 'displacement loss', must be deducted from an integration of wall pressure distribution. These losses are so termed since they are associated with and may be computed from knowledge of the boundary-layer momentum and displacement thicknesses. Curves of these quantities are presented from calculations covering the cases of conical, square and two-dimensional nozzles with both turbulent and laminar boundary layers, for various values of throat Reynolds number and design pressure ratio.

A level of peak thrust efficiency around 0·990, based on fully-expanded isentropic thrust for the same mass flow, has been measured for conical convergent-divergent nozzles of half-angle 10 deg. over the range of design pressure ratio 10 to 25 (area ratio 2 to $3\frac{1}{2}$). It is thought that this value of cone angle is about the practical optimum. This level of design-point performance was obtained with a laminar boundary layer at a nozzle throat Reynolds number of $0{\cdot}75 \times 10^6$; in full-scale equipment the level would be slightly lower.

When operated at atmospheric inlet conditions and a humidity around 0·01 lb/lb, a nozzle of design pressure ratio 20 (area ratio 3) gives 2 per cent excess thrust as a result of condensation.

Investigation of some axisymmetric 'tulip' nozzles, with abrupt turn at the throat and concave divergent walls, has shown that for a design pressure ratio of 20, the 'tulip' shape offers in the same length slightly better peak performance than a 10 deg. conical nozzle. This advantage, amounting to around $\frac{1}{4}$ per cent, disappears at lower design pressure ratio and should increase at higher. Such a trend may be explained in terms of the total supersonic expansion angle; as this increases, more expansion can usefully be concentrated in the sharp turn at the throat. At design pressure ratio 20, it is necessary in order not to exceed the conical nozzle length for the throat turn to be made greater than the theoretical limit, and for some outlet divergence to be retained.

A nozzle of square section throughout, having uniform divergence on all four walls, suffers an additional loss of some $\frac{1}{2}$ per cent over and above the losses from friction and outlet divergence. Pressures across a wall at any station are markedly non-uniform, and the extra loss is attributed to the existence of cross-flow. No significant loss from this source appears to arise in a properly two-dimensional nozzle with flat sidewalls.

REFERENCES

No.	Author(s)	Title, etc.
1	P. F. Ashwood, G. W. Crosse and J. E. Goddard	Measurements of the thrust produced by convergent-divergent nozzles at pressure ratios up to 20. A.R.C. C.P. 326. November, 1956.
2	B. S. Stratford and J. C. Ascough	A recent attempt at accurate airflow measurement by pitot-static traverse. Paper A.6. Symposium on flow measurement in closed conduits. September, 1960.
3	B. S. Stratford	The calculation of the discharge coefficient of profiled choked nozzles and the optimum profile for absolute airflow measurement. *Jour. R. Aero. Soc.* Vol. 68, No. 640, p. 237–245. April, 1964.
4	T. E. Stanton	The flow of gases at high speeds. *Proc. Roy. Soc.* Series A. Vol. 111, p. 306. 1926.
5	G. I. Taylor	The flow of air at high speeds past curved surfaces. A.R.C. R. & M. 1381. 1930.
6	B. S. Stratford and G. S. Beavers	The calculation of the compressible turbulent boundary layer in an arbitrary pressure gradient – a correlation of certain previous methods. A.R.C. R. & M. No. 3207. September, 1959.
7	A. D. Young	Skin friction in the laminar boundary layer in compressible flow. *The Aeronautical Quarterly.* Vol. 1, p. 137. August, 1949.
8	E. W. E. Rogers and Miss B. M. Davis	A note on turbulent boundary-layer allowances in supersonic nozzle design. A.R.C. C.P. 333. June, 1956.
9	M. Tucker	Approximate calculation of turbulent boundary-layer development in compressible flow. N.A.C.A. TN. 2337. April, 1951.
10	N. Curle	The steady compressible laminar boundary layer, with arbitrary pressure gradient and uniform wall temperature. *Proc. Roy. Soc.* Series A. Vol. 249, p. 206. January, 1959.
11	A. D. Young	The calculation of the profile drag of aerofoils and bodies of revolution at supersonic speeds. A.R.C. 15970. April, 1953.
12	M. V. Herbert and R. J. Herd	Boundary-layer separation in supersonic propelling nozzles. A.R.C. R. & M. 3421. August, 1964.
13	E. M. Landsbaum	Thrust of a conical nozzle. *Journal A.R.S.* Vol. 29, p. 212. March, 1959.
14	D. M. Hall and G. C. Griffiths	A theoretical investigation into the aerodynamic performance of conical nozzles with a sharp corner at the throat. Bristol Siddeley Engines Ramjet Report 3327. May, 1961.

REFERENCES (*continued*)

No.	*Author(s)*	*Title, etc.*
15	D. M. Hall	Private communication. 1962.
16	I. M. Hall	Transonic flow in two-dimensional and axially-symmetric nozzles. *Quarterly Journal of Mechanics and Applied Mathematics.* Vol. XV, No. 4, p. 487–508. November, 1962. A.R.C. 23347. December, 1961.
17	R. E. Smith and R. J. Matz	A theoretical method of determining discharge coefficients for venturis operating at critical flow conditions. A.S.M.E. Paper No. 61-WA-211. 1962. *Journal Basic Engineering.* Vol. 84, Series D No. 4, p. 434. 1962.
18	H. W. Liepmann	Investigations on laminar boundary-layer stability and transition on curved boundaries. N.A.C.A. A.C.R. No. 3H30. August, 1943, and Investigation of boundary-layer transition on concave walls. N.A.C.A. A.C.R. No. 4J28. February, 1945.
19	G. T. Golesworthy and M. V. Herbert	The performance of a conical convergent-divergent nozzle with area ratio 2·9 in external flow. A.R.C. C.P. 891. November, 1963.
20	J. Hilsenrath *et al*	*Tables of thermodynamic and transport properties.* Pergamon Press. 1960.
21	J. C. Ascough	Real air effects in propelling nozzles. A.R.C. 28513. September, 1966.
22	S. Glasstone	*Thermodynamics for chemists* (page 114). Van Nostrand, New York. 1947.
23	T. A. Cook	Some supersonic wind tunnel tests on the fixing of boundary-layer transition using distributed roughness bands. R.A.E. (Bedford) Tech. Note Aero. 2772. July, 1961.

APPENDIX I

Nozzle definitions

A.P.R. = applied pressure ratio $= \dfrac{\text{nozzle entry total pressure}}{\text{base pressure}}$

D.P.R. = design pressure ratio, which can have three alternative meanings (*see* Appendix V):

(i) the pressure ratio corresponding in one-dimensional theory to the effective area ratio of the nozzle.

(ii) the pressure ratio at which the gross gauge thrust efficiency η_F based on A.P.R. is a maximum.

(iii) the pressure ratio at which the flow is fully expanded – i.e. nozzle outlet pressure = base pressure.

C_D = discharge coefficient $= \dfrac{\text{measured air mass flow}}{\text{isentropic air mass flow for the same throat area at the same total pressure and total temperature}}$

η_F = gross gauge thrust efficiency (variable geometry)

$= \dfrac{\text{measured gauge thrust at a given pressure ratio}}{\text{gauge thrust of an isentropic nozzle, passing the same flow at the same pressure ratio, when fully expanded}}$

η_F' = gross gauge thrust efficiency (fixed geometry: convergent-divergent)

$= \dfrac{\text{measured gauge thrust at a given pressure ratio}}{\text{gauge thrust of an isentropic nozzle, passing the same flow at the same pressure ratio, and having the same D.P.R.}^{\dagger}\text{ as the actual nozzle}}$

$\eta_{F,\text{conv}}$ = gross gauge thrust efficiency (fixed geometry: convergent)

$= \dfrac{\text{measured gauge thrust of convergent nozzle at a given pressure ratio}}{\text{gauge thrust of an isentropic convergent nozzle, passing the same flow at the same pressure ratio}}$

$\eta_{S,\text{conv}}$ = gross vacuum thrust efficiency (fixed geometry: convergent)

$= \dfrac{\text{measured vacuum thrust of convergent nozzle}}{\text{vacuum thrust of isentropic convergent nozzle, passing the same flow}}$

$k = \dfrac{\text{pressure at incipient separation}}{\text{base pressure}}$

X = equivalent flat plate length

= the length of flat plate over which a boundary layer growing at a constant Mach number equal to the actual local Mach number would attain the same thickness as the actual local boundary layer

Notes on definitions of thrust efficiency.

(i) 'Thrust'—by this is meant the internal thrust produced by the nozzle.

(ii) 'Pressure ratio'—in the present work this is usually taken as A.P.R. (*see* Section 5.1), but it is possible to use as reference any other expansion pressure ratio (e.g. P_t/P_∞); the value of thrust efficiency will then depend on the reference pressure ratio.

---

†Using definition (i) above.

APPENDIX II

Notation

The chief symbols used are listed below, others being defined where they occur in the text.

A	Cross-sectional area
C_D	Discharge coefficient or flow efficiency (*see* Appendix I)
D	Diameter
F	Gauge thrust
$\tilde{F}$	Isentropic momentum thrust $= \frac{Qv'}{g}$
G	A function
H	Boundary-layer shape parameter $= \frac{\delta^*}{\theta}$
k	Separation pressure ratio (*see* Appendix I)
M	Mach number
P or P_s	Static pressure
P_t	Total pressure
P_a	Atmospheric pressure
P_w	Nozzle wall pressure
P_∞	Free stream static pressure
Q	Mass flow
R, r	Radius
r_c	Radius of curvature
Re	Reynolds number
S	Vacuum thrust
T_t	Total temperature
T_s	Static temperature
v	Velocity
x	Surface length for boundary-layer growth
α	Nozzle divergence half-angle
β	Frictional displacement loss
γ	Ratio of specific heats
δ	Boundary-layer thickness
δ^*	Boundary-layer displacement thickness
η_d	Divergence loss factor

η_f	Frictional momentum loss factor
η_F	Gauge thrust efficiency } see Appendix I
η_S	Vacuum thrust efficiency } see Appendix I
η_v	Velocity efficiency
θ	Boundary-layer momentum thickness
κ	Air meter form factor
λ	Curvature factor
μ	Air viscosity
ρ	Air density
σ	Throat aspect ratio of two-dimensional nozzle
$X, Y, Z, W_n, W_p, W_s, W_w$	Forces on thrust rig (*see* Fig. 3)
A_o, P_c, P_{pl}	Quantities associated with thrust rig (*see* Fig. 3)

Suffices, etc.

$_b$	Nozzle base
$_c$	Curvature effect
$_e$	Convergent-divergent nozzle exit
$_f$	Friction effect
$_g$	Geometric throat
$_*$	Isentropic throat
$_'$	Isentropic

APPENDIX III

Losses from Nozzles with Divergent Flow at Outlet

In a nozzle with a constant divergence angle, the loss resulting from non-axial direction of the flow at outlet can be estimated by assuming symmetry of flow from a point or line-source. Conditions at outlet are thus regarded as being uniform across a section whose surface is respectively either spherical or cylindrical. In general, if the divergent portion of the nozzle is long enough, the flow will fairly approximate to this state, and the representation is useful in providing a quite close approximation to the performance loss. Notable exception can occur with a nozzle having very little or very rapid divergence (*see* Section 6.1), and the design of throat contour can have an appreciable effect in such cases.

Treating for convenience the effects of friction and divergence in isolation, consider a nozzle with zero thickness of boundary layer throughout. Taking $A_{e,p}$ as the area of the outlet plane, and $A_{e,s}$ as the

area of the curved isobaric surface as above, it can be shown (e.g. Reference 13) that, at any operating pressure ratio at which the nozzle runs full, the axial component of outlet thrust is equal to

$$\eta_d \frac{Qv_e}{g} + A_{e,p}(P_e - P_\infty)$$

or

$$\eta_d \left\{ \frac{Qv_e}{g} + A_{e,s}(P_e - P_\infty) \right\}$$

where the divergence loss factor $\eta_d = \frac{A_{e,p}}{A_{e,s}}$. It is then obvious that the effective area ratio of the nozzle is given by $\frac{A_{e,s}}{A^*}$ $\left(= \frac{1}{\eta_d} \frac{A_{e,p}}{A^*}\right)$. Hence the equivalent fixed geometry ideal nozzle, in which the flow is presumed to be one-dimensional with no outlet divergence, must have the same area ratio $\frac{A_{e,s}}{A^*}$. Its thrust will then amount to

$$\frac{Qv_e}{g} + A_{e,s}(P_e - P_\infty).$$

Thus we obtain the result that, throughout the range in which a nozzle runs full, the thrust defect from outlet divergence is a constant proportion $(1 - \eta_d)$ of the thrust of the ideal fixed geometry nozzle.

In the case of a nozzle with uniform conical divergence of semi-cone angle α, the divergence loss factor is

$$\eta_d = \frac{1 + \cos\alpha}{2}.$$

A two-dimensional nozzle, which has two parallel walls and the other two of constant width and diverging uniformly with a half-angle α gives

$$\eta_d = \frac{\sin\alpha}{\alpha}.$$

A square nozzle in which all four walls have uniform and equal divergence, and whose centrelines each make an angle α with the axis of the nozzle, has a divergence loss factor

$$\eta_d = \left(\frac{\sin\alpha}{\alpha}\right)^2.$$

These relations are plotted in Fig. 39.

Some indication of the influence of throat geometry is given by Hall in Reference 14. This deals with conical nozzles with an abrupt discontinuity of curvature in the throat plane, formed by the junction of a circular arc approach section with the divergent cone. Hall's analysis, by the method of characteristics, suggests that successive reflections of weak shocks, originating from the flow pattern in the neighbourhood of the throat, can result in a net loss of thrust which varies considerably with nozzle length for a given cone angle, the flow being assumed frictionless. Once beyond the region of initial over-expansion near the throat, a length is reached giving minimum loss, which then conforms very closely to η_d as given above. It seems, therefore, that nozzles with smooth throat contour should, provided they are not too short, be adequately described by the foregoing relations.

In comparing the different levels of η_d in Fig. 39, it must be remembered that, in order to achieve the same change of nozzle area in the same length, as would be of interest in practice, it is necessary to vary the divergence angle with nozzle geometry. The resulting values of α will in fact be greatest for the two-dimensional shape and least for the square, which is in the order required to offset the differences between the curves of η_d.

APPENDIX IV

Estimation of the Boundary-Layer Growth in a Nozzle

The measure of assistance afforded by Dr. B. S. Stratford in formulating the treatment is gratefully acknowledged.

1. *General.*

The following conventional assumptions are made:

(i) The static pressure is constant throughout the boundary layer in a plane normal to the nozzle wall at any station.

(ii) In the case of axisymmetric flow, the boundary layer is assumed to be identical to one having the same thickness on a flat surface.

(iii) Outside the boundary layer the flow is isentropic, with $\gamma = 1{\cdot}4$.

(iv) The boundary layer is always thin by comparison with the total flow area, so that second order terms can be neglected. This implies that the treatment is limited to conditions where the momentum and flow defects are small proportions.

In comparing the thrust of an actual nozzle having no losses besides friction with its isentropic counterpart, we use a momentum loss factor defined as

$$\eta_f = \frac{\text{actual momentum thrust}}{\text{isentropic momentum thrust for same mass flow}}$$

it being assumed that the same static pressure and mainstream velocity exist at outlet from both nozzles – which is to say that the outlet area of the actual nozzle is greater than that of the isentropic by an amount corresponding to the displacement thickness. The first object of the present argument is to obtain the relationship between η_f and momentum thickness at any station where these conditions apply.

Now, in general across any section:

$$\eta_f = \frac{\int \rho v^2 \, dA}{\rho_i v_i^2 A_i}$$

where suffix i denotes isentropic stream conditions.

From continuity we have:

$$\int \rho v dA = \rho_i v_i A_i$$

Hence

$$1 - \eta_f = \int \left(1 - \frac{v}{v_i}\right) \frac{\rho v dA}{\rho_i v_i A_i}. \tag{A1}$$

Referring to Figs. 40 and 41, consider first the case of axial symmetry. From Fig. 40a,

$$\begin{cases} dA = \pi(D-2y)dy \\ A_i = \dfrac{\pi}{4}D_i^2 = \dfrac{\pi}{4}(D-2\delta^*)^2. \end{cases}$$

Thus equation (A1) becomes

$$1-\eta_f = 4\int_0^{\delta}\left(1-\frac{v}{v_i}\right)\frac{\rho v}{\rho_i v_i}\cdot\frac{(D-2y)}{(D-2\delta^*)^2}\cdot dy.$$

Within the range $0<y<\delta$, it is in line with our assumptions to write

$$\frac{(D-2y)}{(D-2\delta^*)^2} \simeq \frac{1}{D}$$

whence

$$1-\eta_f = \frac{4}{D}\int_0^{\delta}\left(1-\frac{v}{v_i}\right)\frac{\rho v}{\rho_i v_i}\cdot dy$$

$$= \frac{4\theta}{D} \text{ by definition.} \tag{A2}$$

In the case of two-dimensional flow (Fig. 40b),

$$\begin{cases} dA = 2(D+B-4\bar{y})d\bar{y} \\ A_i = D_i B_i = DB-2(D+B)\bar{\delta}^* \end{cases}$$

where $\bar{y}$ relates to an assumed uniform mean boundary-layer thickness on all four walls, with properties $\bar{\delta}^*$ and $\bar{\theta}$.
Thus equation (A1) gives:

$$1-\eta_f = 2\int_0^{\bar{\delta}}\left(1-\frac{v}{v_i}\right)\frac{\rho v}{\rho_i v_i}\cdot\left\{\frac{D+B-4\bar{y}}{DB-2(D+B)\bar{\delta}^*}\right\}d\bar{y}$$

Putting

$$\frac{D+B-4\bar{y}}{DB-2(D+B)\bar{\delta}^*} \simeq \frac{D+B}{DB}$$

we get

$$1-\eta_f = \frac{2(D+B)}{DB}\cdot\bar{\theta}\,. \tag{A3}$$

This reduces to $4\theta/D$ when $D/B = 1$, which is the same expression as for axisymmetric flow.

The foregoing relations are quite general, and equations (A2) and (A3) can be applied at any station. In the particular case considered in Section 4.3, that is to say the throat plane of an axisymmetric convergent nozzle, we have seen that

$$1-\eta_f = \frac{4}{D_g}\theta.$$

A comparable expression may be obtained for C_D in terms of δ^*. By definition:

$$\begin{cases} C_D = \dfrac{A_i}{\int dA} \\ \delta^* = \displaystyle\int_0^{\delta} \left(1-\frac{\rho v}{\rho_i v_i}\right) dy. \end{cases}$$

As in the foregoing analysis for η_f we shall write

$$\frac{dA}{A_i} \simeq \frac{4dy}{D_g}$$

Hence

$$\begin{aligned} \delta^* &= \frac{D_g}{4}\int \left(1-\frac{\rho v}{\rho_i v_i}\right)\frac{dA}{A_i} \\ &= \frac{D_g}{4}\left\{ \frac{\int dA}{A_i} - \frac{\int \rho v dA}{l_i v_i A_i} \right\} \\ &= \frac{D_g}{4}\ \frac{1}{C_D} - 1. \end{aligned}$$

When $1-C_D \ll 1$, this becomes

$$1-C_D \simeq \frac{4}{D_g}\delta^*$$

and we obtain

$$\frac{\delta^*}{\theta} = \frac{1-C_D}{1-\eta_f} \qquad \text{(A4)}$$

When it comes to evaluating the friction loss in the divergent section of a supersonic nozzle, the further assumption is made that zero boundary-layer thickness exists at the throat. This is clearly inconsistent with equation (A4) for a convergent nozzle, and some examination is required to justify the use of such an assumption. Data based on calculations for some typical conditions are given in the following pages.

Next, consider the case where it is required to obtain the thrust of a nozzle from measurements of pressure along the walls. We are then concerned with the area under a curve relating surface pressure to area of walls projected along the axis of flow. The argument in the case of a nozzle running full will be presented with reference to Fig. 42, which is a graph of this nature. In accordance with assumptions already stated, it can be seen that pressures at corresponding stations in the actual and isentropic nozzles are the same, but that the area of the actual nozzle is always greater than that of the isentropic by the boundary-layer displacement thickness. Both nozzles are taken to be identical and frictionless up to

the throat (*see* above). Now, the area under the 'isentropic' curve in Fig. 42 must give a thrust corresponding to the value of $\eta_f = 1$. It therefore follows that the thrust of the actual nozzle with $\eta_f < 1$ must relate to some curve beneath the isentropic, the area difference amounting to the loss $(1-\eta_f)$. But we have already seen that the curve of measured wall pressures does in fact lie above the isentropic, as shown in the Figure. In order, therefore, to obtain thrust from pressure measurements, it is necessary to deduct an allowance for friction made up of two components, *viz*:

(i) the quantity $(1-\eta_f)$, termed the 'momentum loss';

(ii) an amount given by the difference in area between the two curves in Fig. 42, termed the 'displacement loss'.

This argument may be restated as follows, using the prime to denote conditions in an isentropic nozzle designed for the same expansion. Axial force on divergent walls of actual nozzle is

$$F_e - F_g = \int_{A_g}^{A_e} (P_w - P_\infty) dA - \int \tau dA_s$$

where $\begin{cases} \tau = \text{shear stress at wall} \\ A_s = \text{wall surface area} \end{cases}$

and $$F_e = \frac{Qv_e}{g} + A_e(P_e - P_\infty)$$

while corresponding force on isentropic nozzle is

$$F_e' - F_g = \int_{A_g}^{A_e'} (P_w' - P_\infty) dA$$

where $$F_e' = \frac{Qv_e'}{g} + A_e'(P_e - P_\infty).$$

Now we know

$$\frac{Qv_e}{g} = \eta_f . \frac{Qv_e'}{g}.$$

Hence, from the above relations, the total effect of friction to be deducted is

$$\int \tau dA_s = \{\beta + (1-\eta_f)\} \tilde{F}_e$$

where $$\beta . \tilde{F}_e = \int_{A_g}^{A_e} P_w dA - \int_{A_g}^{A_{ev}} P_w' dA - P_e(A_e - A_e')$$

$$= A_g P_t \text{ [shaded area in Fig. 42]}.$$

The quantity β is the 'displacement loss' and may be obtained from knowledge of the boundary-layer displacement thickness.

Taking first the case of an axisymmetric or square nozzle, and assuming $A_g = A^*$, we can say at any station:

$$\frac{A'}{A} = \left(1-\frac{2\delta^*}{D}\right)^2$$

where the prime is again used to denote isentropic values, whence

$$\frac{\Delta A}{A'} = \frac{A-A'}{A'} \simeq \frac{4\delta^*}{D}. \tag{A5}$$

Therefore

$$\frac{\Delta A}{A^*} = \frac{4\delta^*}{D}\cdot\frac{A'}{A^*}.$$

Secondly, treating a two-dimensional nozzle as before, we get

$$\frac{A'}{A} = \frac{(D-2\bar{\delta}^*)(B-2\bar{\delta}^*)}{DB}.$$

Hence

$$\frac{\Delta A}{A'} \simeq 2\frac{(D+B)}{DB}\bar{\delta}^*. \tag{A6}$$

There is symmetry between equations (A2) and (A5), and between equations (A3) and (A6), so that for all forms of nozzle considered the same relation holds:

$$\frac{\Delta A}{A^*} = \frac{\delta^*}{\theta}(1-\eta_f)\frac{A'}{A^*}.$$

Now the 'displacement loss' β has been defined above in relation to Fig. 42 as

$$\beta = \frac{\int_{P_e/P_t}^{P_s^*/P_t} \frac{\Delta A}{A^*} d\left(\frac{P_w}{P_t}\right)}{\frac{\tilde{F}_e}{A^*P_t}} \tag{A7}$$

which therefore gives

$$\beta = \frac{\int_{P_e/P_t}^{P_s^*/P_t} \frac{\delta^*}{\theta}(1-\eta_f)\frac{A'}{A^*} d\left(\frac{P_w}{P_t}\right)}{\frac{\tilde{F}_e}{A^*P_t}} \tag{A8}$$

where $\left(\frac{A'}{A^*}\right)$, $\left(\frac{P_w}{P_t}\right)$ and $\left(\frac{\tilde{F}_e}{A^*P_t}\right)$ are functions of M. In the calculations one-dimensional relations have been used.

2. *Turbulent Boundary Layer.*

A one-seventh power law is assumed for the velocity profile.

For a flat plate in uniform flow conditions the boundary-layer thickness δ is effectively independent of Mach number (*see*, for instance, References 6 and 8). We can therefore consider the classical relation for incompressible flow

$$\delta = 0{\cdot}37x.Re_x^{-\frac{1}{5}}$$

which may be compared with an equivalent expression derived from Reference 9,

$$\delta = 0{\cdot}157x.Re_x^{-\frac{1}{7}}.$$

These both give substantially the same result at values of Re_x around 10^6 (Reference 8), but a general preference exists for the lower exponent of Re_x in this range[6], which we shall accordingly adopt.

When dealing with expanding flow in nozzles, two additional effects must be included: first, the favourable pressure gradient, which can be considered as acting along a two-dimensional surface of constant width; and second, the possible divergence of the surface in the presence of the same Mach number distribution. Supposing that appropriate factors can be applied to the above form of expression, ε for divergence and I_t for pressure gradient, we have

$$\delta = 0{\cdot}37\varepsilon I_t x.Re_x^{-\frac{1}{5}} \tag{A9}$$

where x is now the distance measured along the nozzle contour.

In the case of the correction for divergence, no direct experimental evidence can be produced; for the diverging sidewalls of two-dimensional nozzles, where pronounced secondary flows can occur, Rogers[8] is content to accept that no allowance is worth making. Over a small interval of growth a fair theoretical approach is as follows. Consider a uniform non-diverging passage with a specified pressure gradient, and a diverging passage with the same pressure gradient and length and the same total wetted surface area, the initial boundary-layer thickness being zero in each case. Since the wetted areas are equal the friction drags must be equal, and hence the cross-sectional area of boundary layer leaving the passage must be the same for each. It therefore follows that the boundary-layer thicknesses are inversely proportional to the outlet perimeters, whence for the diverging passage:

$$\varepsilon = \frac{\text{mean perimeter}}{\text{exit perimeter}}.$$

An approximate correcton of this sort is used, for instance, by Tucker[9] for increments of radial flow. Its validity when applied to the whole divergent length of a nozzle is less obvious, but calculations for a particular series of conical nozzles by the method of Reference 6 have in fact shown it to be a very close approximation up to Mach number 2·5 and quite acceptable up to 3.

It is not possible to formulate a general relation for the effect of favourable pressure gradient comparable to the simple treatment of divergence given above. But some idea of how the factor I_t behaves can be deduced from experimental data given in the survey of Reference 8, for two-dimensional expansion surfaces of constant width ($\varepsilon = 1$). Rogers (Fig. 5 of Reference 8) presents a wide range of results in terms of $\frac{\Delta\delta}{l}$ and Re_l, to which we have applied the relation

$$\Delta\delta = 0{\cdot}37I_t l\ Re_l^{-\frac{1}{5}}$$

where

$\Delta\delta$ = boundary-layer growth from throat to run-out

l = distance along nozzle from throat to run-out.

The resulting values of I_t are shown in Fig. 43 as a function of M. Rather considerable scatter is exhibited at the higher Mach numbers, which may be associated with differences in the steepness of pressure gradient, i.e. the Mach number achieved in a given measure of length. It is this variation which must make any estimate of boundary-layer effects in nozzles in general only approximate at best. For accuracy it is clearly necessary to consider any particular shape individually and use a treatment such as Reference 6. Some calculations by this method (which assumes zero heat transfer to the walls) have been made in order to examine how appropriate is the mean line drawn on Fig. 43 to the nozzles with which we are mainly concerned in the present work. These are axisymmetric, with a throat profile given by $r_c = \frac{1}{2}D_g$, followed by a conical divergence of 10 deg. semi-angle, and the measured pressure distribution along the wall has been taken. Values of δ computed at various stations along such a nozzle according to the relation[6]

$$\delta = 0{\cdot}37X.Re_X^{-\frac{1}{5}} \tag{A10}$$

where X is the 'equivalent flat plate length', defined by

$$X = \frac{1}{P'r^{1{\cdot}25}}\int_0^x P'r^{1{\cdot}25}dx$$

and

$$P' = \left(\frac{M}{1+0{\cdot}2M^2}\right)^4$$

were compared with equation (A9), giving

$$I_t = \frac{1}{\varepsilon}\left(\frac{X}{x}\right)^{0{\cdot}8}$$

In both cases the boundary-layer thickness was taken as zero at the throat. Substituting for ε the relation already verified, the dotted line in Fig. 43 was obtained, which falls quite satisfactorily amongst the experimental data. It seems, therefore, that a factor I_t of this form may be justified for a generalised treatment.

Applying the relation for compressible flow

$$\frac{\theta}{\delta} = 0{\cdot}097(1+0{\cdot}1M^2)^{-\frac{5}{7}}$$

we then obtain:

$$\theta = 0{\cdot}036\varepsilon I_t x.Re_x^{-\frac{1}{5}}(1+0{\cdot}1M^2)^{-\frac{5}{7}} \tag{A11}$$

The corresponding expression for displacement thickness will be[6]:

$$\delta^* = 0{\cdot}046\varepsilon I_t x.Re_x^{-\frac{1}{5}}(1+0{\cdot}8M^2)^{\frac{3}{7}} \tag{A12}$$

At this point let us examine the effect of throat boundary-layer thickness on the growth down the divergent portion. Now, at a given station in any particular nozzle, M and r are independent of variations in boundary-layer thickness to a first order, whence, for fixed entry conditions of P_t and T_t, the boundary-layer thickness calculated according to equation (A10) depends only on the term $\left[\int P'r^{1{\cdot}25}dx\right]^{\frac{4}{5}}$.

Calling this integral inside the bracket N, we have

$$[N]_0^{x_e} = [N]_0^{x^*} + [N]_{x^*}^{x_e}$$

or

$$N_e = N^* + \Delta N$$

where ΔN is the growth of the integral between throat and nozzle exit, which is unaffected by the nature of any assumption regarding N^*. Hence the boundary-layer thickness at exit is proportional to

$$(N^* + \Delta N)^{\frac{4}{5}}.$$

Taking by way of example the same shape of axisymmetric nozzle as was considered above, with stagnation entry conditions of 1 atm and 300 deg. K, and throat diameter 2 in., let us see the effect of assuming in turn the following conditions in the throat:

(i) $\theta = 0$, hence $N^* = 0$

(ii) $\theta = 0{\cdot}001$ inches. From equation (A2) this would correspond to a local velocity efficiency of 0·998. It is found that this gives $N^* = 0{\cdot}147$.

Now the value of N_e clearly depends on the outlet Mach number of the nozzle, and we will consider $M_e = 2{\cdot}6$ (area ratio 2·9). For this $\Delta N = 9{\cdot}10$. Hence the two cases above give values of boundary-layer thickness at exit proportional to

(i) $(N_e)^{\frac{4}{5}} = (9{\cdot}10)^{\frac{4}{5}} = 5{\cdot}851$

(ii) $(N_e)^{\frac{4}{5}} = (9{\cdot}10 + 0{\cdot}147)^{\frac{4}{5}} = 5{\cdot}927$

from which the error introduced by taking $N^* = 0$ can be seen to be only 1·3 per cent. For nozzles of smaller area ratio this error will increase, and be reduced for nozzles of greater area ratio. But such magnitudes are insignificant against the general accuracy of this treatment.

An interesting comparison may be made between this result and the factor by which the boundary-layer thickness increases from throat to outlet in case (ii) above. The appropriate figures are:

Boundary-layer thickness	At throat (in.)	At outlet (in.)	Ratio $\frac{\text{outlet}}{\text{throat}}$
δ	0·0110	0·0753	6·85
δ^*	0·00177	0·0223	12·60
θ	0·00100	0·00512	5·12

Even in the case of δ^* where the ratio of growth is largest, the throat thickness amounts to about 8 per cent of that at outlet – a figure considerably higher than the error introduced by neglecting throat thickness altogether. To put it another way, the momentum efficiency of the divergent section is, from equation (A2), effectively 0·994 regardless of whether the efficiency at the throat is taken as 0·998 or 1·0.

3. *Laminar Boundary Layer.*

An accurate expression for the boundary-layer momentum thickness in laminar flow, taking account of pressure gradient but with no radial divergence, can be extracted from the work of Curle[10]. Taking his equations 4.23 to 4.26 at the condition of zero heat transfer (as in the case of the turbulent boundary layer), and inserting an allowance for axial symmetry according to the treatment of Young[11], we arrive eventually[12] at the following relations:

$$\theta = 0{\cdot}671 X . Re_X^{-\frac{1}{2}} \qquad \text{(A13)}$$

where X is once more the 'equivalent flat plate length' (i.e. the length of flat plate over which a boundary layer growing at a constant Mach number equal to the actual local Mach number would attain the same thickness as the actual local boundary layer[6]), now defined by

$$X = \frac{1}{P''r^2}\int_0^x P''r^2\,dx$$

with

$$P'' = \frac{M^5}{(1+0{\cdot}2M^2)^4}.$$

The term r^2 is omitted when dealing with two-dimensional flow.

These expressions are closely similar in form to equation (A10) above for a turbulent boundary layer, and in the same way can only be used for a particular nozzle of known pressure distribution. In order to obtain a simple relation for general application, separate factors for divergence and pressure gradient must again be isolated. The former, ε, is that already defined above for a turbulent boundary layer, as it depends only on surface geometry. For the latter, denoted now by I_l, no experimental evidence is this time available. Considering as before the conical nozzles used in the present tests, calculations according to the treatment above show a dependence of I_l on Mach number as in Fig. 44. This curve is very similar to, but rather flatter than, that for I_t taken from Fig. 43. Within the range of nozzle design pressure ratio of current interest, corresponding to a limit of Mach number 3, only 11 per cent error would be introduced by taking the same values of I for both laminar and turbulent conditions – a figure which is probably comparable with the general level of accuracy in an approximate treatment of this nature.

It is interesting to compare equation (A13) with the classical relation for incompressible flow on a flat plate:

$$\theta = 0{\cdot}664x.Re_x^{-\frac{1}{2}}.$$

These should conform when $M = 0$, so that adjustment of the constant derived from Curle's analysis[10] to 0·664 seems legitimate. Hence our final form is:

$$\theta = 0{\cdot}664\varepsilon I_l x.Re_x^{-\frac{1}{2}}. \tag{A14}$$

If the displacement thickness δ^* is required, it is convenient to multiply equations (A13) or (A14) by Young's relation[7]:

$$\frac{\delta^*}{\theta} = 2{\cdot}59(1+0{\cdot}277M^2). \tag{A15}$$

Dividing equation (A11) by (A14) and putting

$$\Lambda = \frac{\theta, \text{ turbulent}}{\theta, \text{ laminar}}$$

we have

$$\Lambda = 0{\cdot}0542Re_x^{0{\cdot}3}.\frac{I_t}{I_l}(1+0{\cdot}1M^2)^{-\frac{5}{7}}. \tag{A16}$$

Now for a given shape of nozzle the quantity $\frac{Re_x}{Re^*}$ depends predominantly on M, and slightly on T_t. In Fig. 45 is shown the form of this relation for our family of 10 deg. conical nozzles. It is thus approximately true to write

$$\Lambda = 0{\cdot}0542(Re^*)^{0{\cdot}3}.\,\text{function}\,(M). \tag{A17}$$

For these particular nozzles curves of Λ are given in Fig. 46 for values of $Re^* = 10^5$ and 10^6, taking I_t/I_l from Fig. 44. Our tests (*see* Section 6.2) have indicated that a laminar boundary layer can exist at a value of Re^* at least as high as $0{\cdot}75 \times 10^6$, at which condition the boundary-layer momentum thickness and hence the thrust loss due to friction in the divergent section are in general only about 45 per cent of what they would be were the boundary layer turbulent.

Likewise, we may define

$$\Omega = \frac{\delta^*, \text{turbulent}}{\delta^*, \text{laminar}}$$

and obtain

$$\Omega = 0{\cdot}02675\, Re_x{}^{0{\cdot}3} \frac{I_t}{I_l}(1+0{\cdot}8M^2)^{\frac{3}{7}}(1+0{\cdot}277M^2)^{-1} \tag{A18}$$

which is similar in form to equations (A16) and (A17). Fig. 47 gives values of Ω for the same conditions as were used in Fig. 46. The laminar boundary-layer displacement thickness and hence the 'displacement loss' is about 75 per cent of the turbulent at $Re^* = 0{\cdot}75 \times 10^6$.

It is interesting to note the behaviour of the ratio $\frac{\Omega}{\Lambda}$. We know that

$$\frac{\Omega}{\Lambda} = \frac{H, \text{turbulent}}{H, \text{laminar}}$$

which, from inspection of equations (A16) and (A18), is obviously independent of Re_x and hence of T_t. In fact it is also independent of M to a very close approximation, having the value $0{\cdot}55 \pm 0{\cdot}002$ throughout the range $1{\cdot}5 < M < 3{\cdot}5$. This value agrees quite well with the incompressible figure of 0·5.

4. *'Momentum Loss' for Axisymmetric Nozzles.*

Let suffix e denote nozzle exit conditions, and l be the nozzle length from throat to outlet measured along the contour. Then let us define an 'equivalent semi-cone angle' α' such that

$$\sin\alpha' = \frac{D_e - D^*}{2l}.$$

We also have

$$\varepsilon = \frac{D_e + D^*}{2D_e}.$$

Hence

$$\frac{4l\varepsilon}{D_e} = \operatorname{cosec}\alpha' \left(1 - \frac{A^*}{A_e}\right).$$

Then, for a turbulent boundary layer, by equations (A2) and (A11)

$$1-\eta_f = \frac{4\theta_e}{D_e}$$

$$= 0{\cdot}036 \operatorname{cosec}\alpha' \, Re_l^{-\frac{1}{5}} \, I_{t,e} \left(1-\frac{A^*}{A_e}\right) \left(1+0{\cdot}1 M_e^{\,2}\right)^{-\frac{5}{7}}.$$

Now $$\frac{Re_l}{Re^*} = \frac{A^*}{A_e} \cdot \frac{\mu^*}{\mu_e} \cdot \frac{l}{D^*}.$$

Sutherland's formula for viscosity can be written as:

$$\frac{\mu^*}{\mu} = \left(\frac{T_t + 117(1+0{\cdot}2M^2)}{T_t + 140{\cdot}4}\right) \left(\frac{1+0{\cdot}2M^2}{1{\cdot}2}\right)^{0{\cdot}5}.$$

An approximation to this which eliminates T_t as a variable within the range of interest is:

$$\frac{\mu^*}{\mu} \doteq \left(1+\frac{M^2}{20}\right) \left(\frac{1+0{\cdot}2M^2}{1{\cdot}2}\right)^{0{\cdot}5}$$

giving $$\frac{Re_l}{Re^*} = \frac{1}{2} \operatorname{cosec}\alpha' \sqrt{\frac{A^*}{A_e}} \left(1-\sqrt{\frac{A^*}{A_e}}\right) \left(1+\frac{M_e^{\,2}}{20}\right) \left(\frac{1+0{\cdot}2M_e^{\,2}}{1{\cdot}2}\right)^{0{\cdot}5}.$$

Therefore $$1-\eta_f = 0{\cdot}036 \, (\operatorname{cosec}\alpha')^{\frac{4}{5}} \, Re^{*-\frac{1}{5}} \left\{\frac{1}{2}\sqrt{\frac{A^*}{A_e}} \left(1-\sqrt{\frac{A^*}{A_e}}\right) \left(1+\frac{M_e^{\,2}}{20}\right) \times \right.$$

$$\left. \times \left(\frac{1+0{\cdot}2M_e^{\,2}}{1{\cdot}2}\right)^{0{\cdot}5} \right\}^{-\frac{1}{5}} . I_{t,e} \left(1-\frac{A^*}{A_e}\right) \left(1+0{\cdot}1 M_e^{\,2}\right)^{-\frac{5}{7}}$$

$$\propto (\operatorname{cosec}\alpha')^{\frac{4}{5}} \, Re^{*-\frac{1}{5}} . \text{ function } (M_e). \qquad \text{(A19)}$$

The corresponding expression for a laminar boundary layer is, from equation (A14):

$$1-\eta_f = 0{\cdot}664 \, (\operatorname{cosec}\alpha')^{\frac{1}{2}} \, Re^{*-\frac{1}{2}} \left\{\frac{1}{2}\sqrt{\frac{A^*}{A_e}} \left(1-\sqrt{\frac{A^*}{A_e}}\right) \left(1+\frac{M_e^{\,2}}{20}\right) \times \right.$$

$$\left. \times \left(\frac{1+0{\cdot}2M_e^{\,2}}{1{\cdot}2}\right)^{0{\cdot}5} \right\}^{-\frac{1}{2}} . I_{l,e} \left(1-\frac{A^*}{A_e}\right)$$

$$\propto (\operatorname{cosec}\alpha')^{\frac{1}{2}} \, Re^{*-\frac{1}{2}} . \text{ function } (M_e). \qquad \text{(A20)}$$

In the calculations that follow two values of Re^* have been taken:

(i) $0{\cdot}6 \times 10^6$, for both turbulent and laminar

(ii) 4×10^6, for turbulent only.

Where values widely different to these are encountered, correction may readily be made according to equations (A19) and (A20). Departing now from particular nozzles of known properties, the one-dimensional values of A_e/A^* have been taken corresponding to M_e, and $I_{t,e}$ in equation (A19) according to the full line in Fig. 43. A range of conditions of α' from 5 deg. to 20 deg. has been covered, and of M_e from 1·5 to 4 – although the results above $M_e = 3{\cdot}5$ are of doubtful accuracy.

Figs. 48 and 49 show the values obtained for a turbulent boundary layer. These have been converted to the case of a laminar boundary layer, for want of better knowledge concerning $I_{t,e}$ in the general case, by the expedient of factoring according to Fig. 46 for $Re^* = 0{\cdot}6 \times 10^6$, derived from equation (A17). The resulting values appear in Fig. 50.

For convenience Figs. 51 to 53 present the product $\eta_d \eta_f$ for uniformly conical nozzles – i.e. where the equivalent semi-cone angle α' is the same as the outlet divergence angle α. It is interesting to note here how the compromise between the effects of friction and divergence varies the cone angle for peak thrust performance. The optimum value of α is seen to depend severally upon design pressure ratio, Reynolds number, and whether the boundary layer is laminar or turbulent. In the laminar case (Fig. 53) the lowest angle taken (5 deg.) is superior at all values of D.P.R. for the Reynolds number shown. At low Re with a turbulent boundary layer, Fig. 52 shows that $7\frac{1}{2}$ deg. is to be preferred when the D.P.R. is above 12. Increase of Re then removes much of this advantage, and at conditions corresponding to an engine in flight (Fig. 51) parity is not achieved until a D.P.R. around 40.

If any secondary flow effects are neglected, the case of a square nozzle with four diverging walls all alike may be treated to a close approximation by the method presented above for axisymmetric nozzles. The angle α' then becomes the 'equivalent divergence semi-angle' of opposite walls. Exception must, however, be made in the case of Figs. 51 to 53, since the divergence loss factor η_d is now different – *see* Appendix III. The appropriate new values of $\eta_d \eta_f$ for square nozzles of uniform divergence are shown in Figs. 54 to 56. For any particular divergence angle α the value of η_d is reduced, which results in the optimum angle now being the lowest considered (5 deg.) in all cases except that of a turbulent boundary layer with low Re and D.P.R. above 35.

5. *'Momentum loss' for Two-Dimensional Nozzles.*

Consider a rectangular nozzle with two parallel sides spaced B apart, and two diverging walls separated by a distance D which increases with nozzle length. As before, the treatment will assume a uniform mean boundary-layer thickness on all four walls. Then:

$$\varepsilon = \frac{D_e + D^* + 2B}{2(D_e + B)}$$

Now let us define an 'equivalent wedge semi-angle' α' such that

$$\sin \alpha' = \frac{D_e - D^*}{2l}$$

where l is the surface length of the diverging walls. The effective length of the parallel walls will be somewhat less than l [lying between l and the axial length $(D_e - D^*)/2\tan\alpha'$], but for small values of α' little error will be introduced by treating all four sides as having the same length l. Thus

$$\frac{2(D_e + B)}{D_e B} l\varepsilon = \operatorname{cosec} \alpha' \frac{(D_e + D^* + 2B)(D_e - D^*)}{2 D_e B}$$

$$= \operatorname{cosec} \alpha' \left(1 - \frac{A^*}{A_e}\right) \left\{1 + \frac{1}{2\sigma}\left(1 + \frac{A_e}{A^*}\right)\right\}$$

where $\sigma = \dfrac{B}{D^*}$, the aspect ratio of the throat.

Therefore
$$1-\eta_f = 0{\cdot}036 \operatorname{cosec}\alpha' \, Re_l^{-\frac{1}{5}} \, I_{t,e} \left(1-\frac{A^*}{A_e}\right) \times$$
$$\times \left\{1+\frac{1}{2\sigma}\left(1+\frac{A_e}{A^*}\right)\right\} (1+0{\cdot}1M_e^{\,2})^{-\frac{5}{7}}.$$

If Re^* is now based upon the throat height D^* (rather than on width B), we have:

$$\frac{Re_l}{Re^*} = \frac{1}{2}\operatorname{cosec}\alpha' \left(1-\frac{A^*}{A_e}\right)\left(1+\frac{M_e^{\,2}}{20}\right)\left(\frac{1+0{\cdot}2\,M_e^{\,2}}{1{\cdot}2}\right)^{0{\cdot}5}$$

whence

$$1-\eta_f = 0{\cdot}036\,(\operatorname{cosec}\alpha')^{\frac{4}{5}}\, Re^{*-\frac{1}{5}} \left\{\frac{1}{2}\left(1+\frac{M_e^{\,2}}{20}\right)\left(\frac{1+0{\cdot}2\,M_e^{\,2}}{1{\cdot}2}\right)^{0{\cdot}5}\right\}^{-\frac{1}{5}} \times$$
$$\times I_{t,e}\left(1-\frac{A^*}{A_e}\right)^{\frac{4}{5}} \left\{1+\frac{1}{2\sigma}\left(1+\frac{A_e}{A^*}\right)\right\} (1+0{\cdot}1\,M_e^{\,2})^{-\frac{5}{7}}$$
$$\propto (\operatorname{cosec}\alpha')^{\frac{4}{5}}\, Re^{*-\frac{4}{5}}.\ \text{function}\,(M_e;\sigma) \qquad \text{(A21)}$$

The corresponding expression for a laminar boundary layer is:

$$1-\eta_f = 0{\cdot}664\,(\operatorname{cosec}\alpha')^{\frac{1}{2}}\, Re^{*-\frac{1}{2}} \left\{\frac{1}{2}\left(1+\frac{M_e^{\,2}}{20}\right)\left(\frac{1+0{\cdot}2\,M_e^{\,2}}{1{\cdot}2}\right)^{0{\cdot}5}\right\}^{-\frac{1}{2}} \times$$
$$\times I_{l,e}\left(1-\frac{A^*}{A_e}\right)^{\frac{1}{2}} \left\{1+\frac{1}{2\sigma}\left(1+\frac{A_e}{A^*}\right)\right\}$$
$$\propto (\operatorname{cosec}\alpha')^{\frac{1}{2}}\, Re^{*-\frac{1}{2}}.\ \text{function}\,(M_e;\sigma). \qquad \text{(A22)}$$

The same conditions for calculation have been taken as for the axisymmetric case, and where values of Re^* are required widely different from those given, a similar means of correction can be applied using equations (A21) and (A22). For the two-dimensional nozzles a range of α' from 10 deg. to 30 deg. has been covered, with throat aspect ratios between 1 and 10. Results appear in Figs. 57 to 59.

The product $\eta_d\eta_f$ is shown for two-dimensional nozzles with flat divergent surfaces in Figs. 60 to 62.

6. *'Displacement loss' for Axisymmetric and Two-Dimensional Nozzles.*

Having already computed the 'momentum loss' term $(1-\eta_f)$ for each shape of nozzle, it is convenient to use the general equation (A8) which gives the 'displacement loss' β as:

$$\beta = \frac{1}{\bar{F}_e/A^*P_t}\int_{P_e/P_t}^{P_s^*/P_t} H(1-\eta_f)\frac{A}{A^*}\,d\left(\frac{P}{P_t}\right).$$

For a turbulent boundary layer, from equations (A11) and (A12):

$$H = 1{\cdot}278\,(1+0{\cdot}8M^2)^{\frac{3}{7}}(1+0{\cdot}1M^2)^{\frac{5}{7}}$$

while for a laminar boundary layer, [equation (A15)]:

$$H = 2{\cdot}59\,(1+0{\cdot}277M^2).$$

Since H, $\tilde{F}/A^*P_t$, A/A^* and P/P_t are all functions of M only, equation (A8) can be re-cast in the form

$$\beta = G_1(M_e)\int_1^{M_e}(1-\eta_f)G_2(M)\,dM.$$

Values of $(1-\eta_f)$ against M may be taken from Figs. 48 to 50 and 57 to 59, for various conditions of α' and Re^*, and, in the case of two-dimensional nozzles, of σ. From the resulting calculations we emerge with Figs. 63 to 65 for axisymmetric and square nozzles, and Figs. 66 to 68 for two-dimensional nozzles.

APPENDIX V

Nozzle Design Pressure Ratio

In Appendix I three quite usual but incompatible ways of defining D.P.R. were given, viz:

(i) the pressure ratio corresponding in one-dimensional theory to the effective area ratio† of the nozzle.

(ii) the pressure ratio at which the gross gauge thrust efficiency η_F based on A.P.R. is a maximum.

(iii) the pressure ratio at which the flow is fully expanded,i.e. nozzle outlet pressure = base pressure.

The geometric outlet area of a nozzle (A_e) must include the effects of divergent flow at outlet as discussed in Appendix III. In the case of a conical nozzle for example, using the notation of Appendix III, it is equal to $A_{e,s}$ or $\frac{A_{e,p}}{\eta_d}$. However, the effective outlet area is reduced below the geometric by the presence of a boundary layer. Putting A_e' for the isentropic flow area corresponding to A_e, we have

$$A_e' = A_e\left(1-\frac{4\delta^*}{D}\right)_e$$

and hence the effective area ratio becomes (*see* sketch)

$$\frac{A_e'}{A^*} = \frac{A_e}{A_g}\cdot\frac{\left(1-\frac{4\delta^*}{D}\right)_e}{C_D}$$

from which D.P.R. (i) can be determined. It is to be understood that the same pressure P_e' is here considered as existing at the outlet of both the actual nozzle and its isentropic one-dimensional counterpart, as in Fig. 42. For convenience the above expression is rewritten as

$$\frac{A_e'}{A^*} = \frac{A_e}{A_g}\cdot\frac{1}{C_D}\left\{1-H_e(1-\eta_f)\right\}$$

---

† 'Effective area ratio' is defined as the ratio of the isentropic one-dimensional flow areas at outlet and throat.

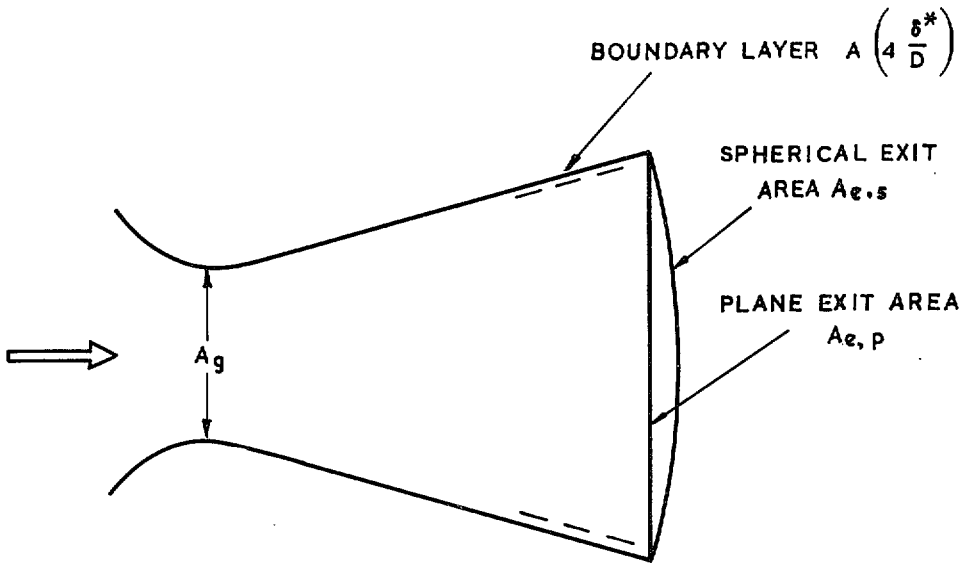

ACTUAL NOZZLE

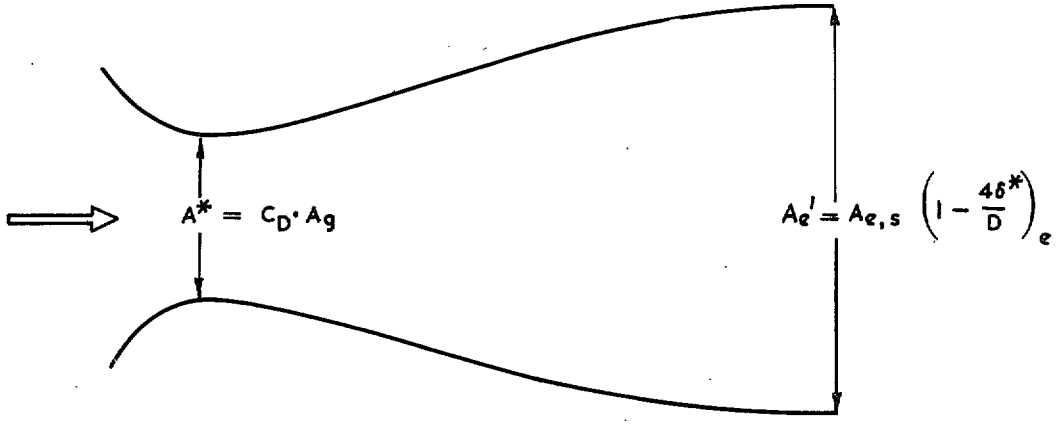

IDEAL NOZZLE

since the term $(1-\eta_f)$ can be obtained from Figs. 48 to 50; if required, relations for H will be found in Section 6 of Appendix IV.

Taking as an example a conical nozzle with

$$\begin{cases} \dfrac{A_{e,p}}{A_g} = 2{\cdot}9; \quad C_D = 0{\cdot}99 \\ Re^* = 4\times10^6; \alpha = 10 \text{ deg.} \end{cases}$$

we get $$\eta_d = 0{\cdot}9924 \text{ and } \left(1-\frac{4\delta^*}{D}\right)_e = 0{\cdot}9824$$

so that $$\frac{A_{e,s}}{A_g} = \frac{2{\cdot}9}{0{\cdot}9924} = 2{\cdot}922$$

and $$\frac{A_e'}{A^*} = \frac{2{\cdot}9\times0{\cdot}9824}{0{\cdot}9924\times0{\cdot}99} = 2{\cdot}900.$$

Thus the readily measured quantity $A_{e,p}/A_g$ may in some cases approximate quite closely to the effective area ratio.

Now take the case of an internal-expansion nozzle with some inherent and substantial loss in the divergent portion, over and above the losses from friction and outlet divergence, such as a discontinuity of profile, sudden over-expansion, secondary air injection slot, etc. It is found that with the nozzle running full the pressure in the outlet plane (P_e) can then be considerably higher than the pressure P_e', as represented in Fig. 69. The peak thrust efficiency occurs around a pressure ratio of P_t/P_e' [= D.P.R.(i)], while D.P.R. (iii) has the much lower value P_t/P_e. This effect may be regarded as an attempt by nature to afford some measure of compensation for the loss of $\int P_w dA$ occurring within the nozzle; the wall pressure having earlier fallen below the isentropic curve, it can later rise above it. There is a fundamental understanding that the 'gain' in area under the curve can never exceed the preceding 'loss'. In practice, with a nozzle designed on the basis of $P_e' = P_\infty = P_b$[†], but having $P_e > P_e'$ and hence $> P_\infty$, the full potential gain is not achieved (point 1 in sketch); and in terms of η_F at the given pressure ratio (P_t/P_∞) it will pay to assist nature by extending the nozzle walls to give a new P_e closer to P_∞ (point 2 in sketch). This, of course, involves an increase in nozzle area ratio (from nozzle A to nozzle B in sketch), which brings with it a shift in the curve of η_F to peak at a new pressure ratio above P_t/P_∞ (point 3 in sketch). That is to say we should deliberately design a nozzle with such an imperfection to have D.P.R. (i) greater than the pressure ratio at which it is required to operate, in order to allow the extra amount of divergent wall for recovery.

We therefore see that with a nozzle working over a certain expansion pressure ratio P_t/P_∞, it does not of necessity imply over-expansion to have D.P.R. (i) $> P_t/P_\infty$. Since the completeness of expansion ultimately governs the performance of an exhaust system, we shall always obtain the best η_F at this particular pressure ratio (P_t/P_∞) when D.P.R. (iii) $\simeq P_t/P_\infty$.

[†] For the purpose of this argument base pressure is treated as equal to ambient at the nozzle design-point, as is approximately the case in quiescent air testing.

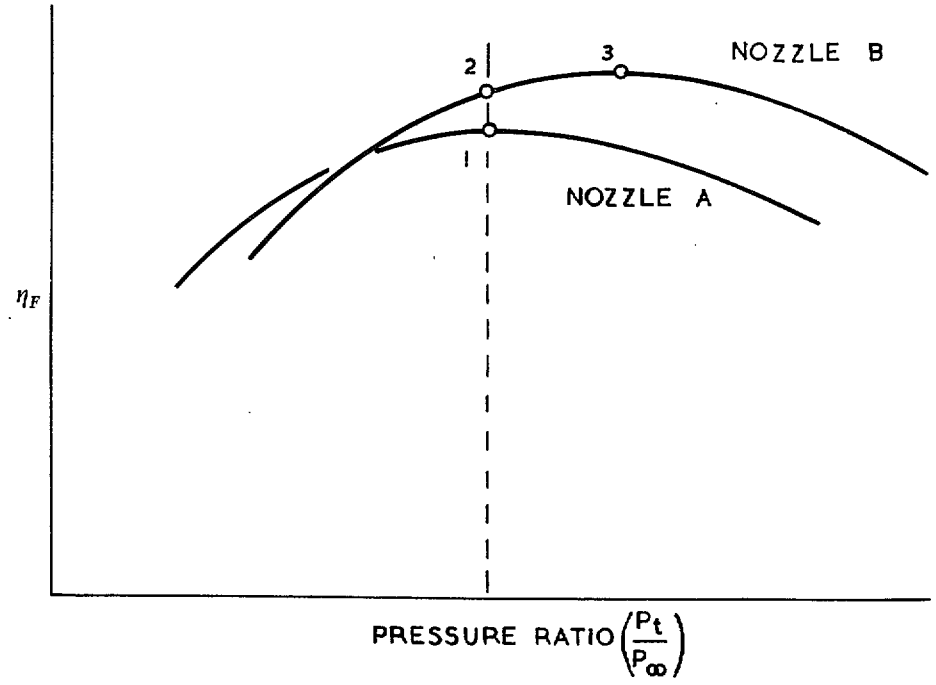

It remains to be shown why definitions (ii) and (iii) can differ, i.e. why peak internal thrust efficiency ($\eta_{F,\max}$) may occur at a condition when the flow is under-expanded. The expression for thrust efficiency can be written

$$\eta_F = \frac{1{\cdot}26789\, C_D \eta_{S,\text{conv}} + \int_0^{\left(\frac{A_e}{A_g}-1\right)} \frac{P_w}{P_t} d\left(\frac{A}{A_g}\right) - \frac{1}{A.P.R.} \cdot \frac{A_e}{A_g} - \phi}{C_D \left[\frac{\tilde{F}}{A^* P_t}\right]_{\text{APR}}}$$

where

$\eta_{S,\text{conv}}$ is obtained as in Section 4.

(= 1·003 for our nozzles with $C_D = 0{\cdot}990$, when choked)

$\phi = \frac{1}{A_g P_t} \int \tau dA_s$: *see* Appendix IV, Section 1

$\frac{\tilde{F}}{A^* P_t}$ = isentropic momentum thrust function

$$= \gamma \sqrt{\left(\frac{\gamma+1}{\gamma-1}\right)} \left(\frac{2}{\gamma+1}\right)^{\frac{\gamma}{\gamma-1}} \sqrt{\left[1 - \frac{1}{(P.R.)^{\frac{\gamma-1}{\gamma}}}\right]}.$$

It should be noted, since the integration is performed over the component of divergent surface area projected in the axial direction, that A_e in the above expression relates to geometric plane outlet area,

and to be consistent with previous notation should properly be written $A_{e,p}$. The above expression has the form

$$\eta_F = \frac{a - \dfrac{b}{A.P.R.}}{\psi(A.P.R.)}$$

where

$$\begin{cases} a = 1{\cdot}26789\,\eta_{S,\text{conv}} + \dfrac{1}{C_D}\displaystyle\int_0^{\left(\frac{A_e}{A_g}-1\right)} \frac{P_w}{P_t}\,d\left(\frac{A}{A_g}\right) - \frac{\phi}{C_D} \\ b = \dfrac{1}{C_D}\cdot\dfrac{A_e}{A_g} \\ \psi = \text{a function} \end{cases}$$

and both a and b are constants for a given geometry of nozzle running full. Then, for η_F to be a maximum, we have

$$\frac{b}{(A.P.R.)^2} = \left(a - \frac{b}{A.P.R.}\right)\frac{\psi'(A.P.R.)}{\psi(A.P.R.)}.$$

This equation may be solved for A.P.R. for particular conditions of a and b. The resulting value will be D.P.R. (ii), and is dependent mainly on two factors: first and foremost, the nozzle area ratio contained in b; and second, and to a much lesser extent, the value of the term $\int P_w dA$ appearing in a. In general it seems that the case of $P_e > P_e'$ is associated with a reduction in $\int P_w dA$ below the isentropic value, but it is possible for considerable differences in outlet pressure to occur in nozzles of the same area ratio without greatly affecting the net area under the curve.

One therefore reaches the conclusion that D.P.R. (ii) depends primarily on A_e/A_g and to some extent on $\int P_w dA$, and is thus linked most closely with D.P.R. (i). The state of expansion of the flow at outlet – and hence D.P.R. (iii) – has no direct bearing on the value of D.P.R. (ii).

To sum up, for internal-expansion nozzles with substantial imperfections of divergent contour, there are really two cases of interest which must be distinguished:

(*a*) To obtain the maximum thrust efficiency from a given geometry of nozzle, the A.P.R. being variable; i.e. to locate D.P.R. (ii). This condition ($A.P.R._{opt}$) will occur close to the pressure ratio (P_t/P_e') corresponding to the effective (rather than geometric) nozzle area ratio A_e'/A^*; and it may in practice be sufficiently accurate to take $A.P.R._{opt} \simeq$ D.P.R. (i). It is possible for the flow at outlet to be considerably underexpanded.

(*b*) To obtain the maximum thrust efficiency at a particular A.P.R., nozzle area ratio being variable. This requires complete expansion† of the flow at outlet, so that $P_e = P_b$ ($= P_\infty$ by assumption). Hence in this case A.P.R. = D.P.R. (iii)

The above argument (with $P_b = P_\infty$) is given as for operation in quiescent air. In external flow this condition is unlikely still to obtain, and we shall normally find $P_b < P_\infty$. Let us see how this affects the

† Subject to friction effects.

first of the two cases just discussed. In the neighbourhood of its design-point, any internal-expansion nozzle will conform approximately to equation (11), which may be put in general form

$$\frac{\eta}{\eta_{max}} = \frac{K_1 + K_2\left(\frac{1}{D.P.R.} - \frac{1}{R}\right)}{\text{function } [R]}$$

where K_1 and K_2 are constants depending only on effective nozzle geometry and R is any unspecified reference pressure ratio. As before (*see* Section 5.2) it is strictly D.P.R. (i) which occurs in this expression, while the condition for D.P.R. (ii) is of course $\eta = \eta_{max}$. Now this relation clearly gives a unique curve of η/η_{max} versus R regardless of what reference pressure ratio is used. Similarly the analysis above could equally well be conducted in general terms of R rather than specifically A.P.R., and the conclusion would still be that, on the curve of η/η_{max}, the two points R = D.P.R. (i) and R_{opt} = D.P.R. (ii) are very close together. When $P_b \neq P_\infty$, it may be convenient to use in place of A.P.R. a reference which we will call the engine exhaust pressure ratio (E.P.R. = P_t/P_∞). So long as the nozzle runs full, nothing is altered algebraically in case (a) above, and the values of D.P.R. (i) and (ii) are unique.

Some care is required, however, in interpreting case (b) in relation to D.P.R. (iii). The condition for the latter was stated (Appendix I) to be $P_e = P_b$, so that D.P.R. (iii) = P_t/P_e and as such is also unique for an internal-expansion nozzle running full. But the requirements of case (b) are no longer the same. One is now concerned with obtaining the maximum nozzle internal thrust in flight (omitting here any base drag) at a particular E.P.R., and what is wanted is to make $P_e = P_\infty$ rather than $P_e = P_b$. Thus the design condition becomes in this case E.P.R. = D.P.R. (iii).

These differences are, of course, only likely to be significant for the instance originally considered – that is, a nozzle having some large internal loss beyond the normal amount from friction and outlet divergence.

APPENDIX VI

Real Air Effects

(In collaboration with Mr. J. C. Ascough of N.G.T.E.)

Throughout the present work, isentropic thrust quantities have been derived on the basis of the following values for air:

$$\gamma = 1{\cdot}400$$

$$R = 96{\cdot}0 \text{ ft.lbf/lb.deg.}K$$

$$g = 32{\cdot}2 \text{ ft/sec}^2.$$

Nozzle entry stagnation conditions in these tests were approximately 1 Atm and 290 deg.K.

Some thought has been given to the possibility that, during the expansion process, the air may depart sufficiently from the state of being a 'perfect gas' to introduce an error in isentropic thrust evaluated as above. Such departure could take two forms, which will be considered in turn.

1. *Real Air Compressibility.*

The real air equation of state is

$$\frac{P}{\rho} = ZRT,$$

where the compressibility factor Z is known to vary with both temperature and pressure, R being taken as constant. The sense of the variation is such that a combination of low temperature and high pressure produces the greatest difference. During an expansion, therefore, there will be some mutual compensation of the separate influences.

In order to examine the magnitude of this effect, calculations have been made using real air data for enthalpy and entropy given in Reference 20. This problem is considered in detail in Reference 21, on which the present note is based. Fig. 70 shows the factor by which isentropic fully-expanded thrust as conventionally determined must be corrected. It can be seen that, for the particular entry total temperature taken, there is an appreciable sensitivity to pressure level but little to expansion pressure ratio. The latter result stems from the opposing influences of temperature and pressure on the factor Z, which cause this quantity to vary only slightly along any one expansion path for conditions in the present range of interest. The final value of Z, which approximates quite closely to our factor in Fig. 70,

$$\chi = \frac{v_{\text{real}}}{v_{\text{ideal}}}$$

where ideal air is defined by the condition $Z = 1$, thus depends mainly on the initial levels of pressure and temperature and very little on how far the expansion proceeds. It should be noted that the level of curves such as those in Fig. 70 is very sensitive to temperature; values given in that Figure for total temperature 290 deg. K should not be used for other conditions, and quite accurate determination of temperature should precede the use of any correction for this effect.

For our conditions of 1 atm total pressure, the error introduced by neglect of this correction barely exceeds 0·1 per cent in thrust efficiency.

At the same time it is of interest to observe the effect on discharge coefficient. According to definition, A^* is the throat area required to pass the actual mass flow of a nozzle under isentropic conditions, and for any particular nozzle $C_D \propto A^*$. Hence

$$\rho^* v^* C_D = \text{constant}$$

and it follows that

$$\frac{C_{D,\text{real}}}{C_{D,\text{ideal}}} = \frac{(\rho v)^*_{\text{ideal}}}{(\rho v)^*_{\text{real}}}.$$

Fig. 71 shows the values of this ratio calculated for the same total temperature (290 deg. K), and it is evident that the effect is negligible for the conditions of these tests.

2. *Energy Transfer.*

This is an effect essentially similar to that of chemical recombination during the expansion of high temperature gases. The proportion of energy in the vibrational mode in a gas in equilibrium decreases with fall in temperature, and the problem in a high speed expansion is whether sufficient time for this relaxation of vibrational energy is available. If the residence time in a nozzle is comparable with the relaxation time, some of the vibrational energy at the initial high temperature may not follow the equilibrium conversion to translational energy at the low temperature leaving the nozzle. This 'freezing' process constitutes a potential loss in thrust, and will be most serious in nozzles of small scale.

A measure of the order of this effect may be obtained by considering the total amount of vibrational energy initially present: clearly the loss can never exceed this quantity. Available data[22] show this to be highly sensitive to nozzle entry temperature; at 400 deg. K air contains 0·18 per cent energy in the vibrational mode, but at 300 deg. K only 0·03 per cent. It seems, therefore, that in our tests this is a negligible effect and no attempt to derive a correction need be made.

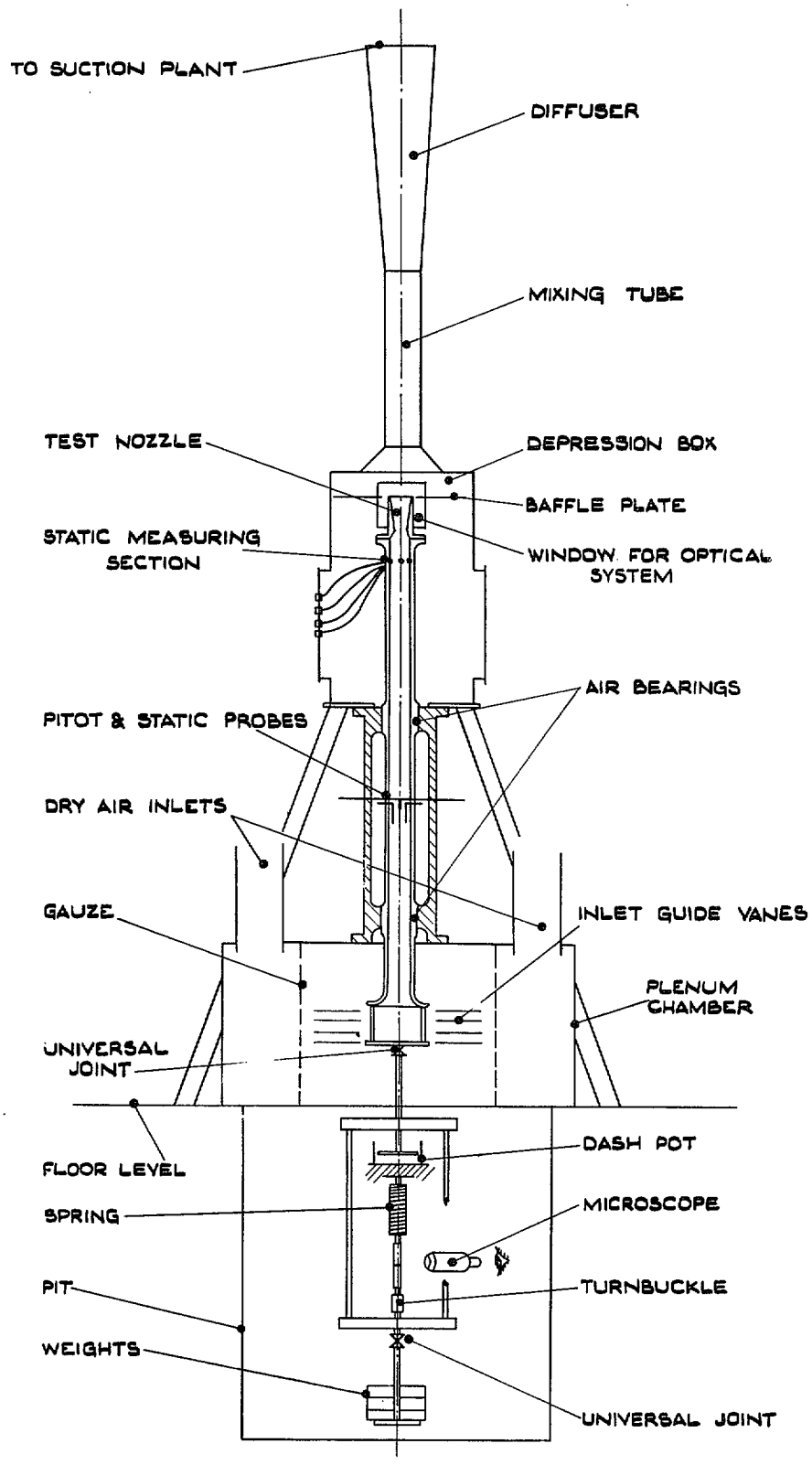

FIG. 1. Layout of thrust rig.

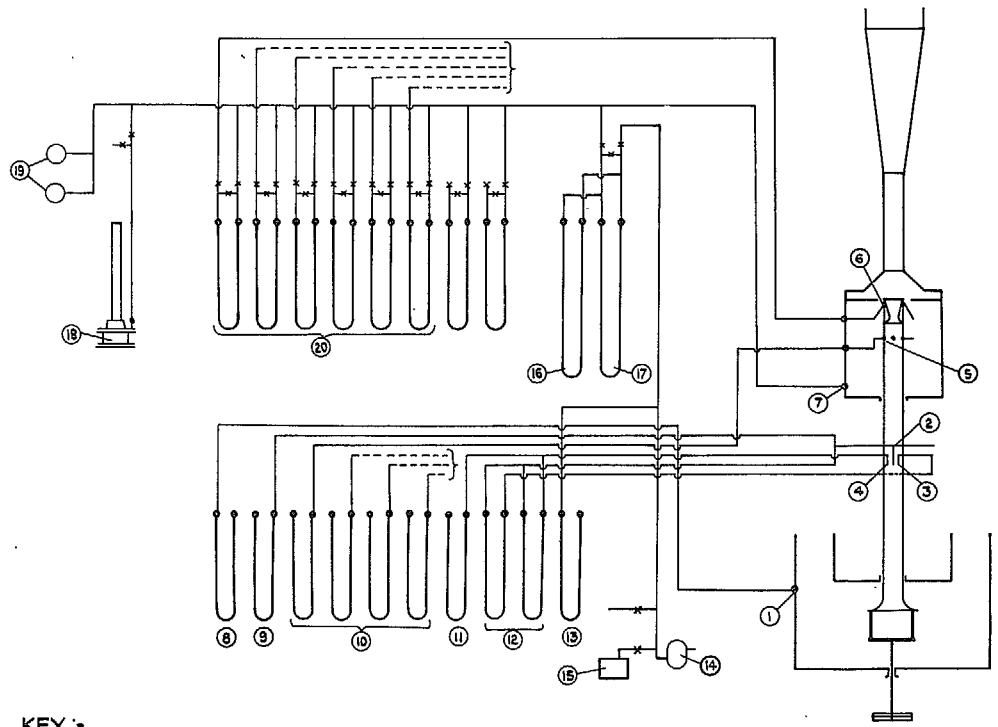

KEY :-

1. PLENUM CHAMBER STATIC. P_{pl}
2. TOTAL HEAD PROBE.
3. STATIC PROBE 1.
4. STATIC PROBE 2.
5. ENTRY SECTION STATIC (4 off)
6. NOZZLE BASE STATICS (USUALLY 6 off) P_b
7. DEPRESSION BOX STATIC. P_c
8. PLENUM STATIC - ATMOSPHERE. (H_2O) $P_{pl} - P_a$
9. ATMOSPHERE - PROBE TOTAL. (H_2O)
10. ATMOSPHERE - ENTRY STATIC 4 off H_2O
11. ATMOSPHERE - PROBE STATIC 2 (H_2O)
12. PROBE TOTAL - PROBE STATICS 1 & 2 (H_2O)
13. ATMOSPHERE - VACUUM. (H_g)
14. VACUUM PUMP.
15. PIRANI VACUUM GAUGE
16. DEPRESSION - VACUUM. (VACUUM OIL)
17. DEPRESSION - VACUUM. (DIBUTYL - PHTHALATE)
18. KEW GAUGE. (P_c OR P_a)
19. CAPSULE TYPE VACUUM GAUGES (HIGH & LOW RANGE)
20. DEPRESSION - BASE 6 off (TETRALIN) $P_c - P_b$

FIG. 2. Pressure instrumentation.

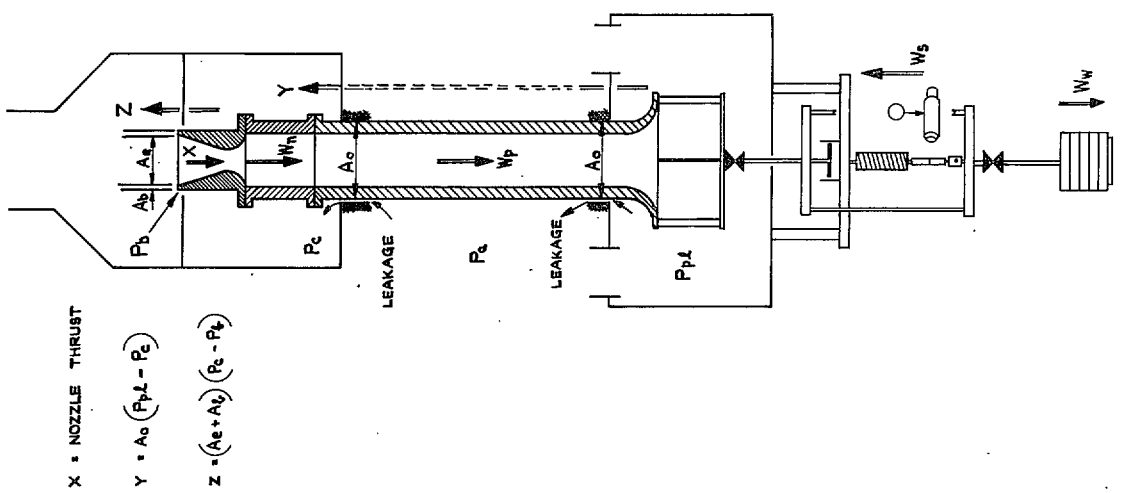

FIG. 3. Diagram of forces on the rig. Drawing not to scale.

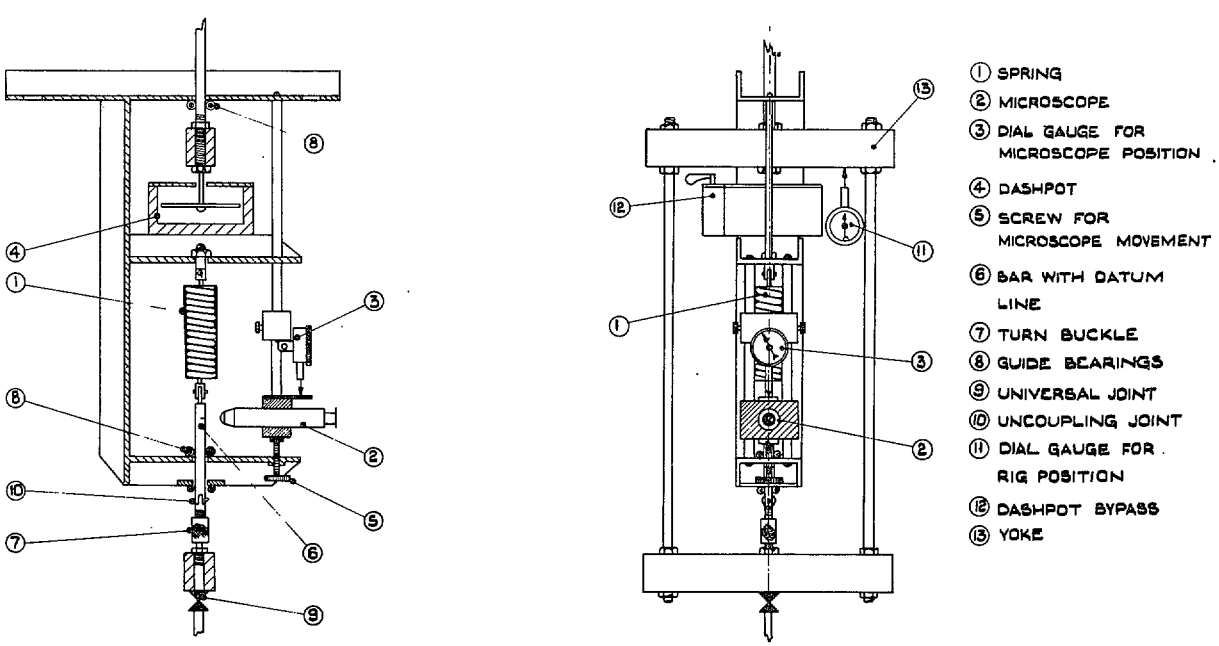

FIG. 4. Thrust balancing equipment.

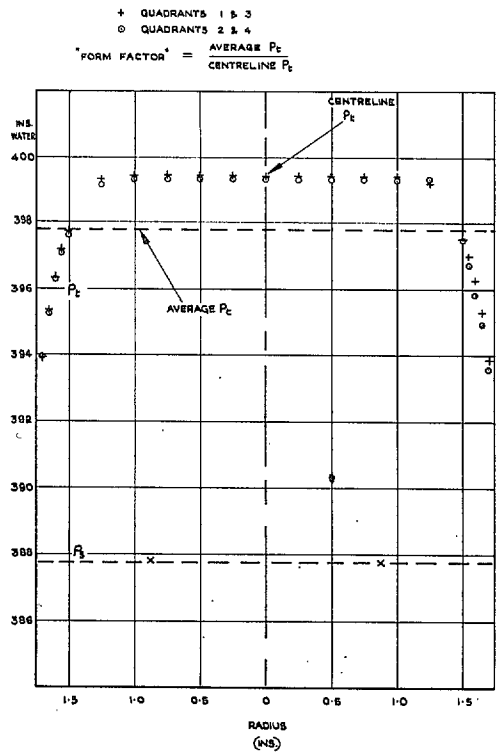

FIG. 5. Air meter pressure distribution.

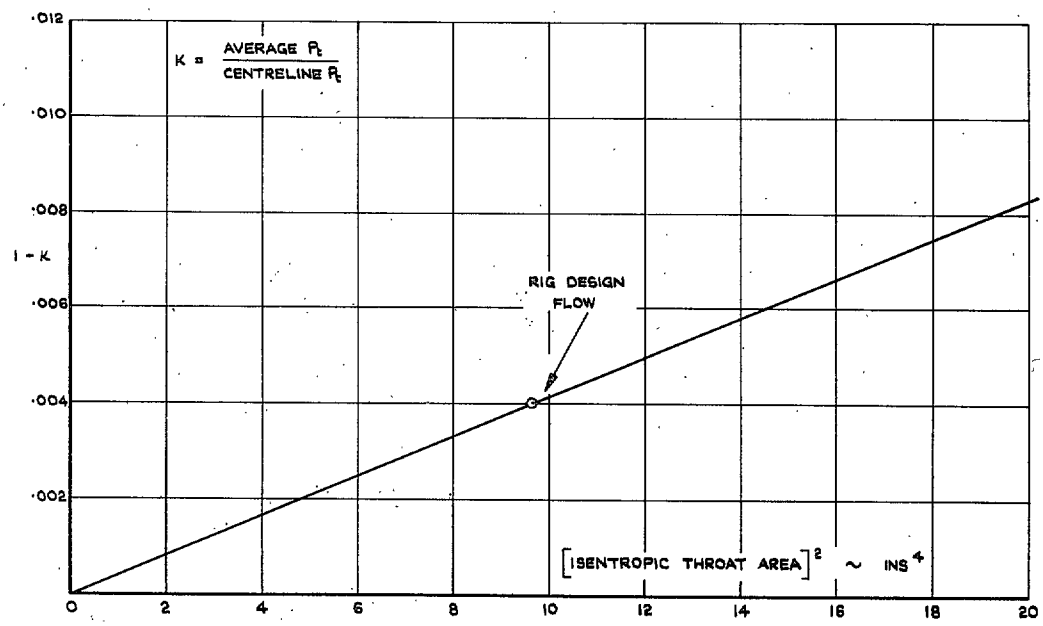

FIG. 6. Variation of form factor with mass flow.

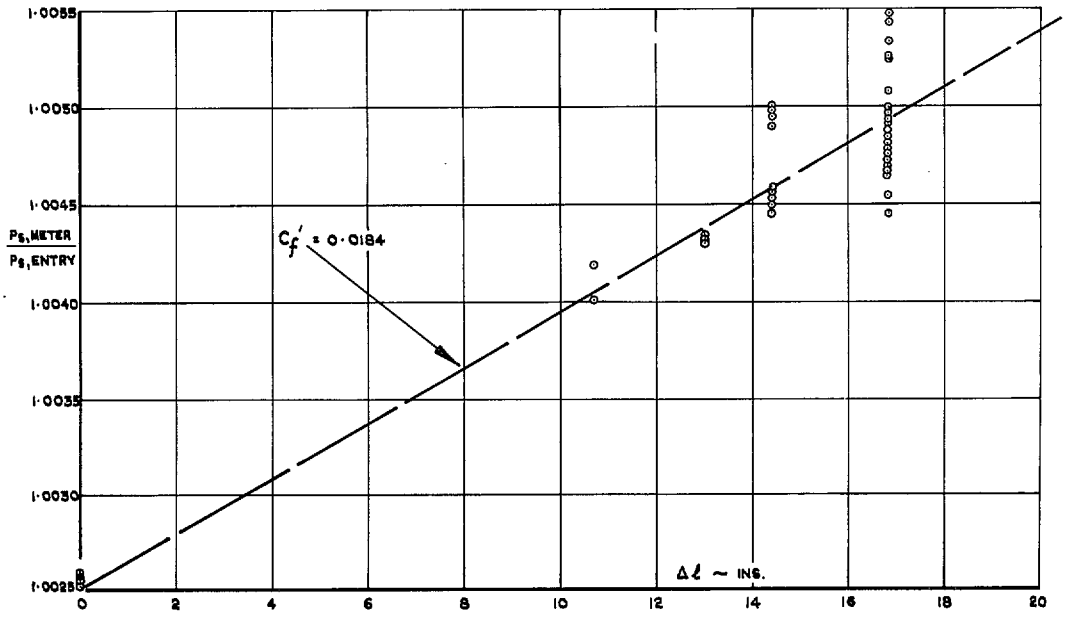

FIG. 7. Friction loss in nozzle entry pipe.

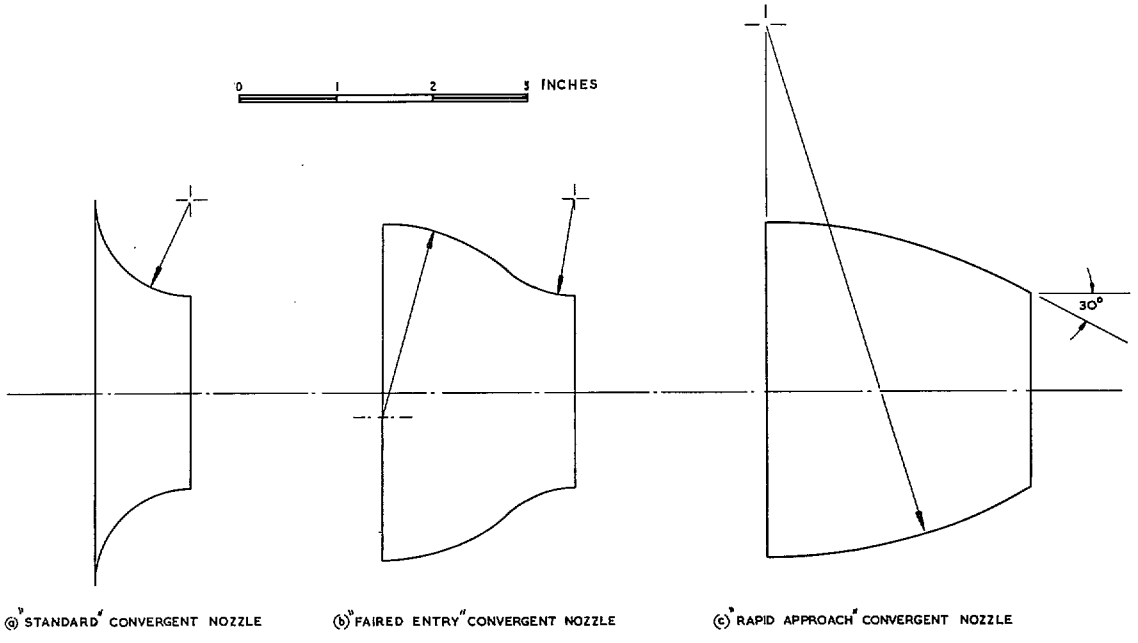

FIG. 8. Convergent nozzle types.

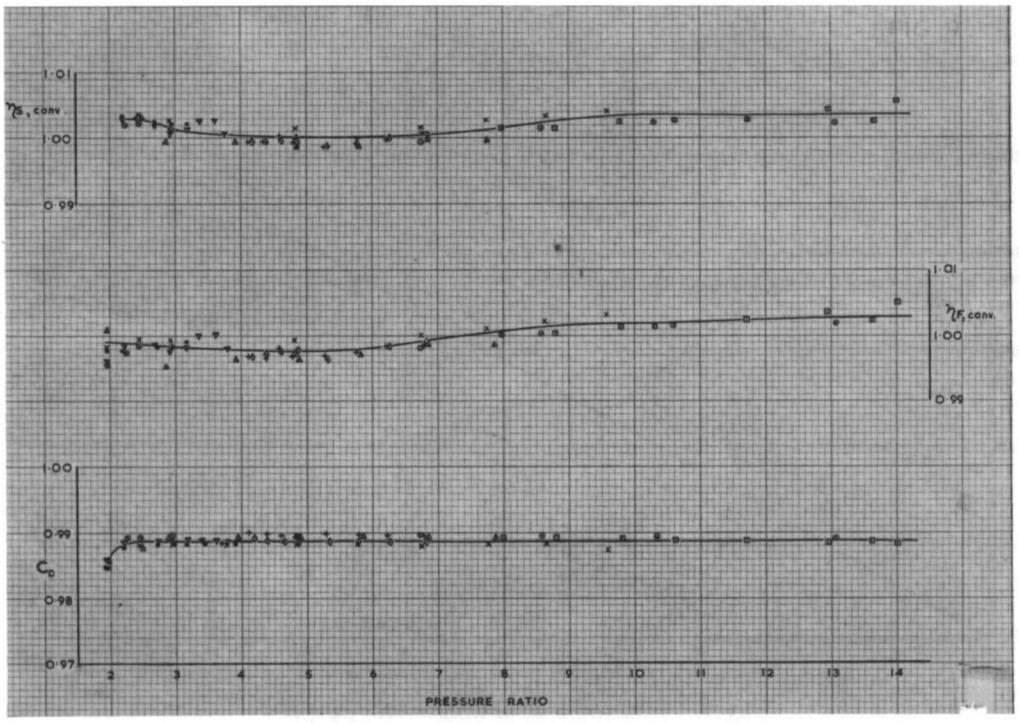

FIG. 9. Performance of 'standard' convergent nozzle.

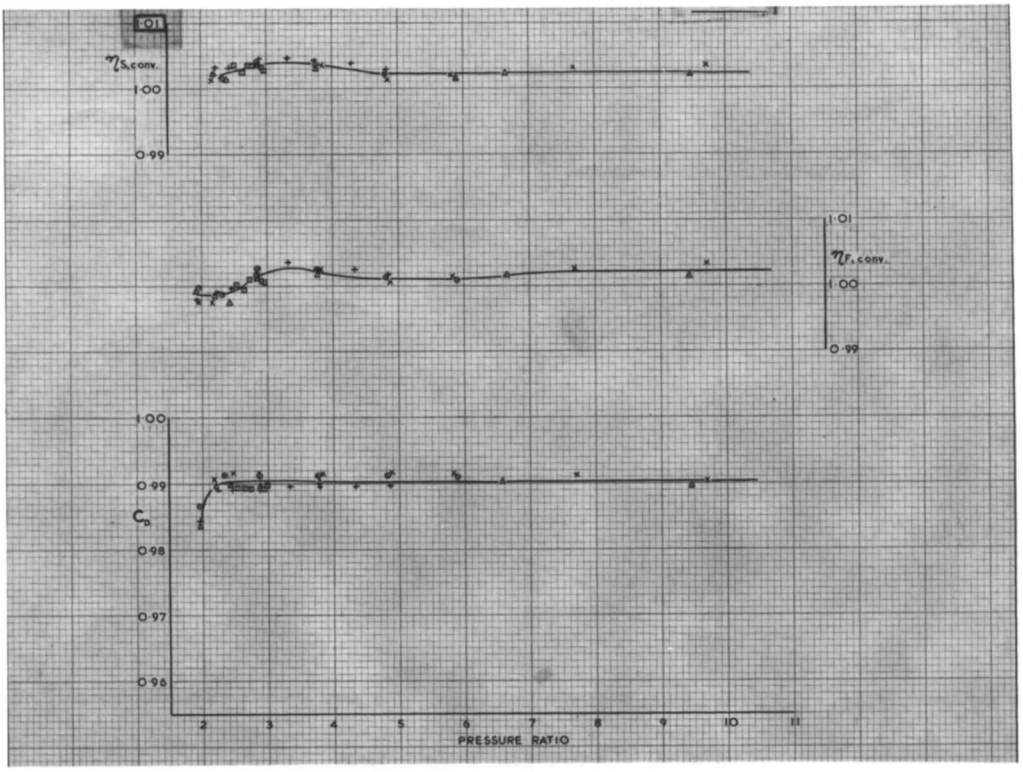

FIG. 10. Performance of 'faired entry' convergent nozzle.

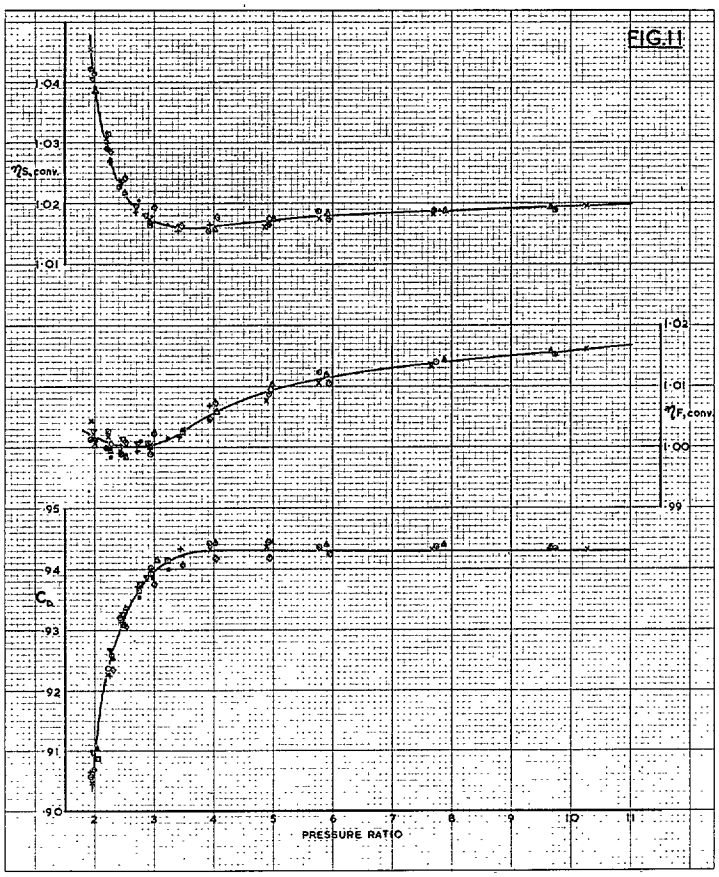

FIG. 11. Performance of 'rapid approach' convergent nozzle.

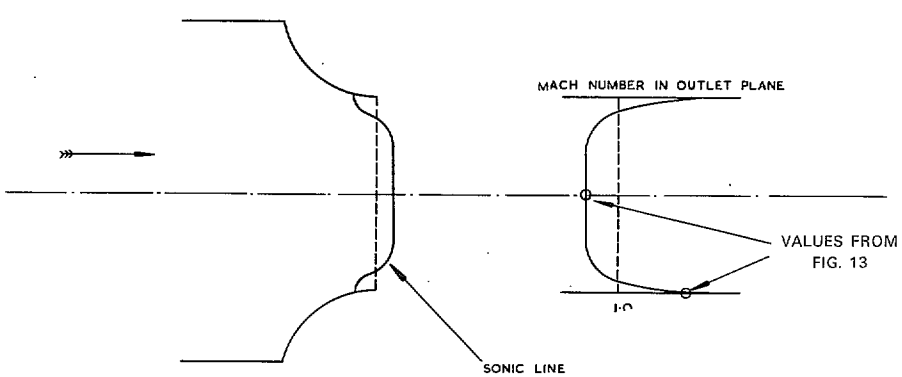

FIG. 12. Representation of flow leaving convergent nozzle with convex curvature.

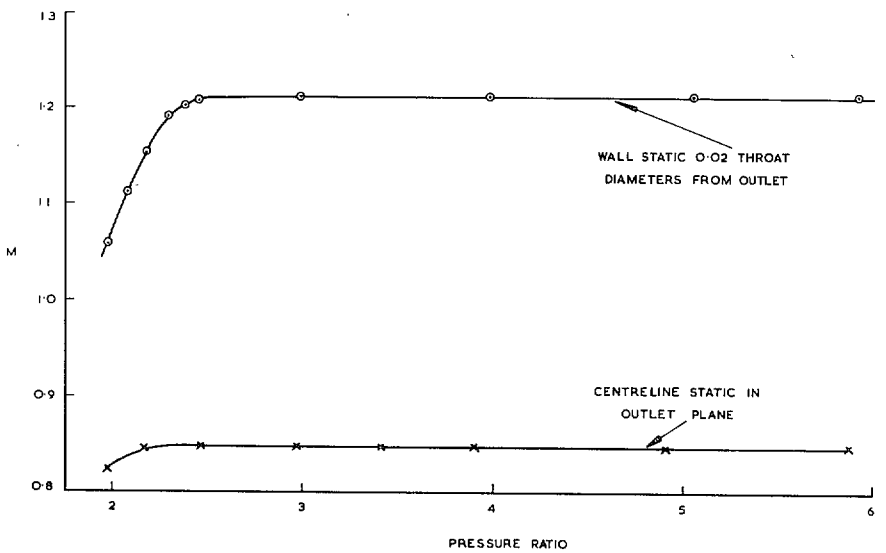

FIG. 13. Mach number of flow leaving 'standard' convergent nozzle.

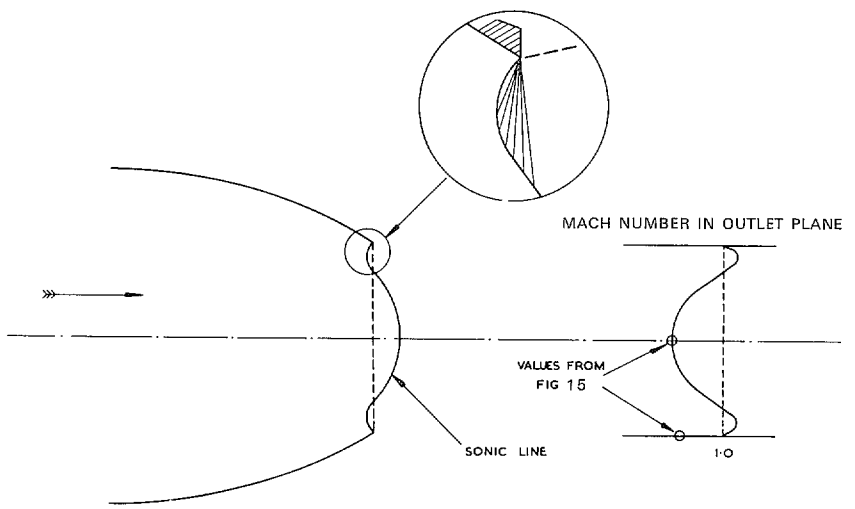

FIG. 14. Representation of flow leaving convergent nozzle with concave curvature.

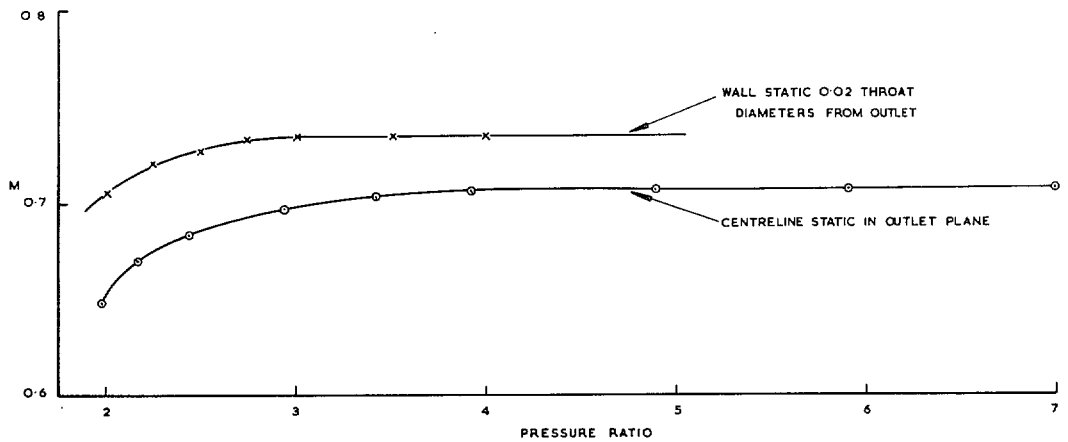

FIG. 15. Mach number of flow leaving 'rapid approach' convergent nozzle.

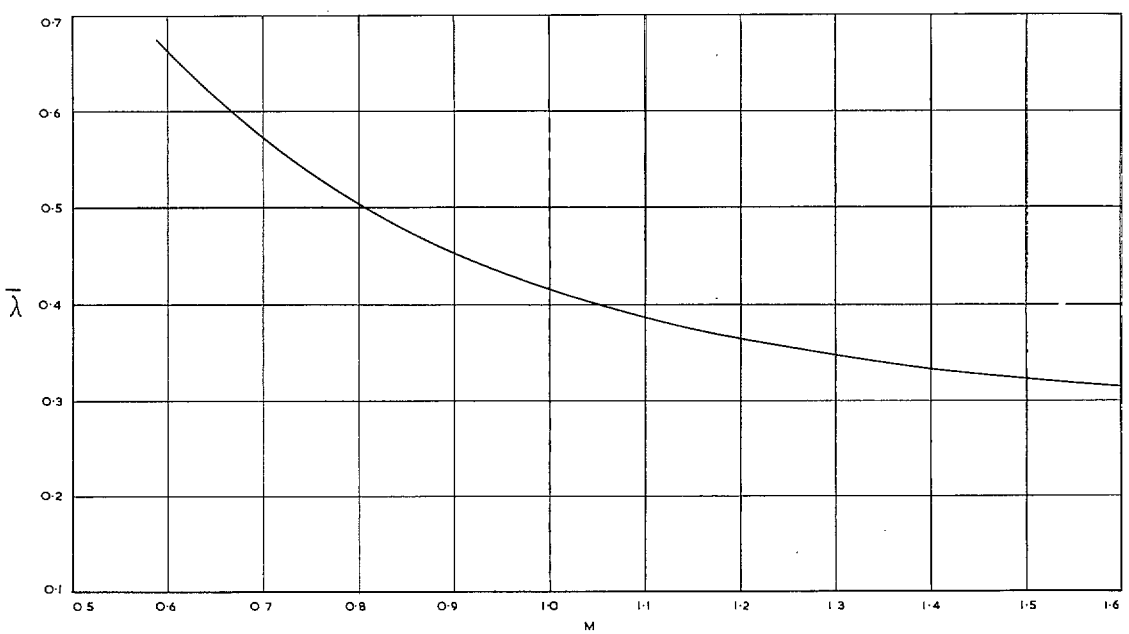

FIG. 16. Variation of curvature factor with Mach number.

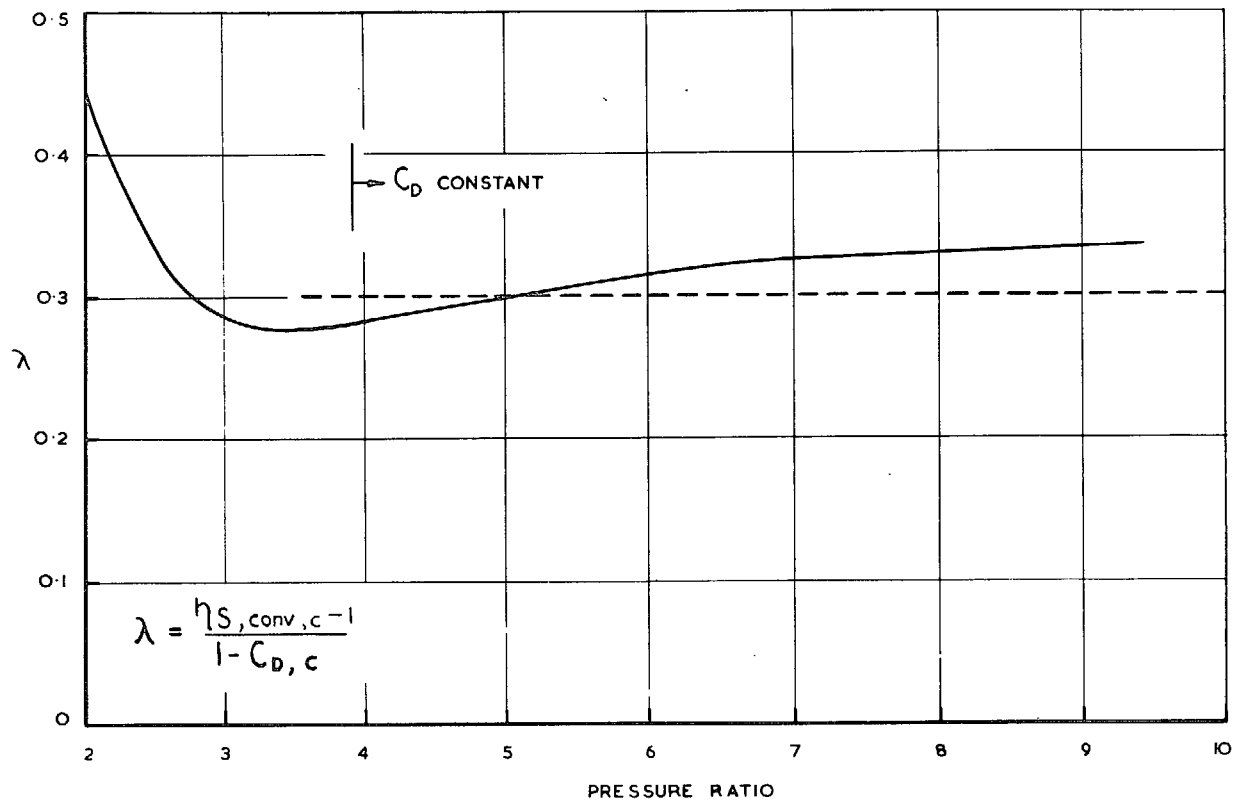

FIG. 17. Values of curvature factor obtained from 'rapid approach' convergent nozzle.

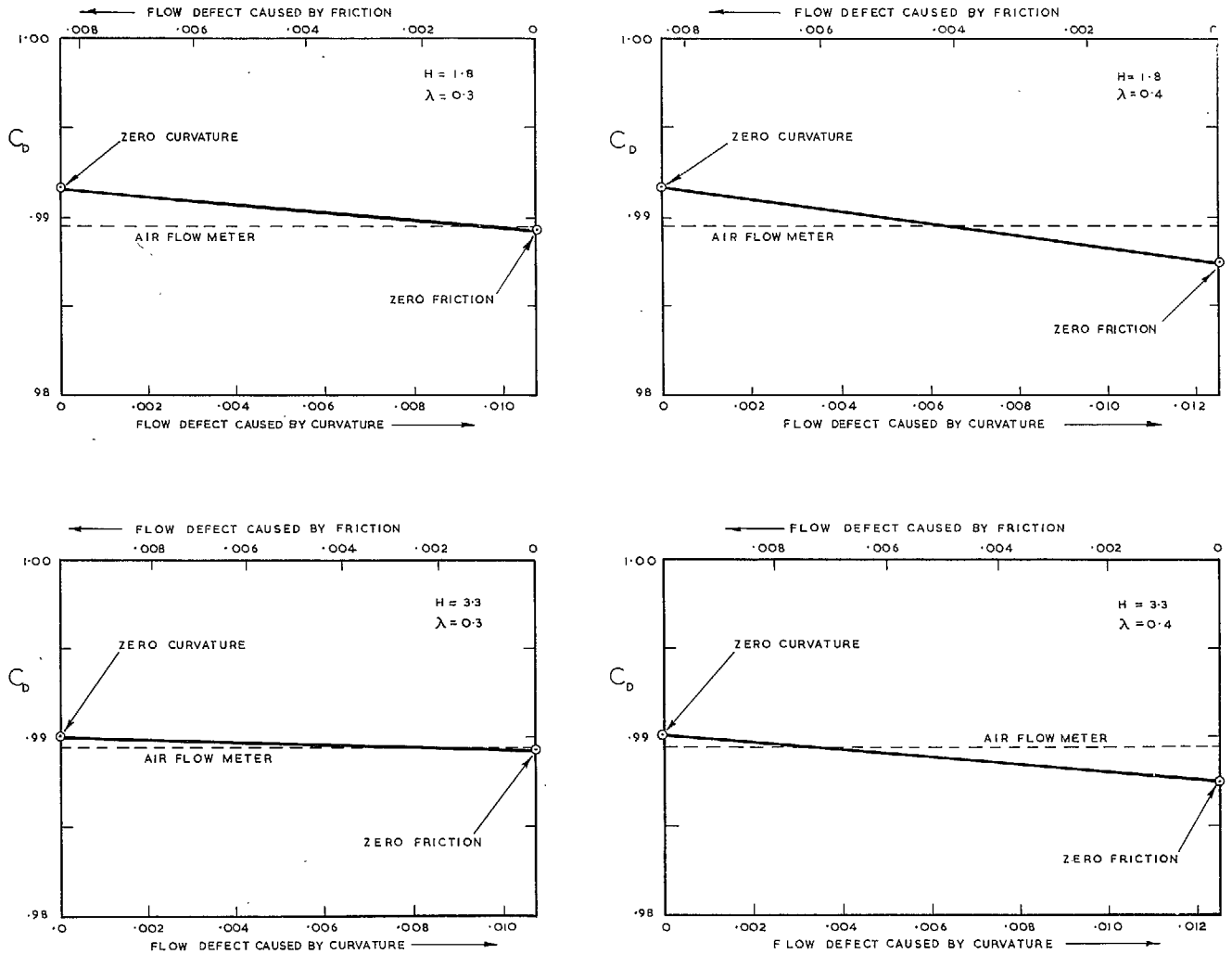

FIG. 18. Breakdown of losses in smooth convergent nozzles.

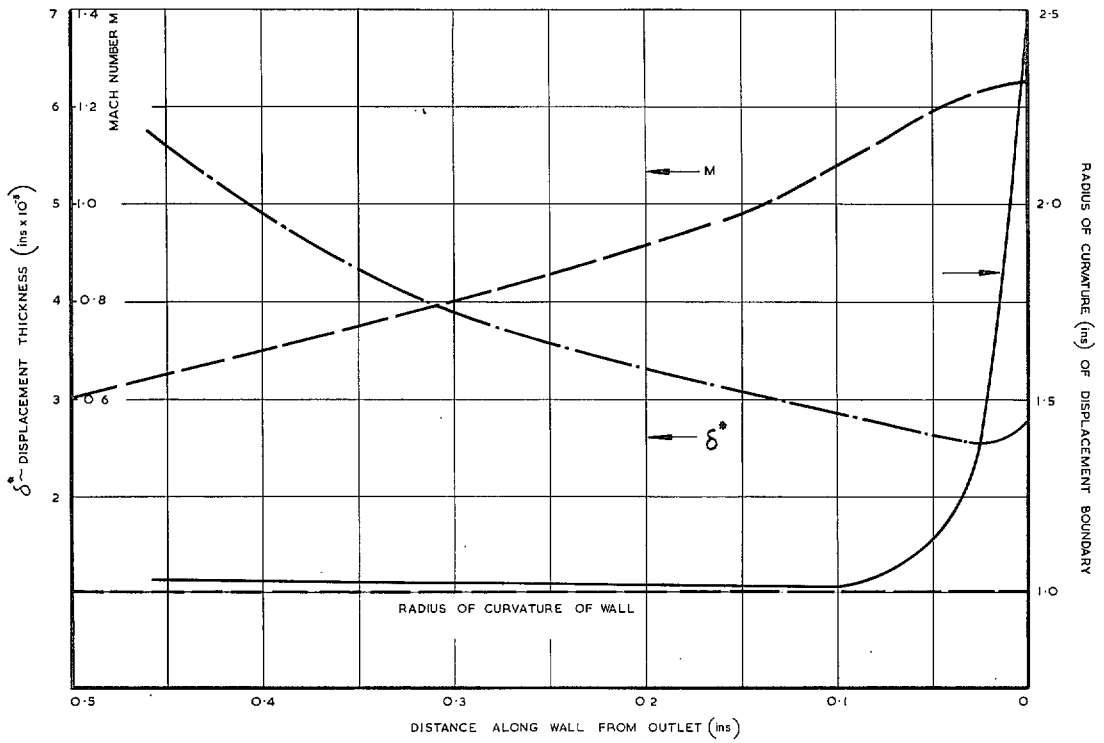

FIG. 19. Effective curvature of 'standard' convergent nozzle.

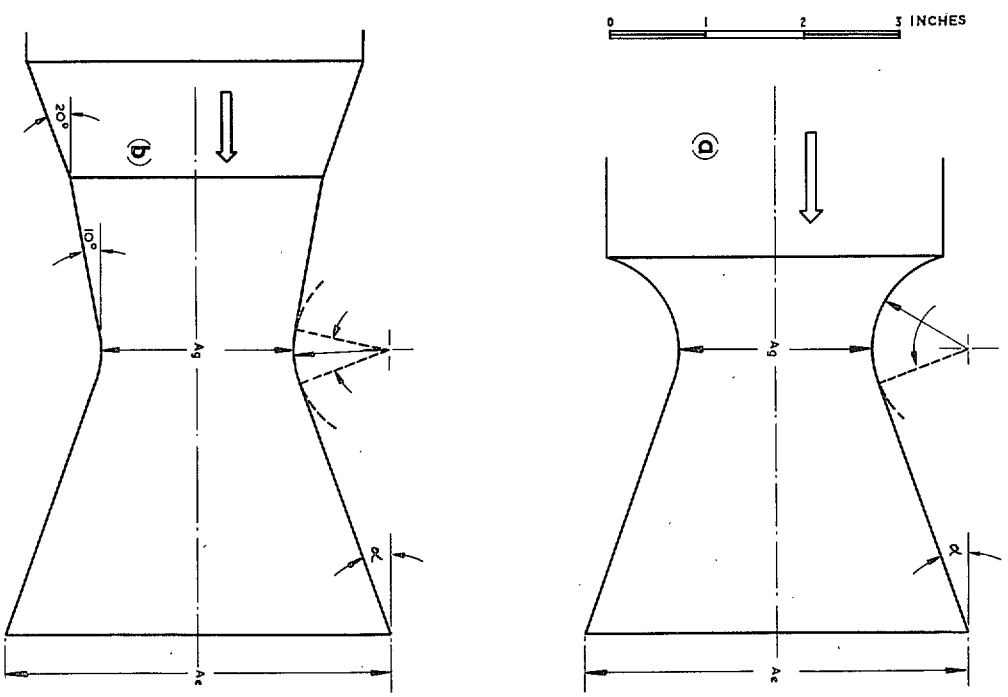

FIG. 20. Conical nozzle geometries.

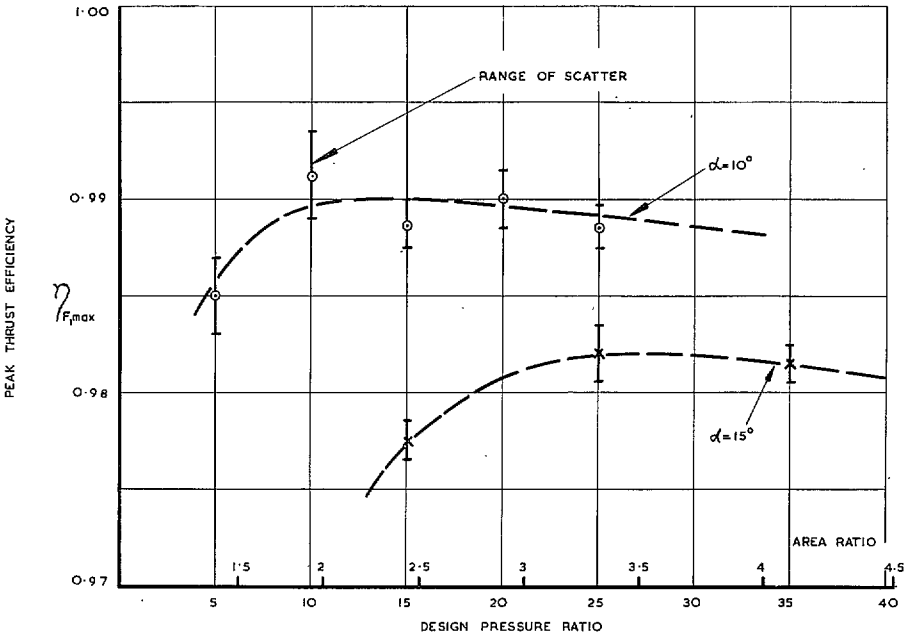

FIG. 21. Design-point performance of conical nozzles.

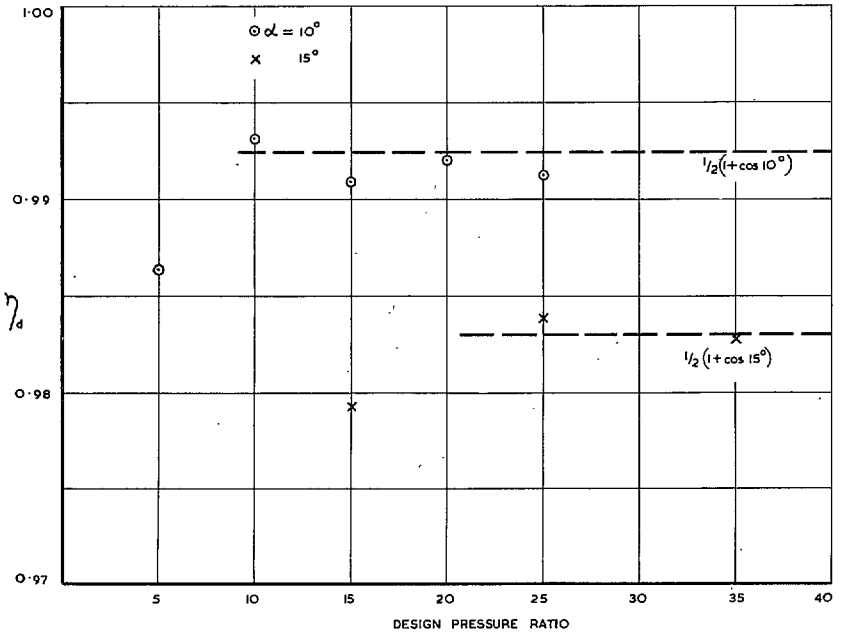

FIG. 22. Divergence loss in conical nozzles obtained from thrust measurement.

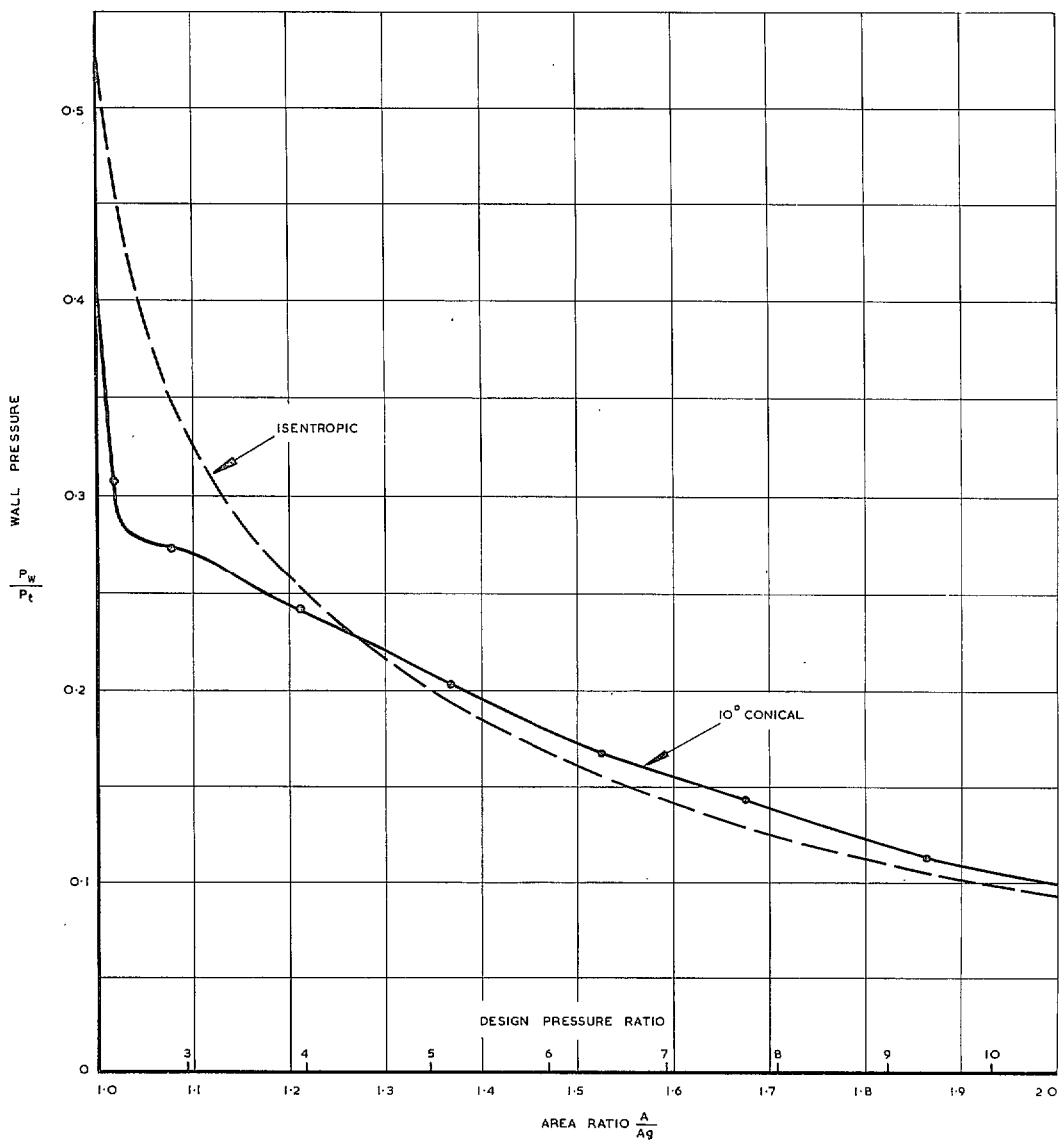

FIG. 23. Wall pressure distribution in conical nozzles – I. (Geometry as Fig. 20a: $\alpha = 10$ deg.).

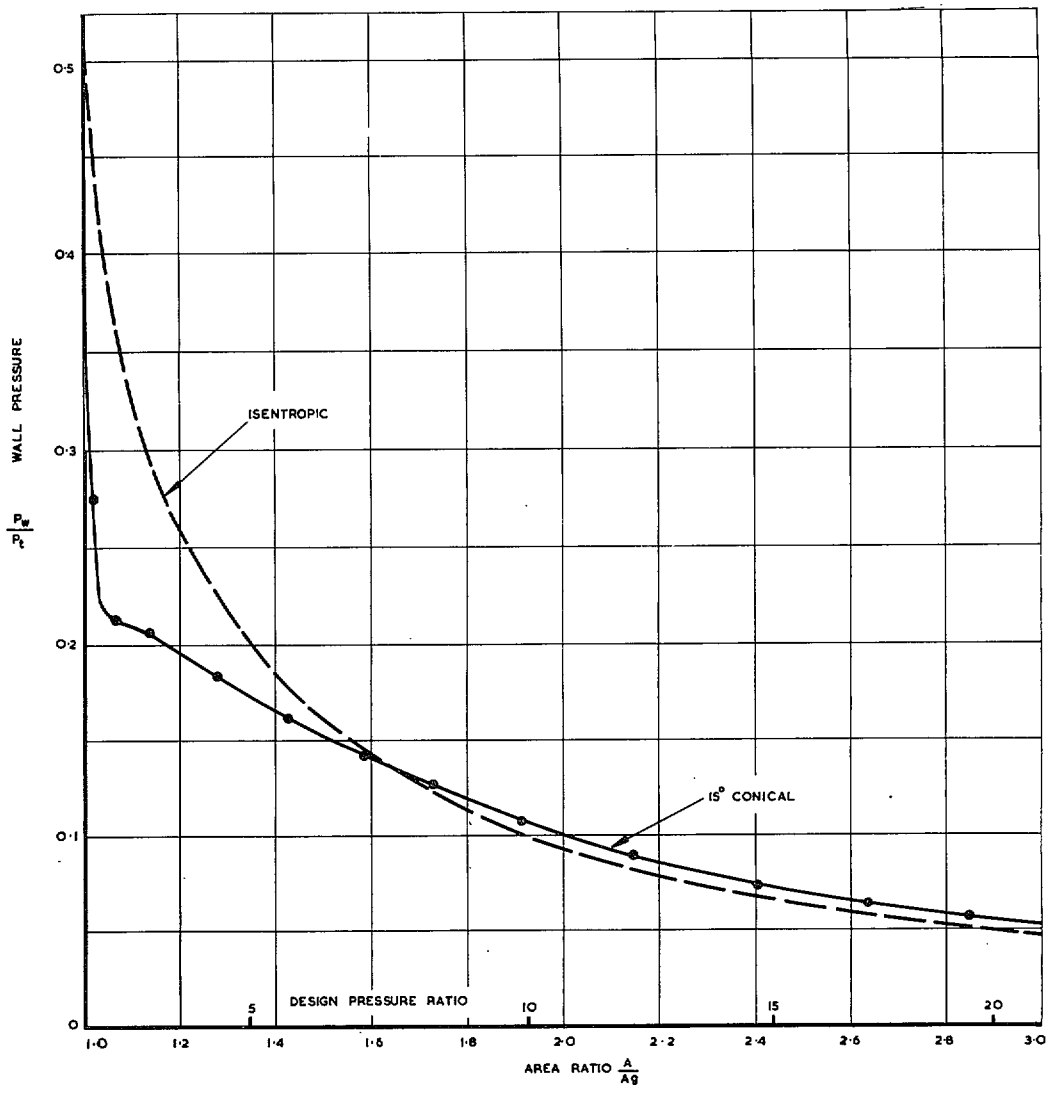

FIG. 24. Wall pressure distribution in conical nozzles – II. (Geometry as Fig. 20a : α = 15 deg.).

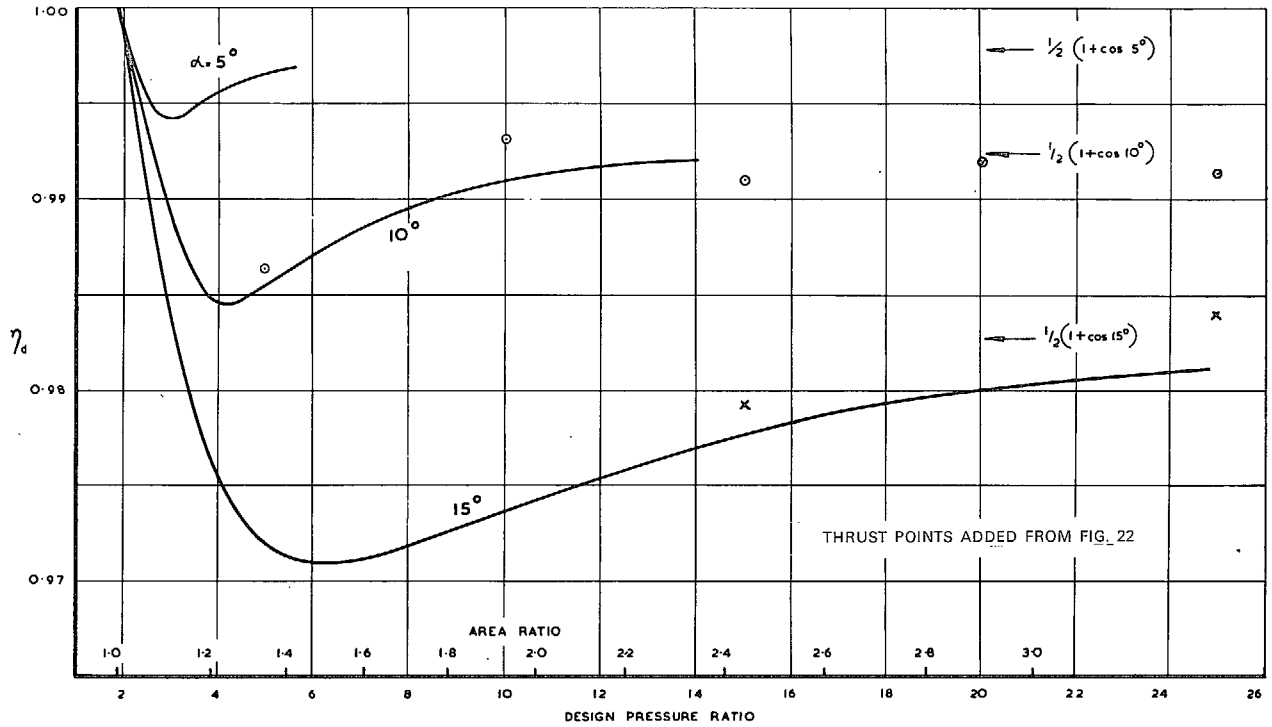

FIG. 25. Divergence loss in conical nozzles obtained from pressure measurement.

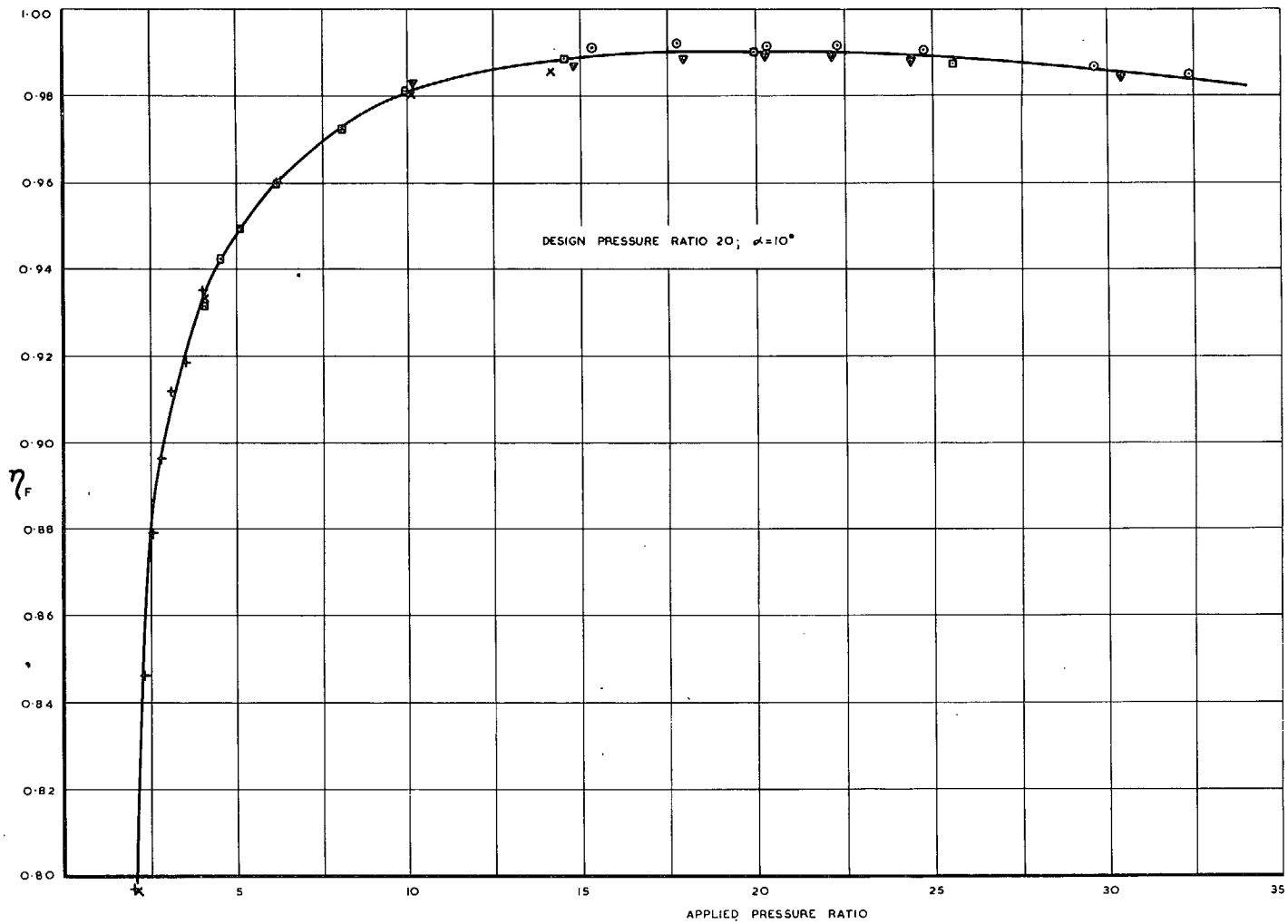

FIG. 26. Variable geometry thrust efficiency of conical nozzle with laminar boundary layer.

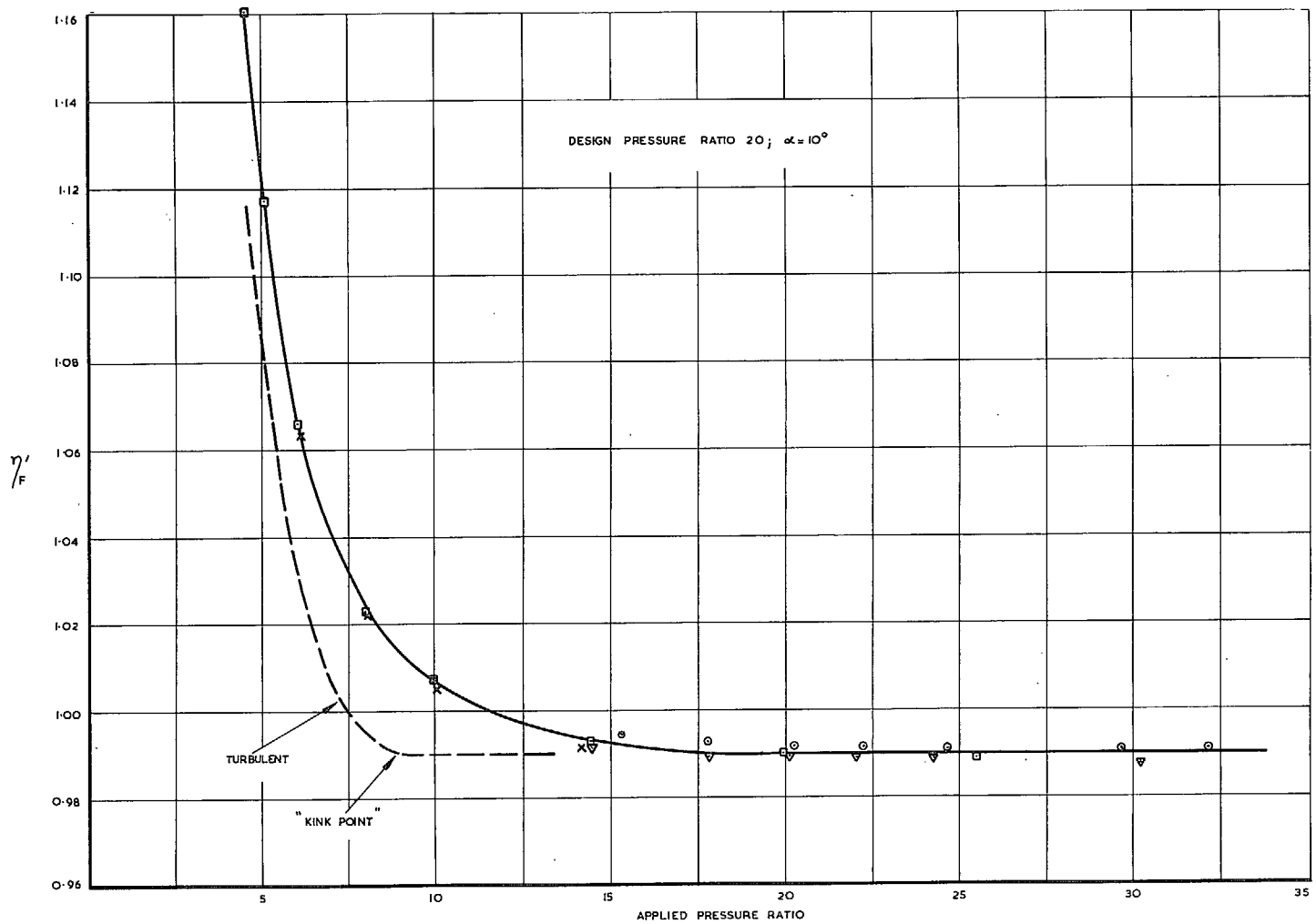

FIG. 27. Fixed geometry thrust efficiency of conical nozzle with laminar boundary layer.

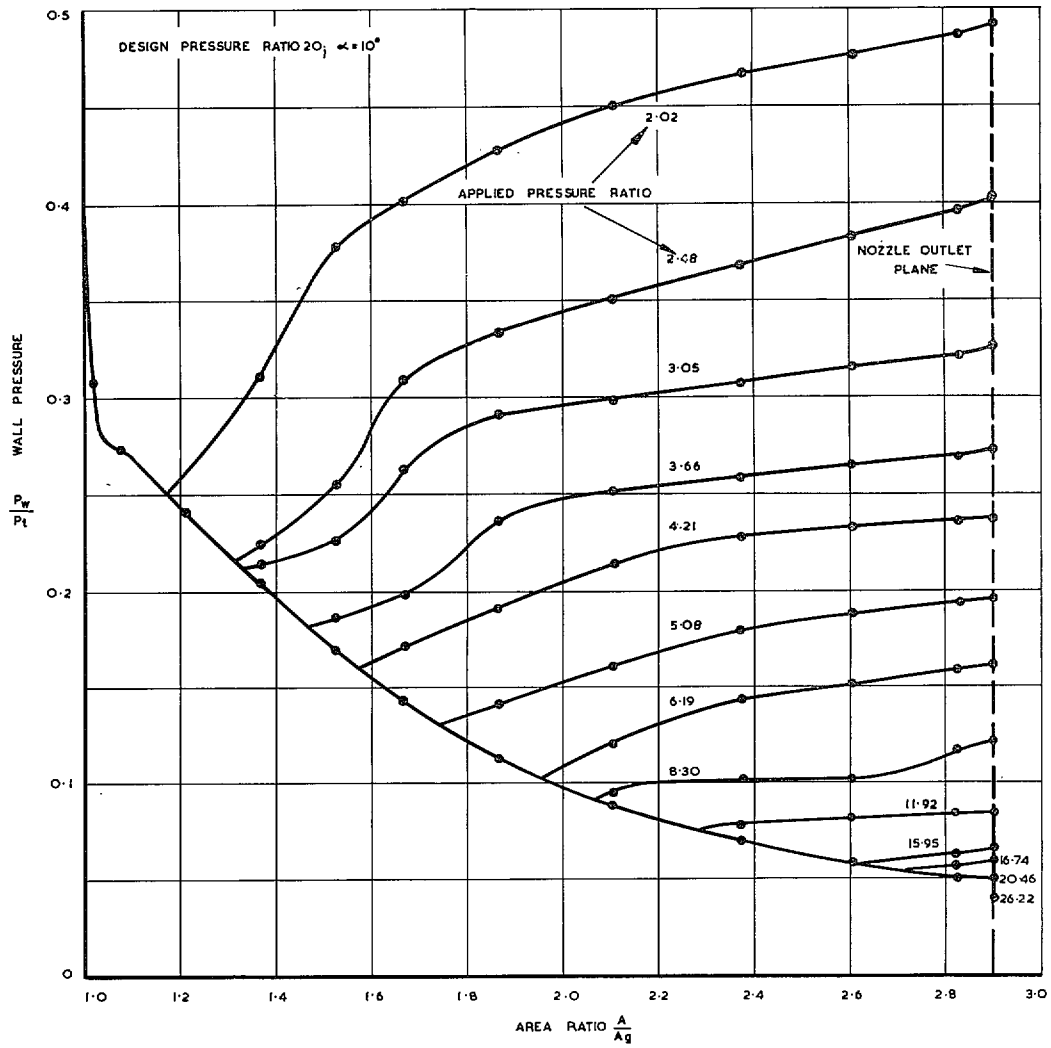

FIG. 28. Wall pressure distribution in conical nozzle with laminar boundary layer.

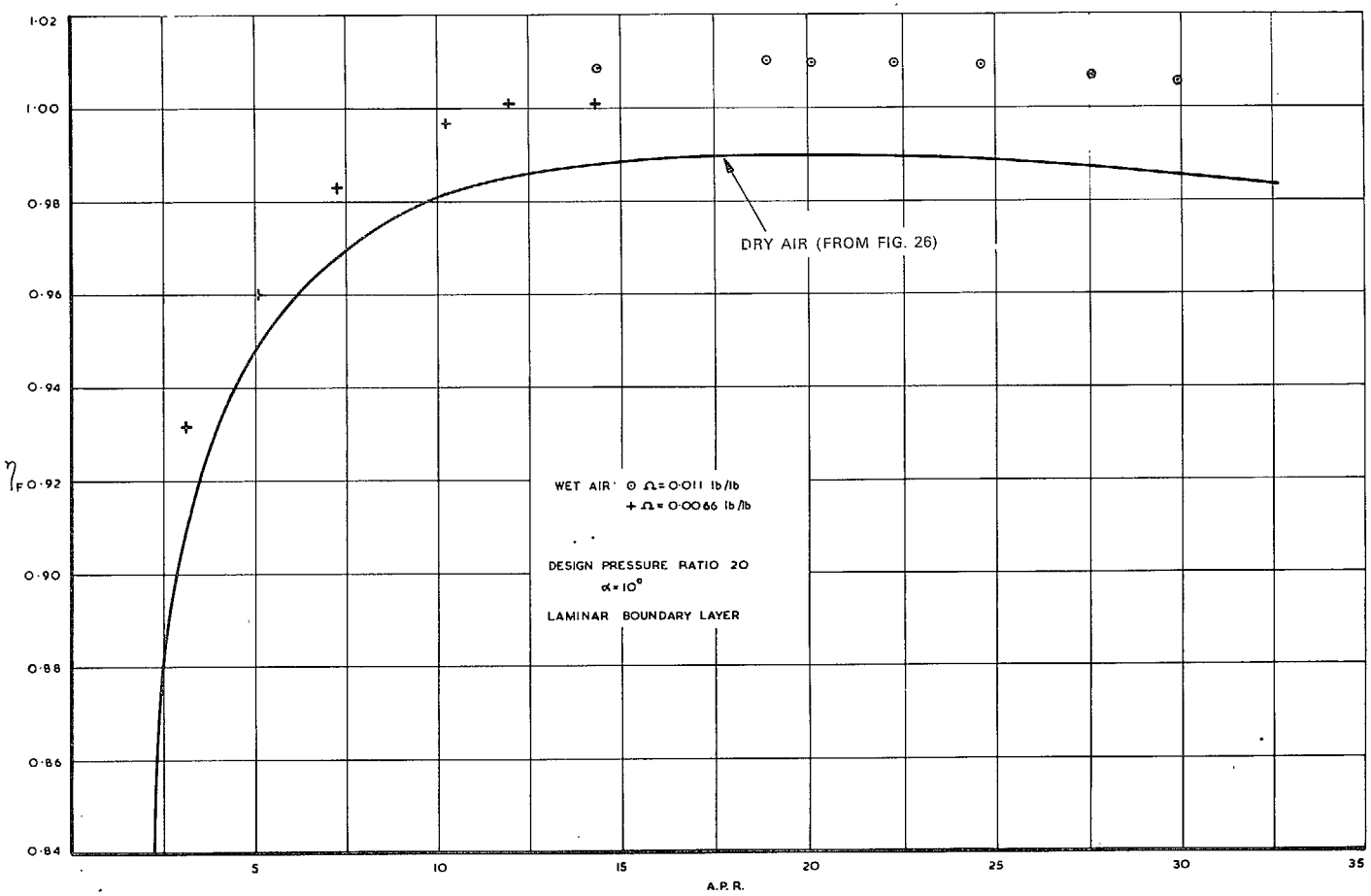

FIG. 29. Effect of humidity on thrust performance of conical nozzles.

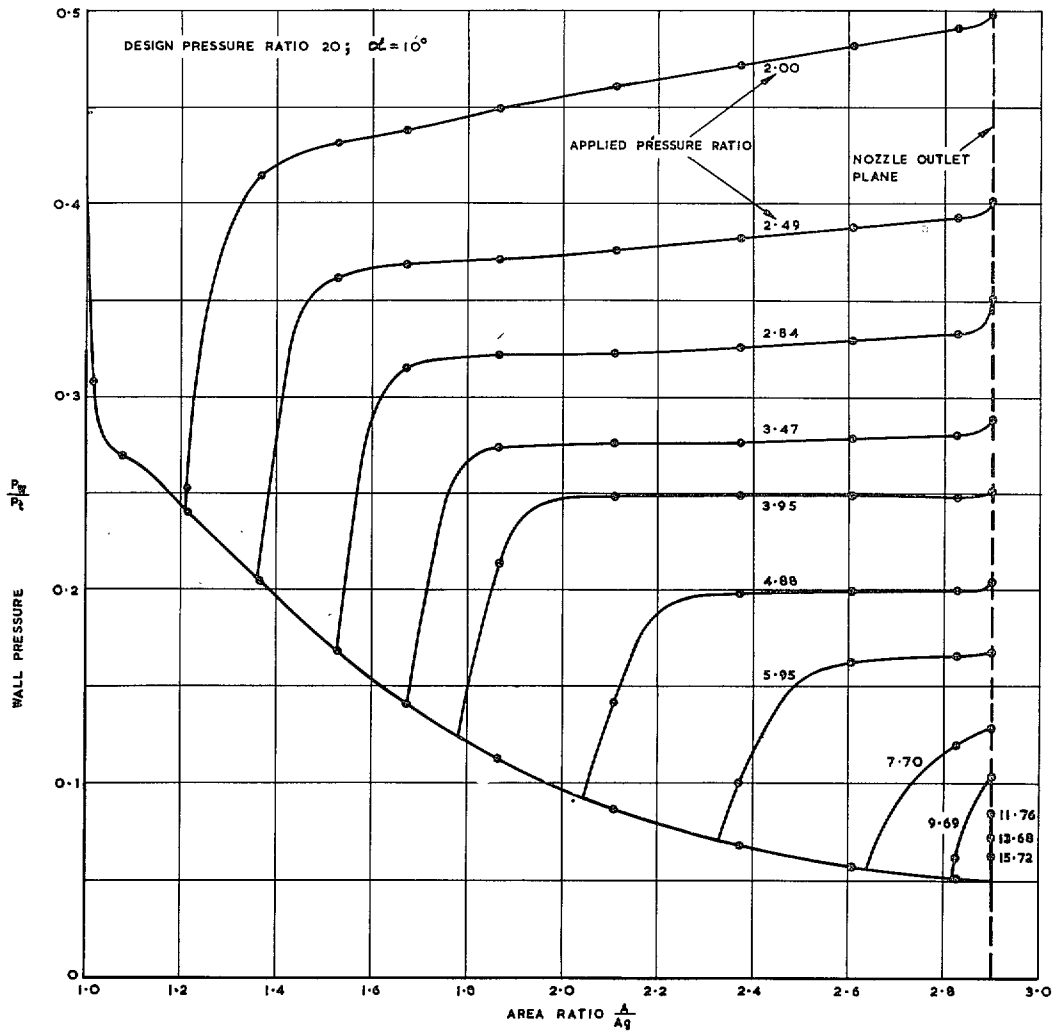

FIG. 30. Wall pressure distribution in conical nozzle with roughened surface.

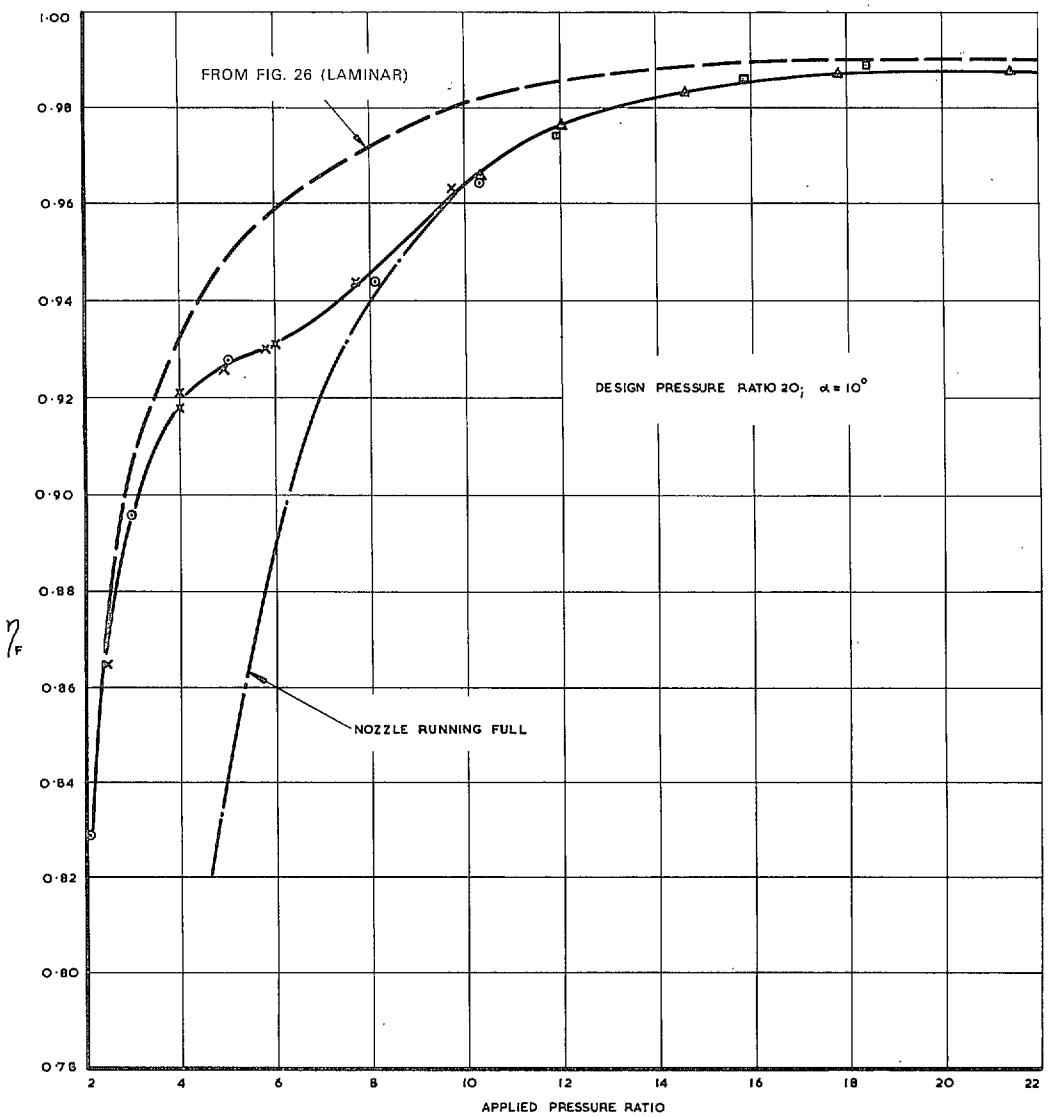

FIG. 31. Thrust efficiency of conical nozzle with roughened surface.

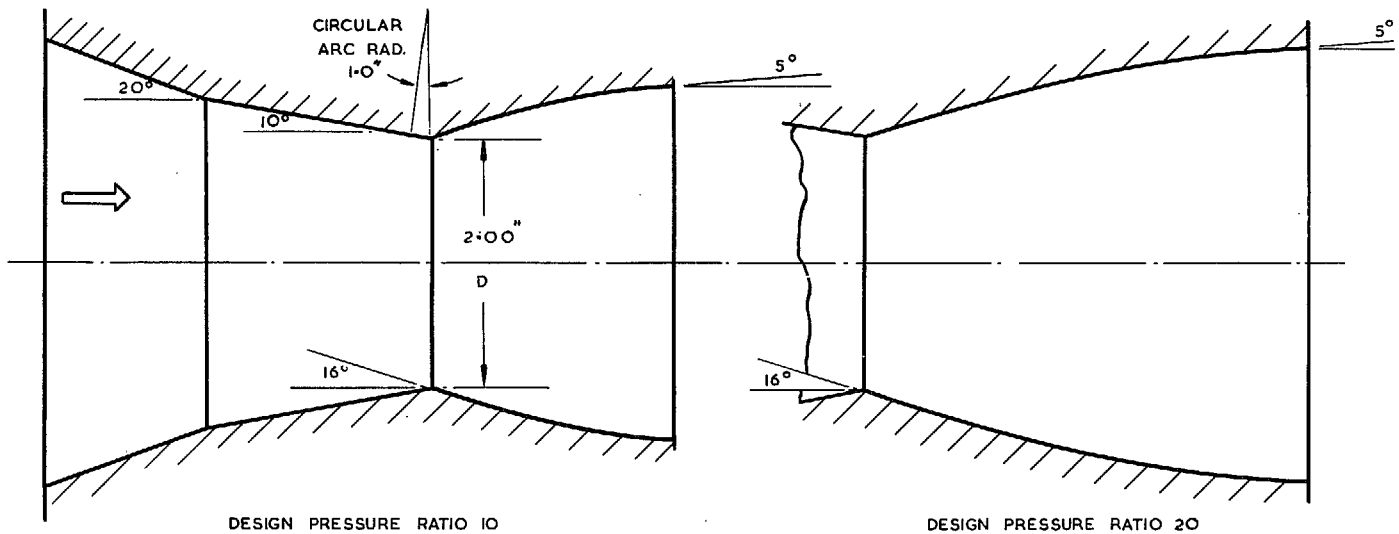

FIG. 32. Axisymmetric 'tulip' nozzle geometry.

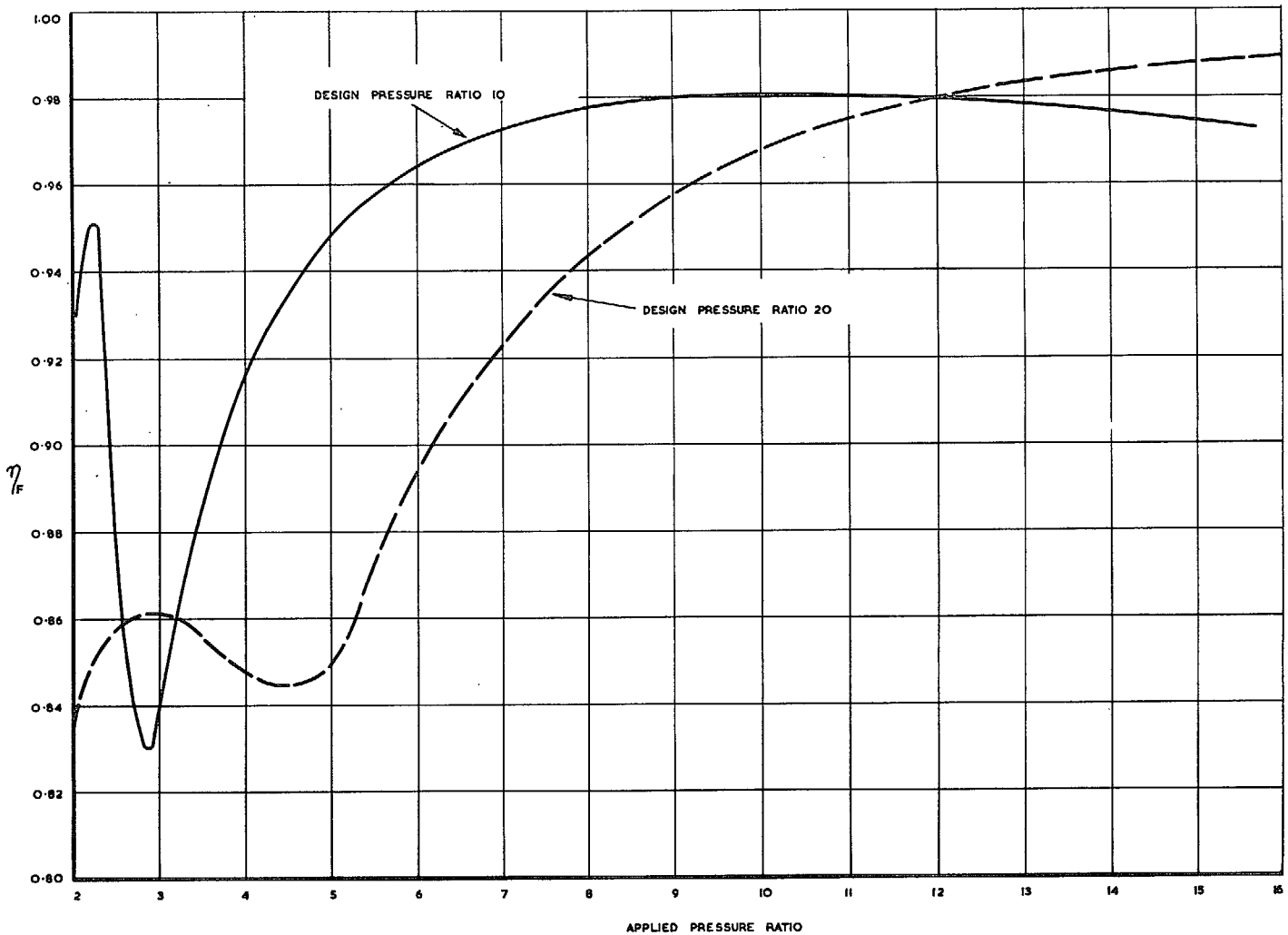

FIG. 33. Thrust efficiency of axisymmetric 'tulip' nozzles.

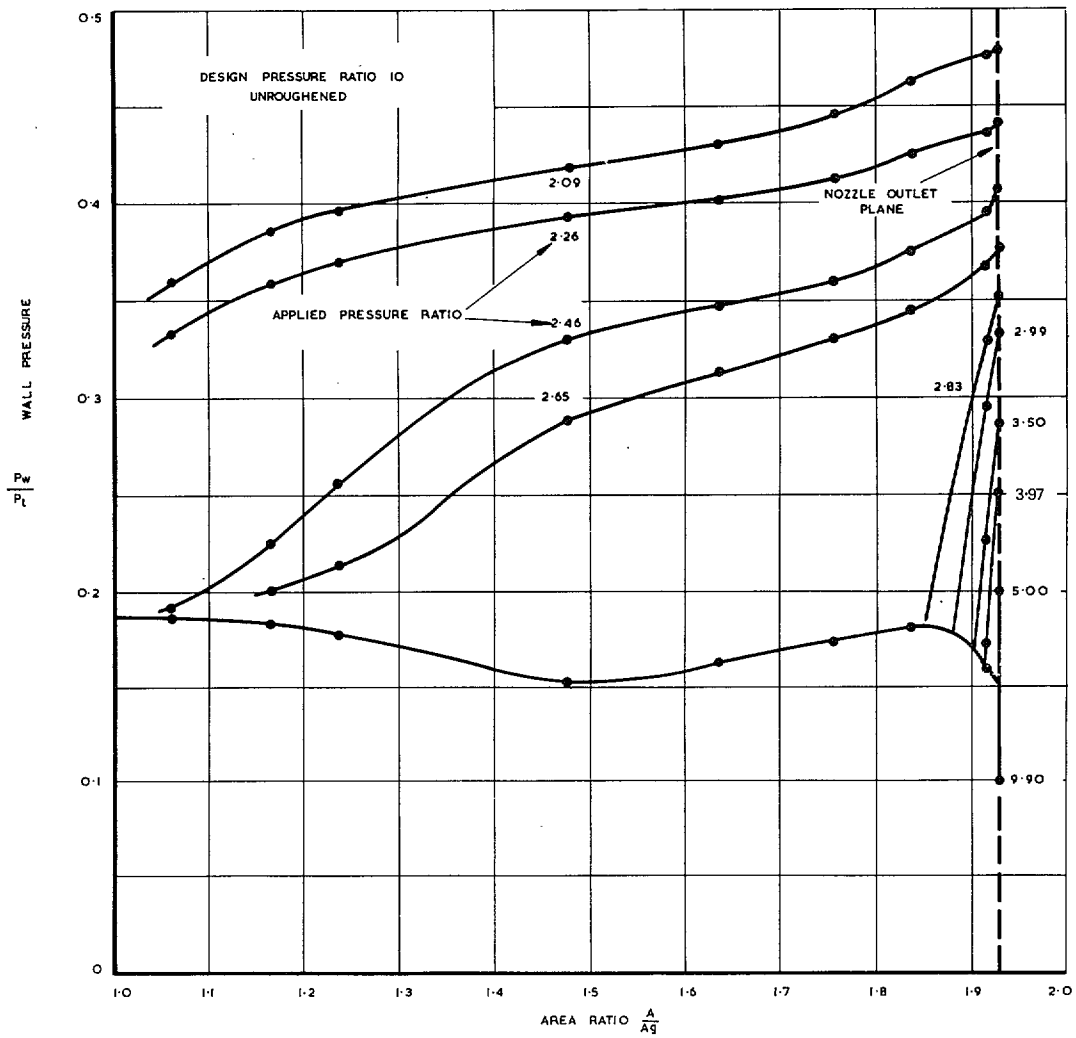

FIG. 34. Wall pressure distribution in axisymmetric 'tulip' nozzles – I.

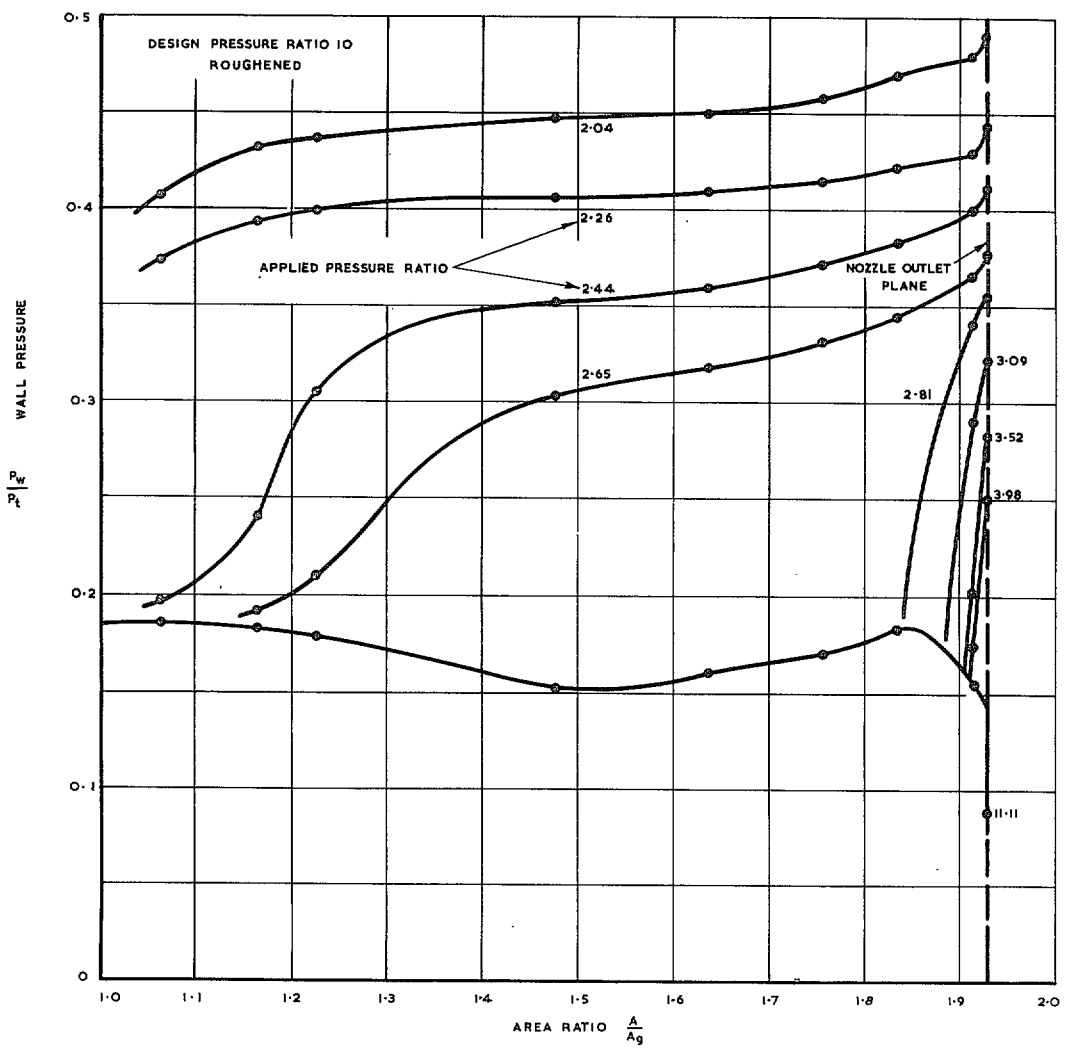

FIG. 35. Wall pressure distribution in axisymmetric 'tulip' nozzles – II.

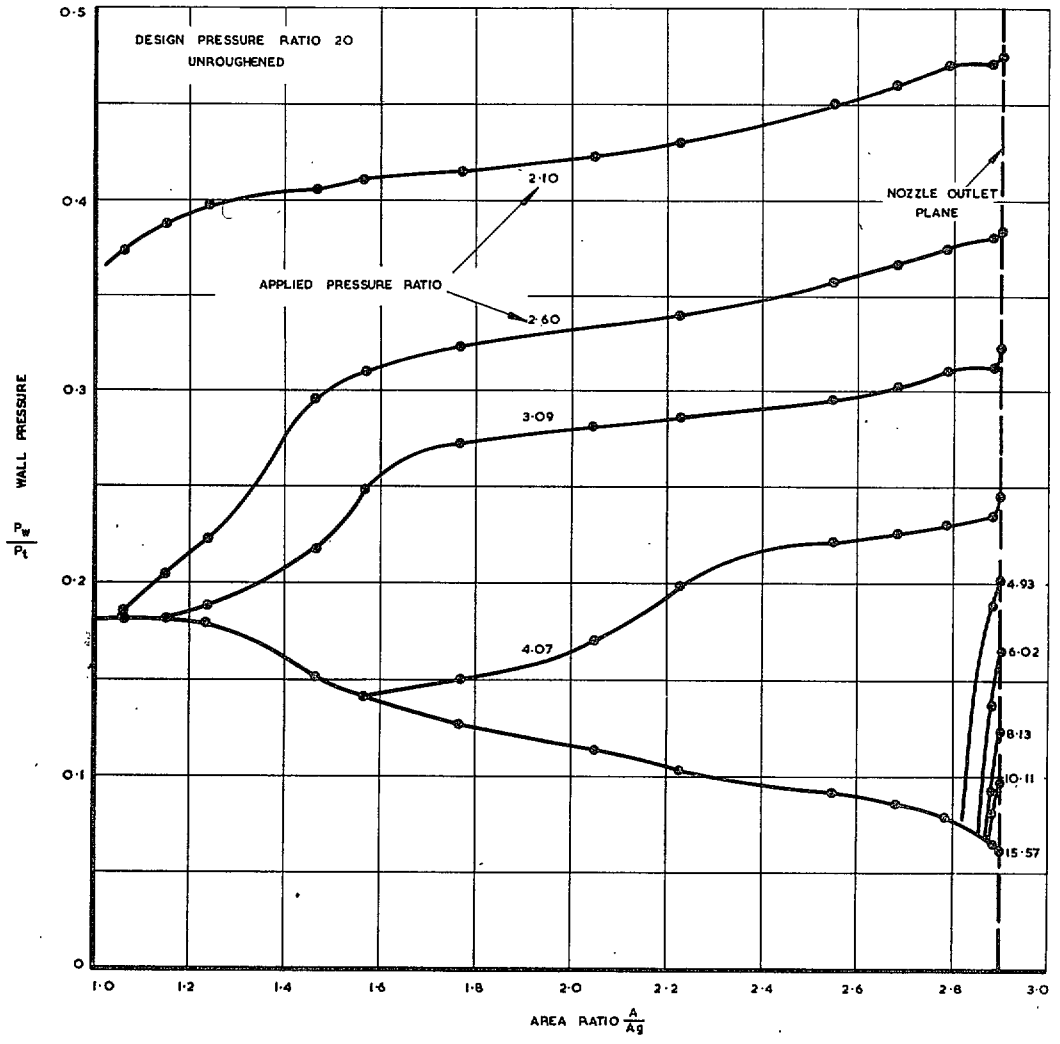

FIG. 36. Wall pressure distribution in axisymmetric 'tulip' nozzles – III.

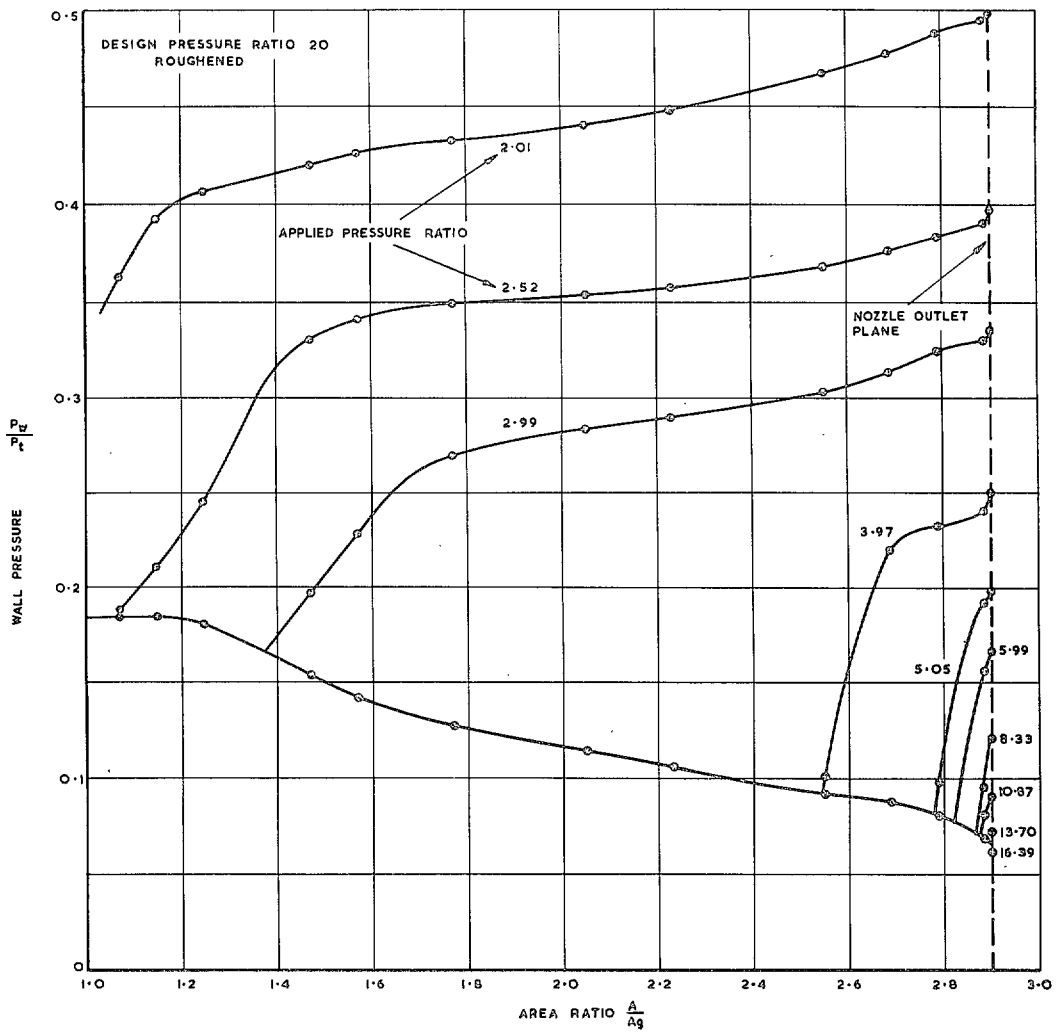

FIG. 37. Wall pressure distribution in axisymmetric 'tulip' nozzles – IV

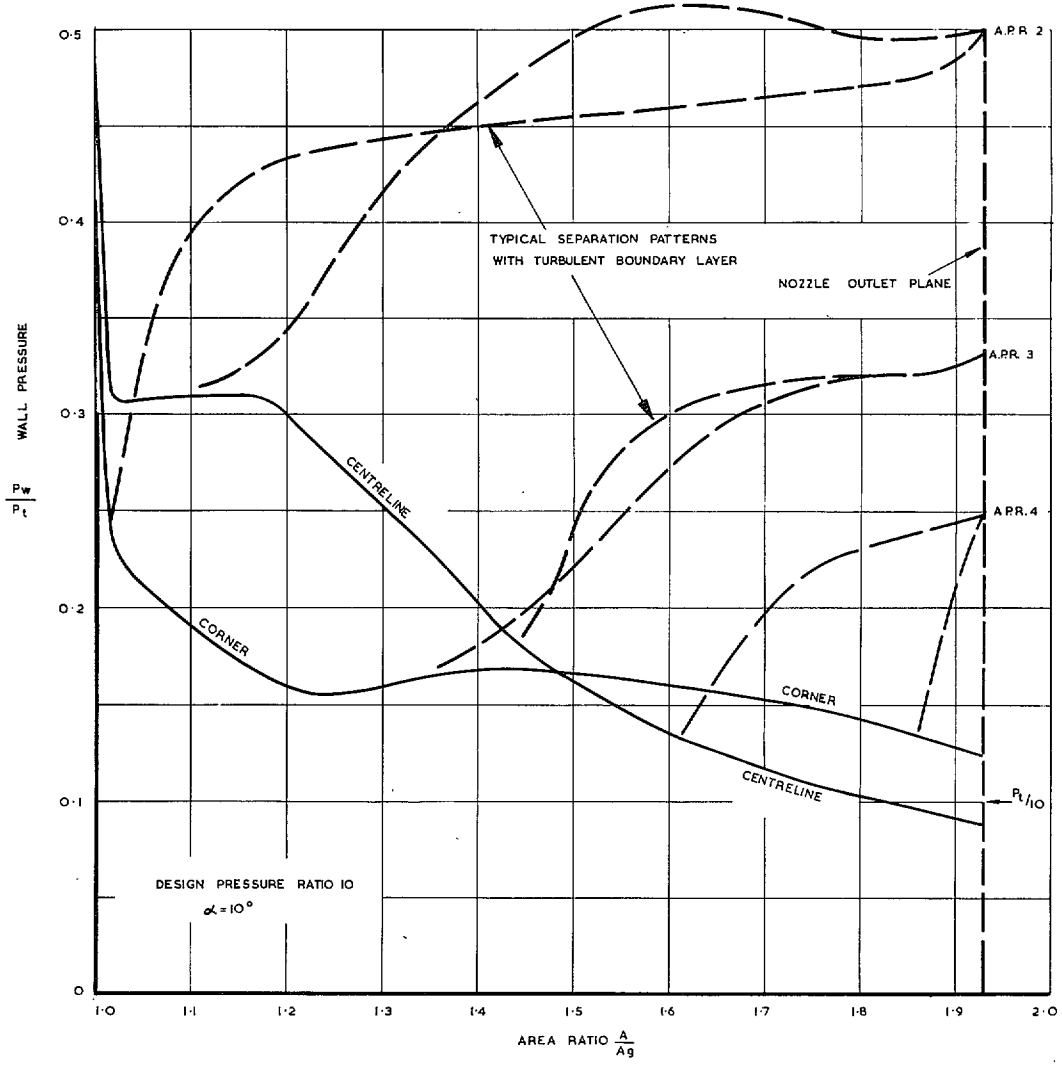

FIG. 38. Wall pressure distribution in square nozzle.

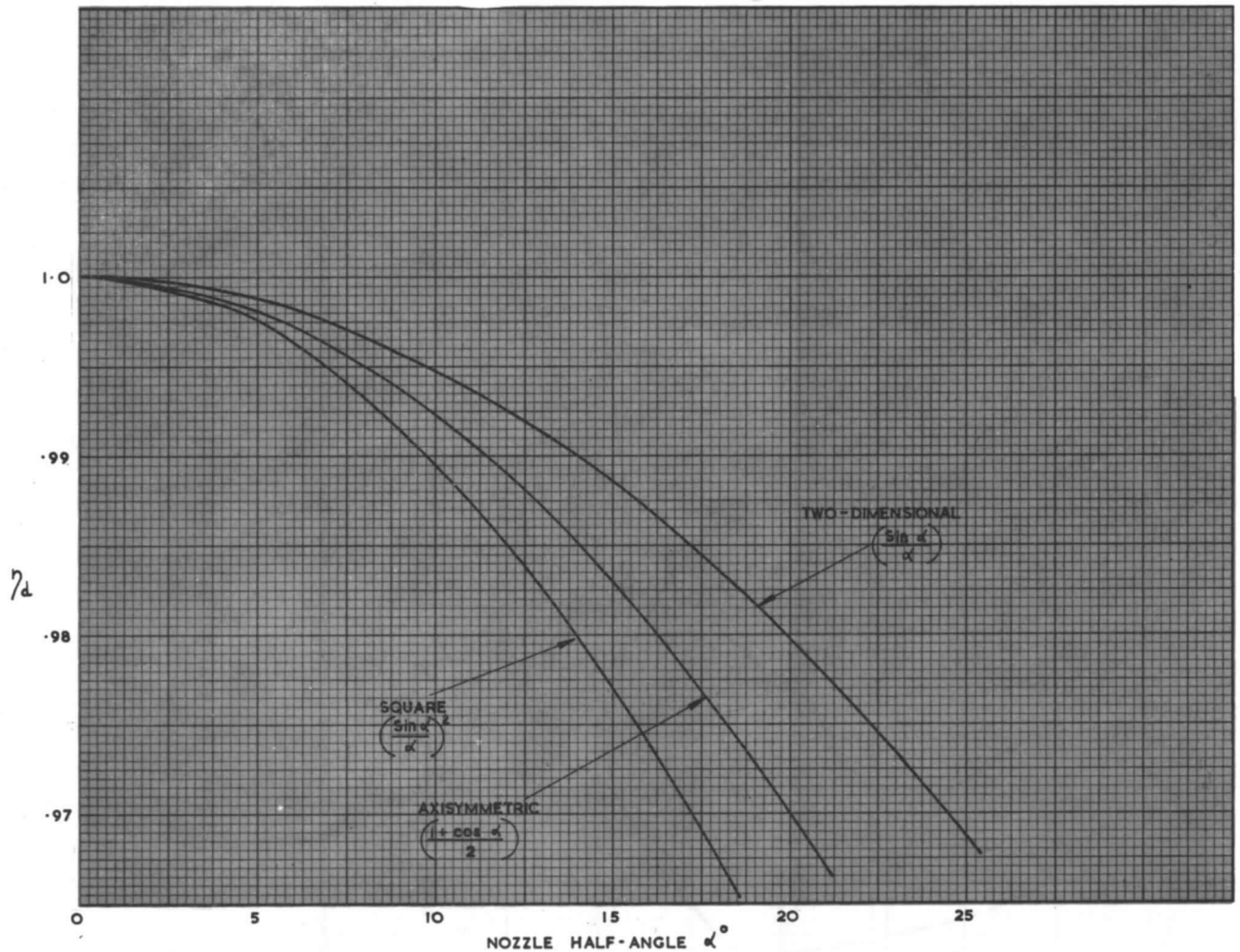

FIG. 39. Divergence loss factors.

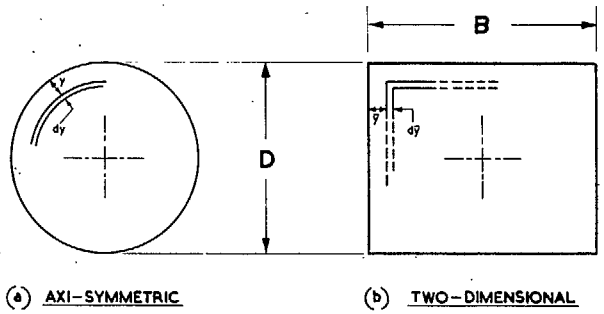

FIG. 40. Definition of nozzle dimensions.

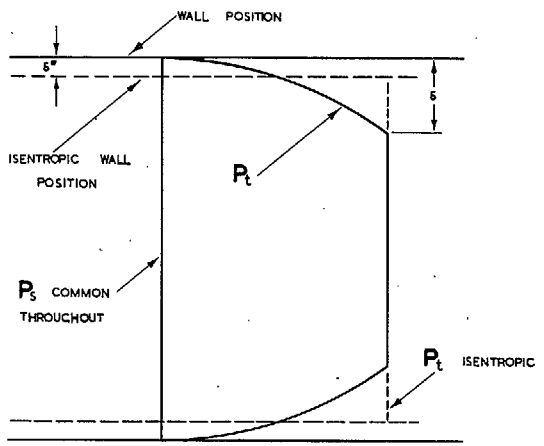

FIG. 41. Nozzle pressure profiles.

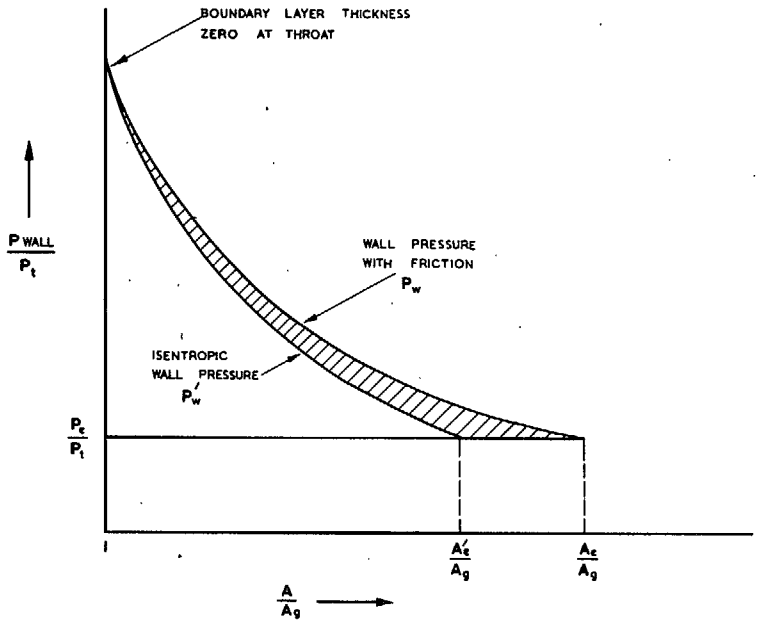

FIG. 42. Diagram describing 'displacement loss'.

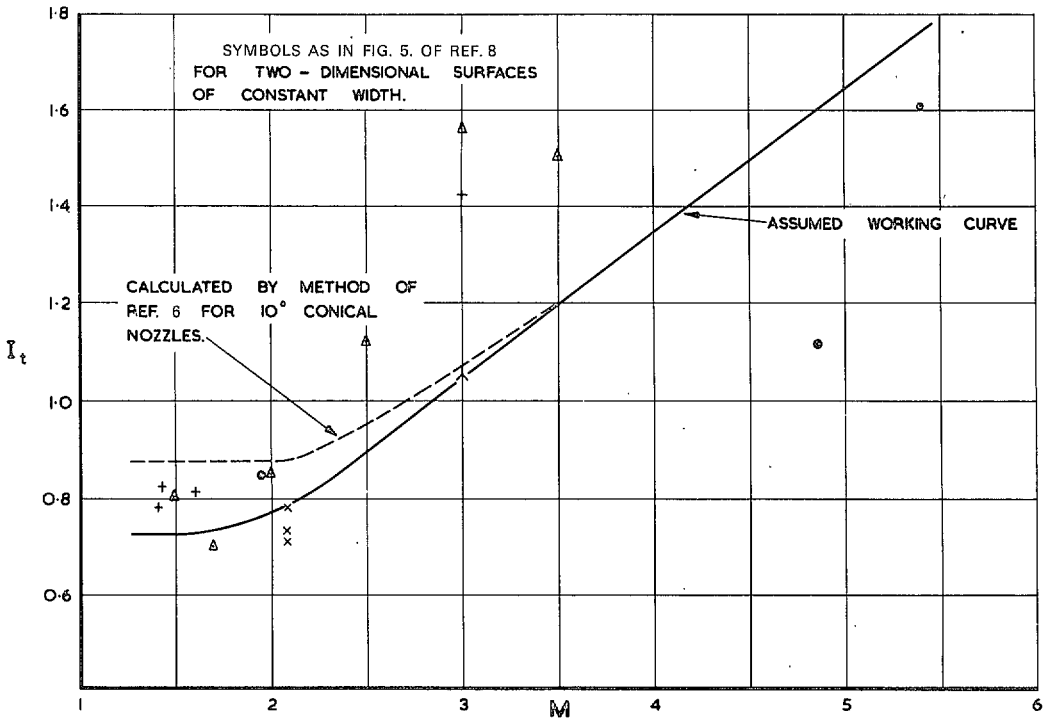

FIG. 43. Pressure gradient factor for turbulent boundary layer.

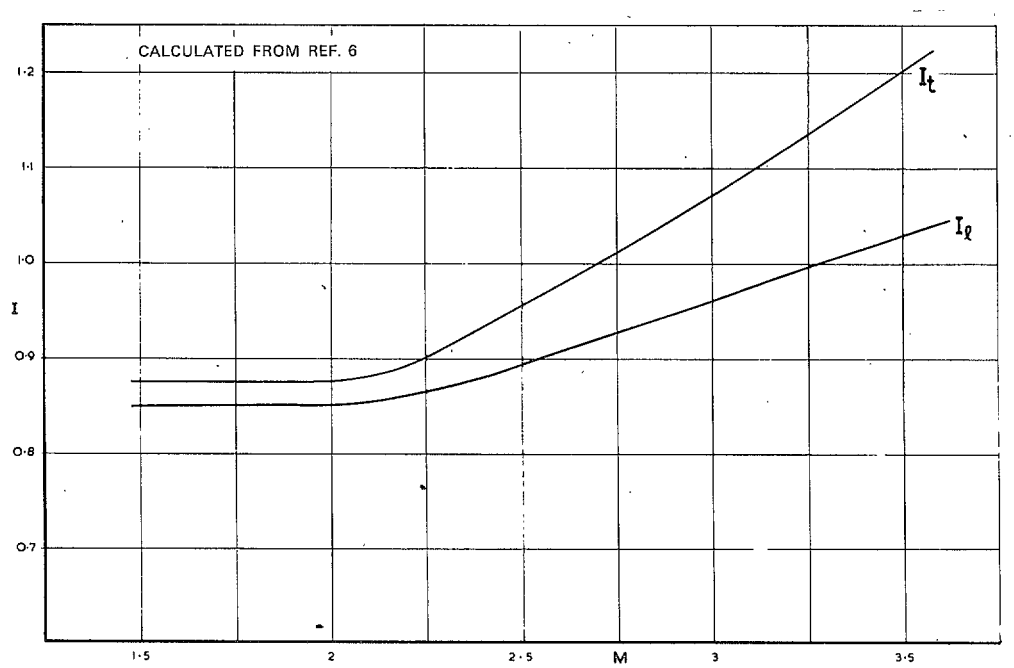

FIG. 44. Laminar and turbulent pressure gradient factors for 10 deg. conical nozzles.

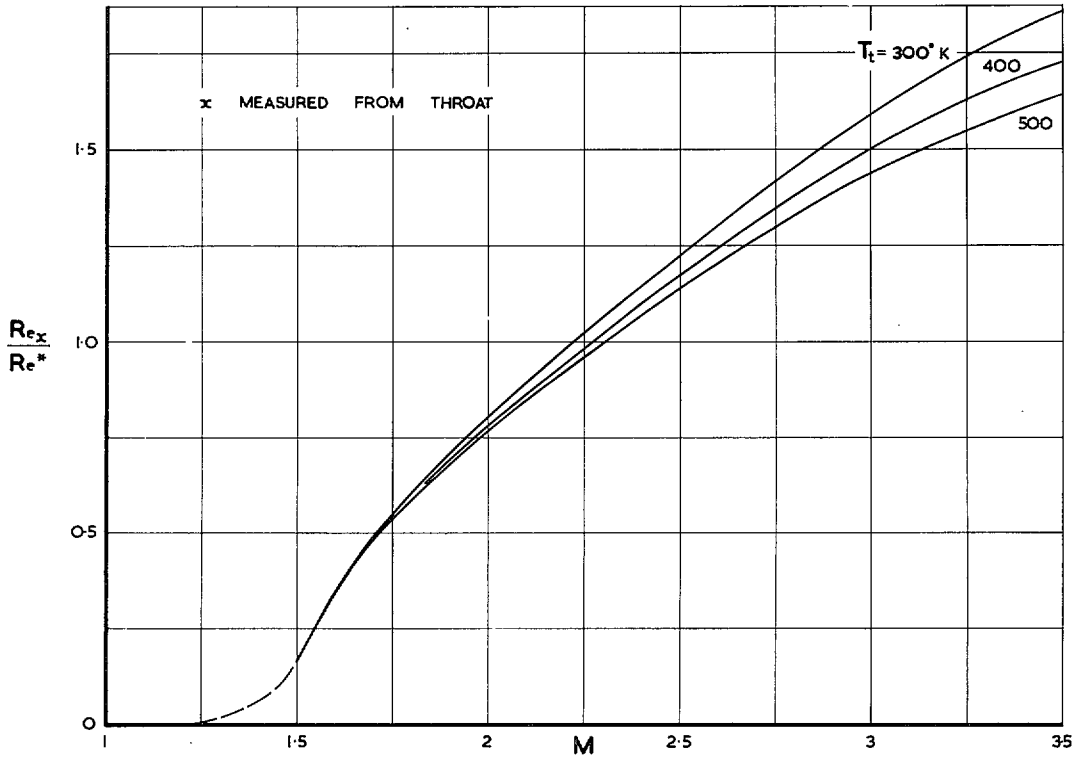

FIG. 45. Reynolds number variation along 10 deg. conical nozzle.

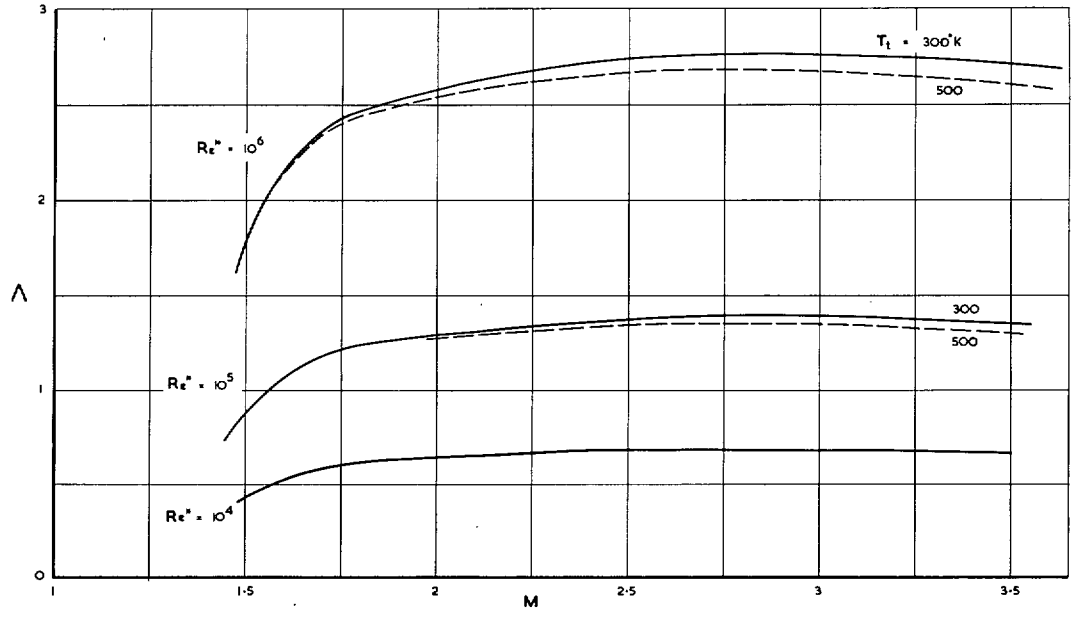

FIG. 46. Ratio of turbulent to laminar momentum thickness.

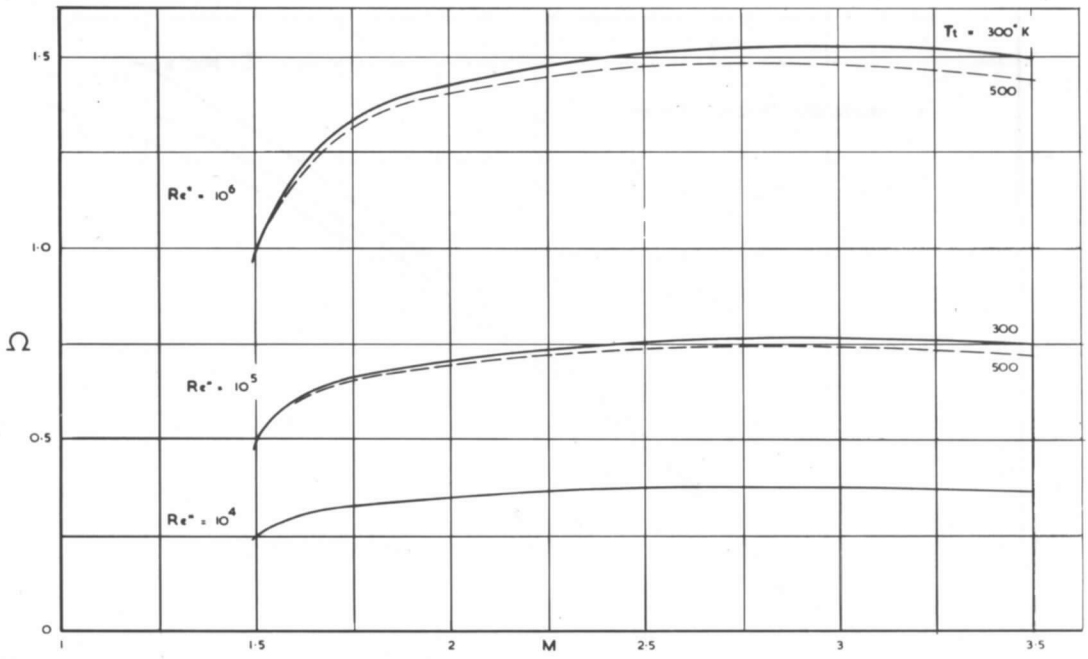

FIG. 47. Ratio of turbulent to laminar displacement thickness.

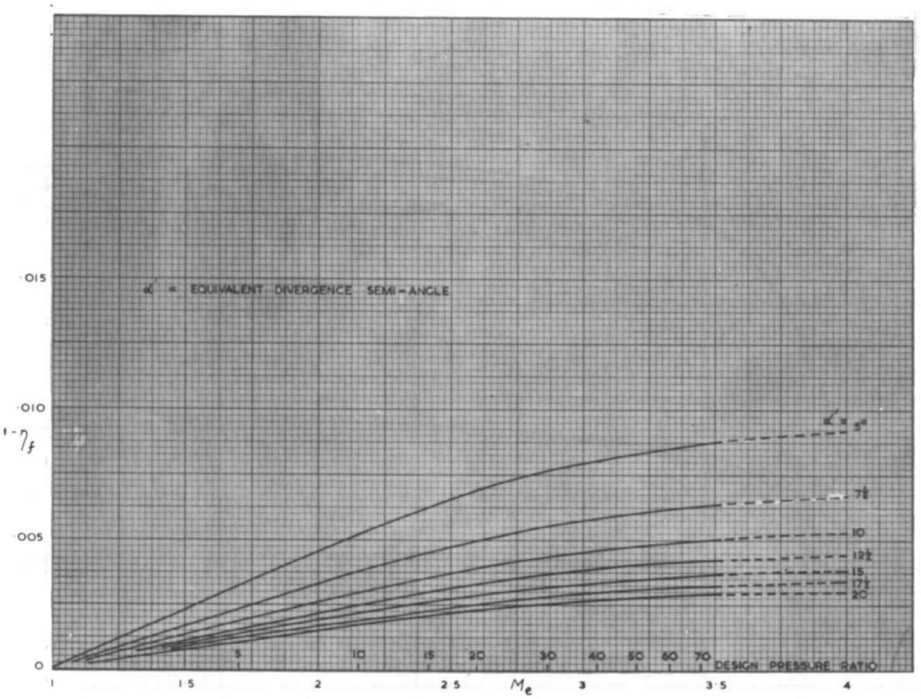

FIG. 48. 'Momentum loss' for axisymmetric & square nozzles – I. Turbulent boundary layer: $Re^* = 4 \times 10^6$.

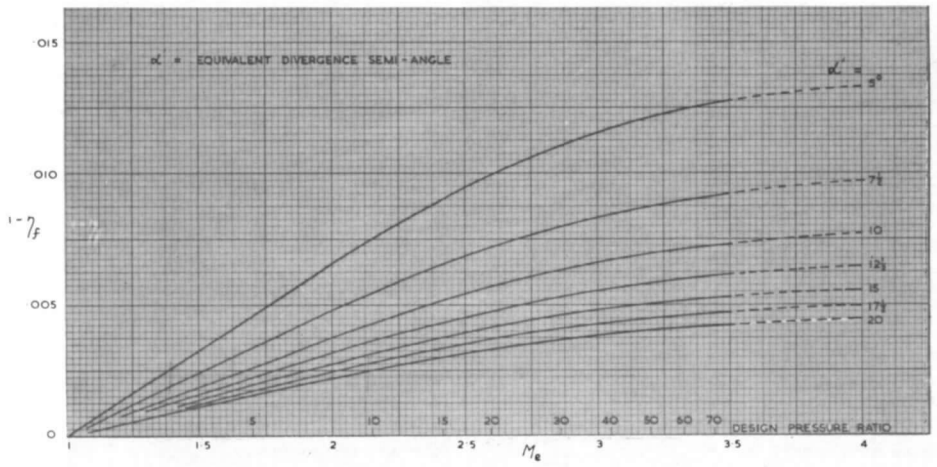

FIG. 49. 'Momentum loss' for axisymmetric & square nozzles – II. Turbulent boundary layer: $Re^* = 0{\cdot}6 \times 10^6$.

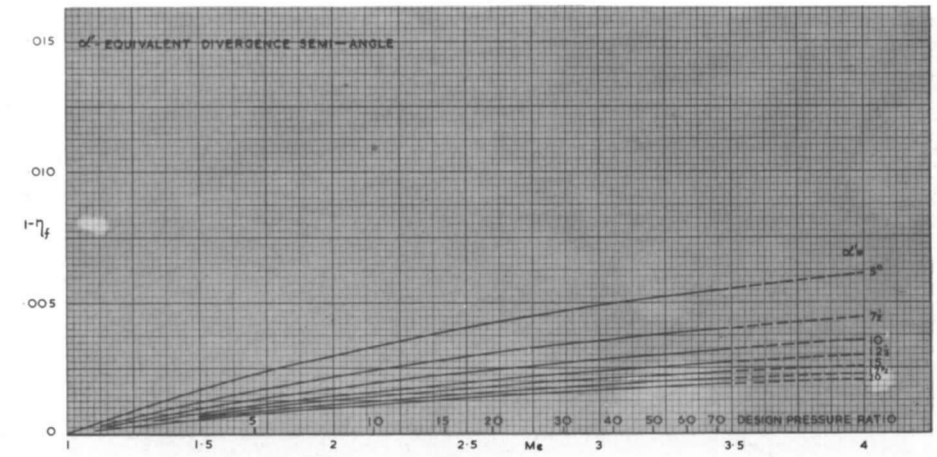

FIG. 50. 'Momentum loss' for axisymmetric & square nozzles – III. Laminar boundary layer: $Re^* = 0{\cdot}6 \times 10^6$.

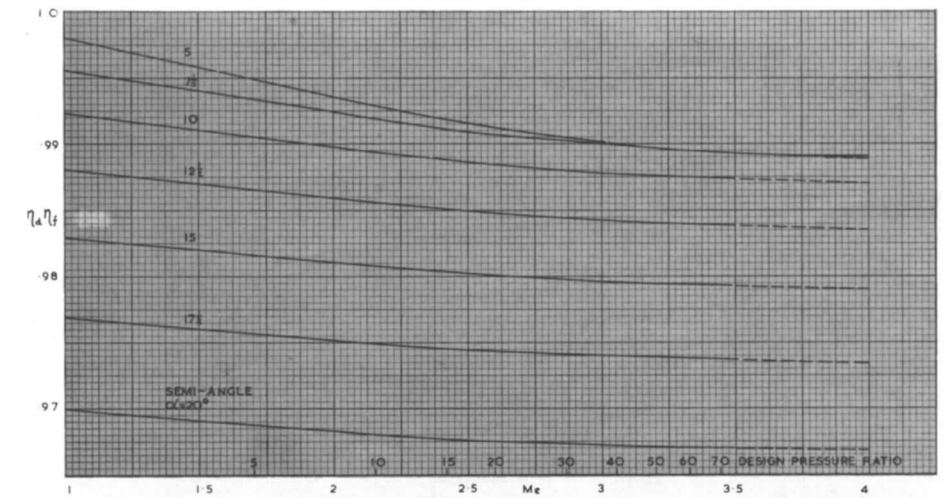

FIG. 51. Momentum & divergence losses for conical nozzles – I. Turbulent boundary layer: $Re^* = 4 \times 10^6$.

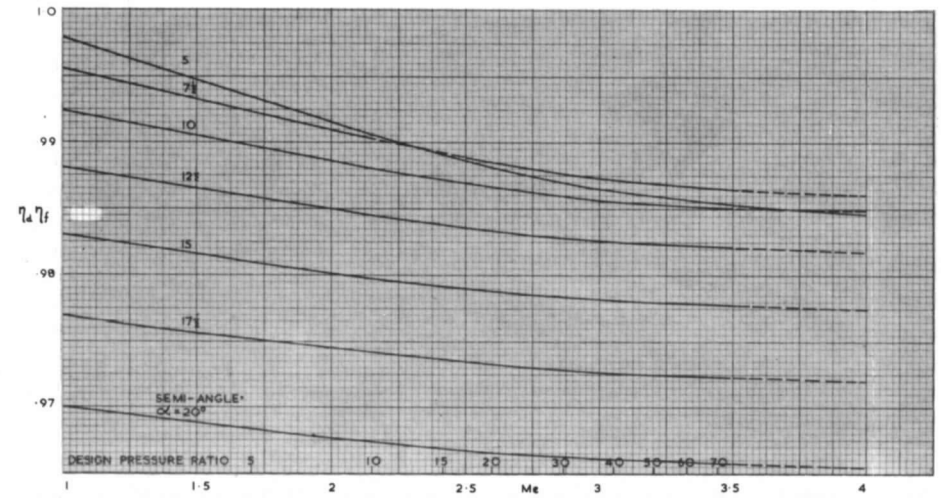

FIG. 52. Momentum & divergence losses for conical nozzles – II. Turbulent boundary layer: $Re^* = 0{\cdot}6 \times 10^6$.

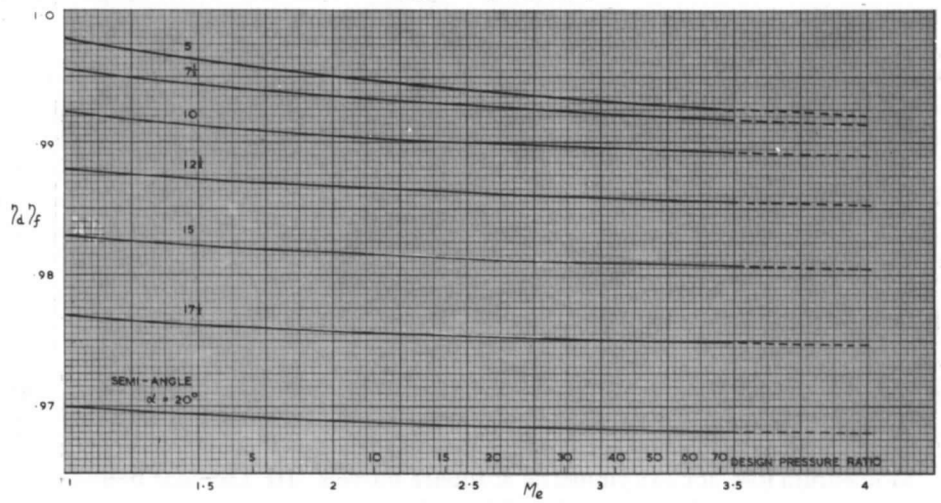

FIG. 53. Momentum & divergence losses for conical nozzles – III. Laminar boundary layer: $Re^* = 0{\cdot}6 \times 10^6$.

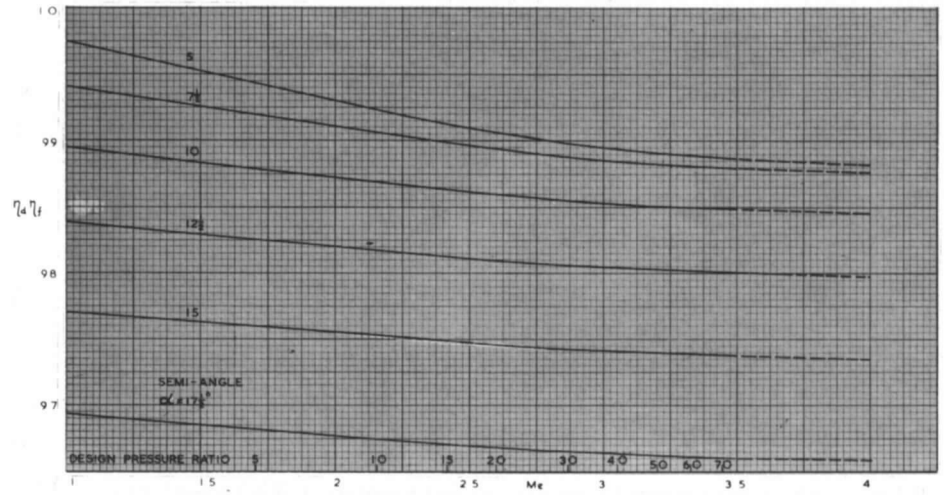

FIG. 54. Momentum & divergence losses for square nozzles – I. Turbulent boundary layer: $Re^* = 4 \times 10^6$.

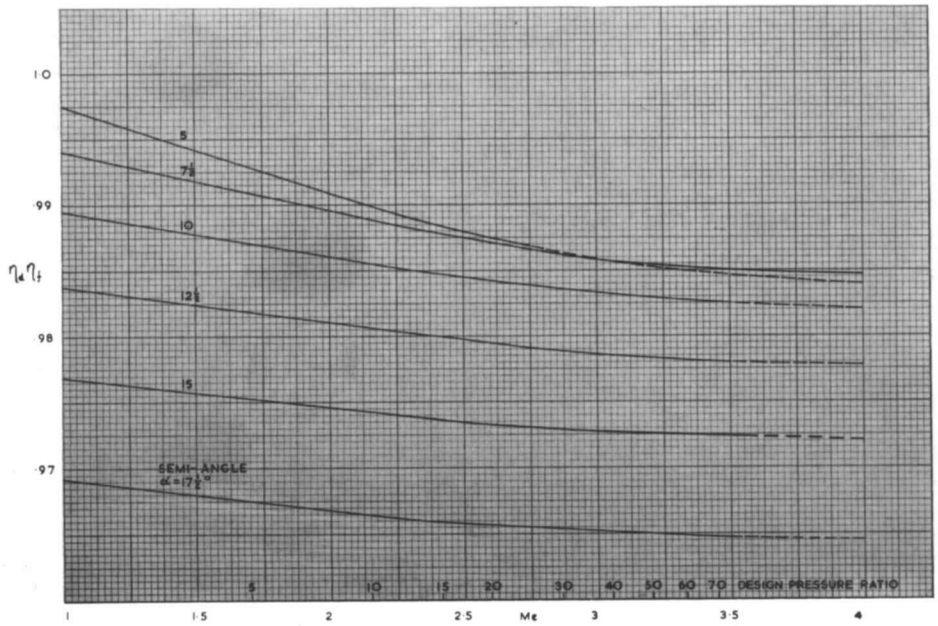

FIG. 55. Momentum & divergence losses for square nozzles – II. Turbulent boundary layer: $Re^* = 0{\cdot}6 \times 10^6$.

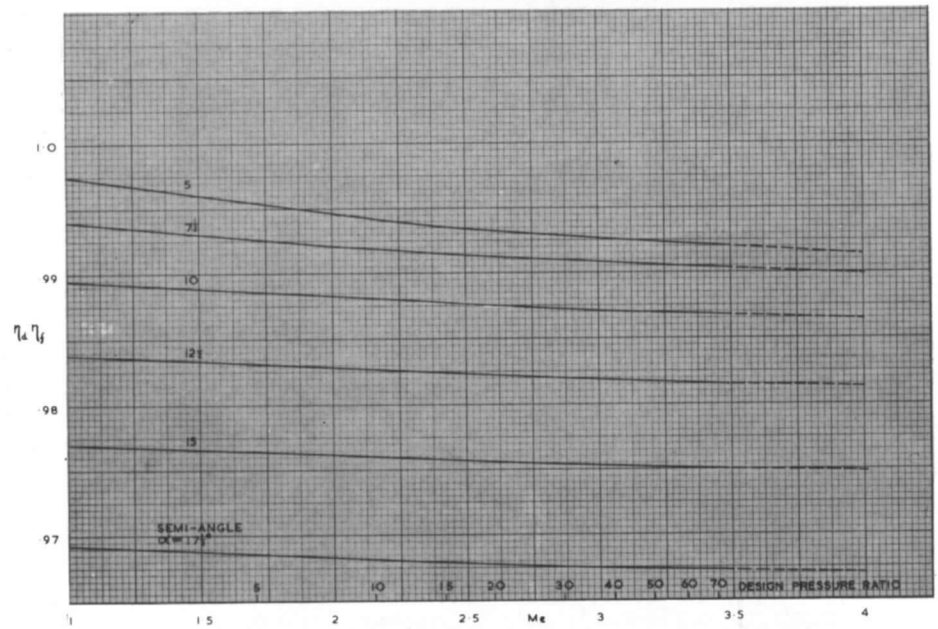

FIG. 56. Momentum & divergence losses for square nozzles – III. Laminar boundary layer: $Re^* = 0{\cdot}6 \times 10^6$.

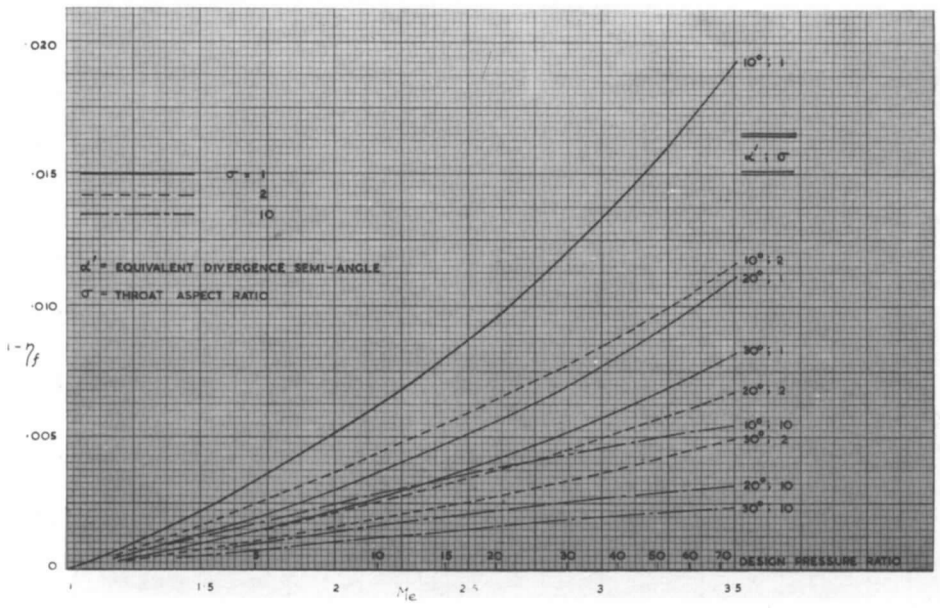

FIG. 57. 'Momentum loss' for two-dimensional nozzles – I. Turbulent boundary layer: $Re^* = 4 \times 10^6$.

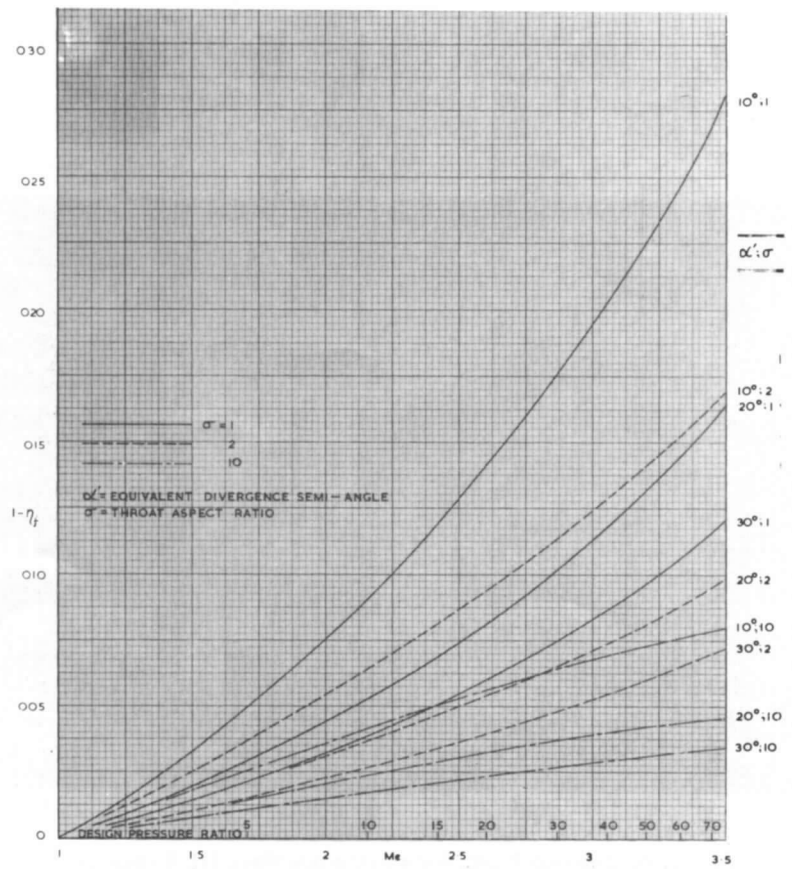

FIG. 58. 'Momentum loss' for two-dimensional nozzles – II. Turbulent boundary layer: $Re^* = 0{\cdot}6 \times 10^6$.

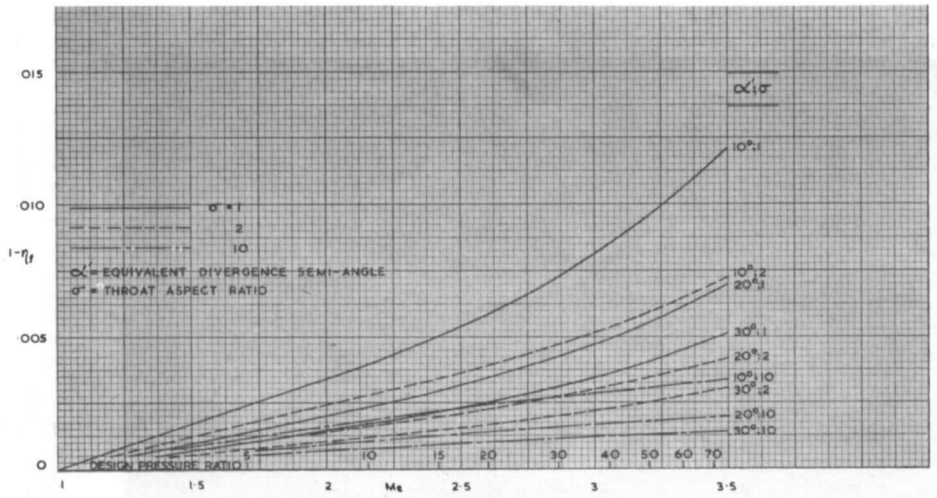

FIG. 59. 'Momentum loss' for two-dimensional nozzles – III. Laminar boundary layer: $Re^* = 0{\cdot}6 \times 10^6$.

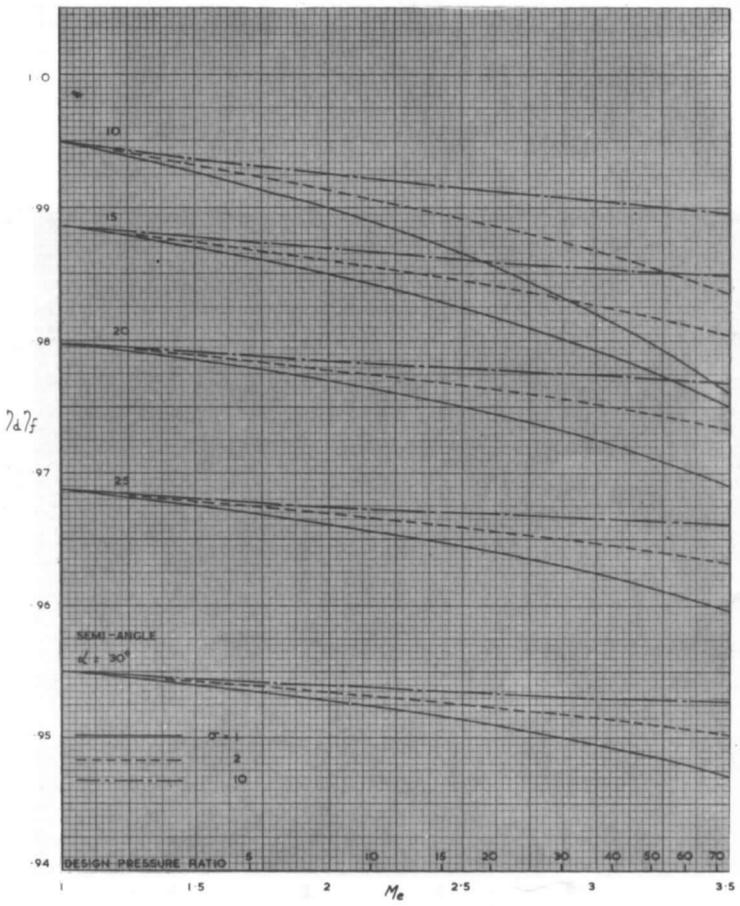

FIG. 60. Momentum & divergence losses for two-dimensional nozzles – I. Turbulent boundary layer: $Re^* = 4 \times 10^6$.

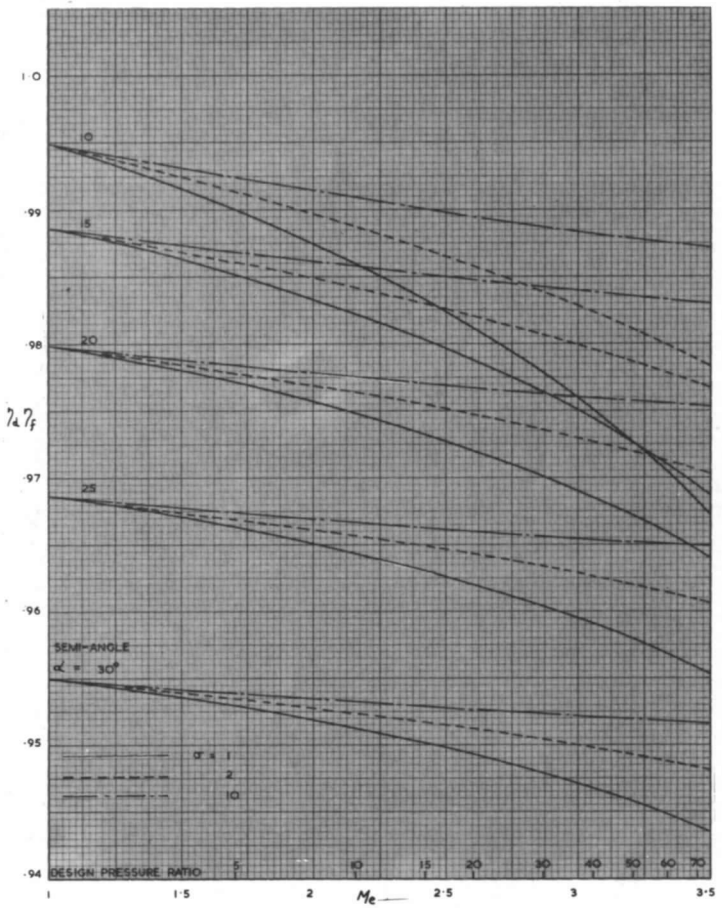

FIG. 61. Momentum & divergence losses for two-dimensional nozzles – II. Turbulent boundary layer: $Re^* = 0{\cdot}6 \times 10^6$.

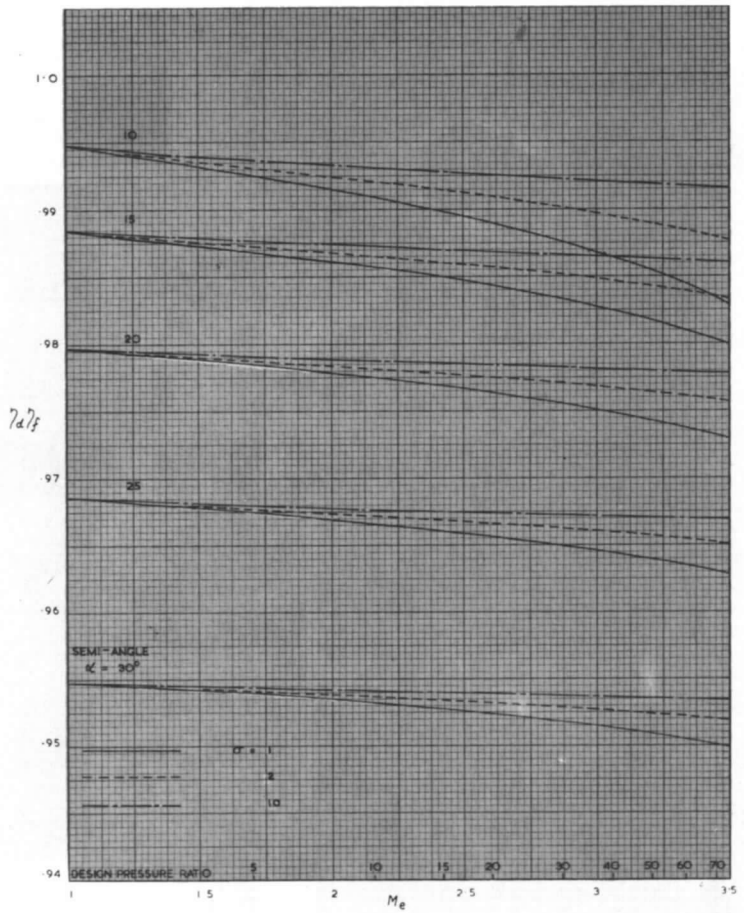

FIG. 62. Momentum & divergence losses for two-dimensional nozzles – III. Laminar boundary layer: $Re^* = 0{\cdot}6 \times 10^6$.

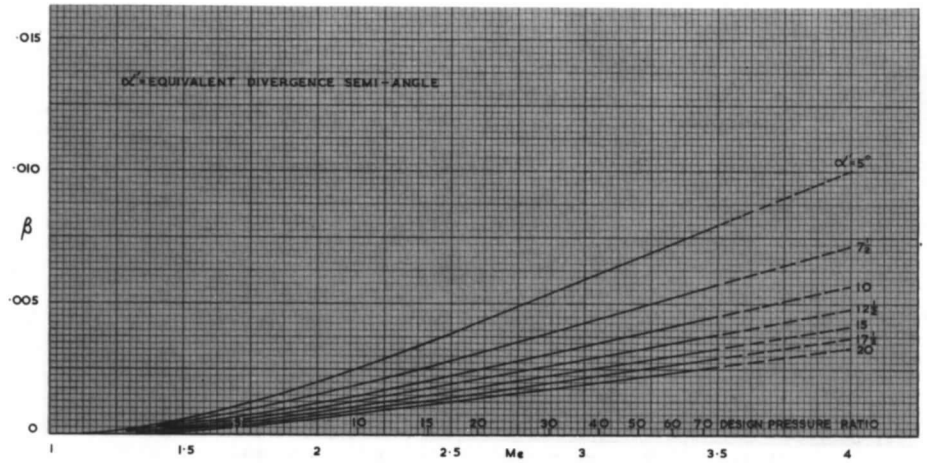

FIG. 63. 'Displacement loss' for axisymmetric & square nozzles – I. Turbulent boundary layer: $Re^* = 4 \times 10^6$.

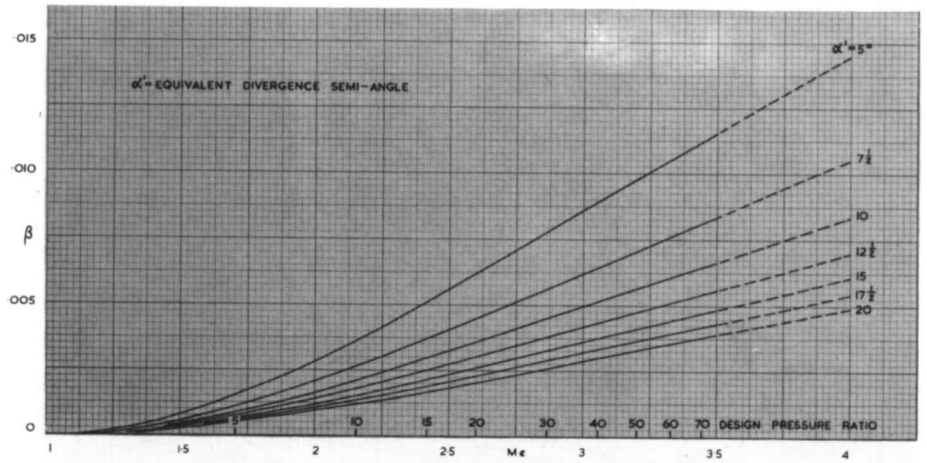

FIG. 64. 'Displacement loss' for axisymmetric & square nozzles – II. Turbulent boundary layer: $Re^* = 0{\cdot}6 \times 10^6$.

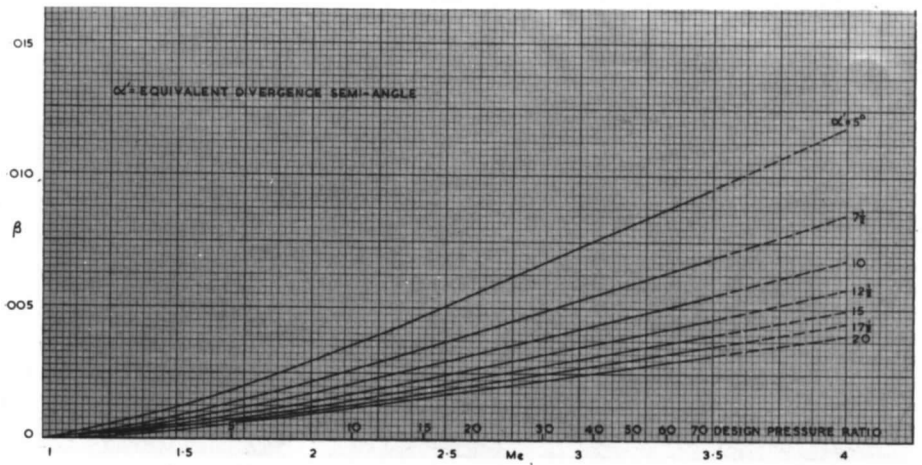

FIG. 65. 'Displacement loss' for axisymmetric & square nozzles – III. Laminar boundary layer: $Re^* = 0{\cdot}6 \times 10^6$.

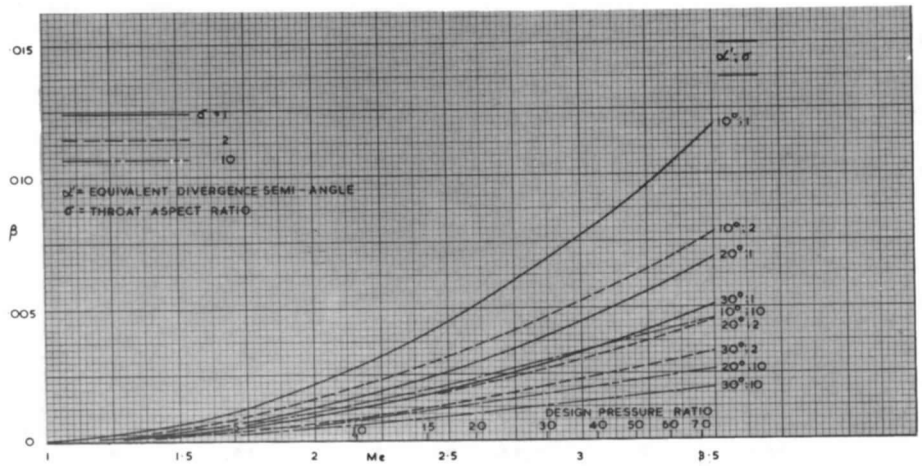

FIG. 66. 'Displacement loss' for two-dimensional nozzles – I. Turbulent boundary layer: $Re^* = 4 \times 10^6$.

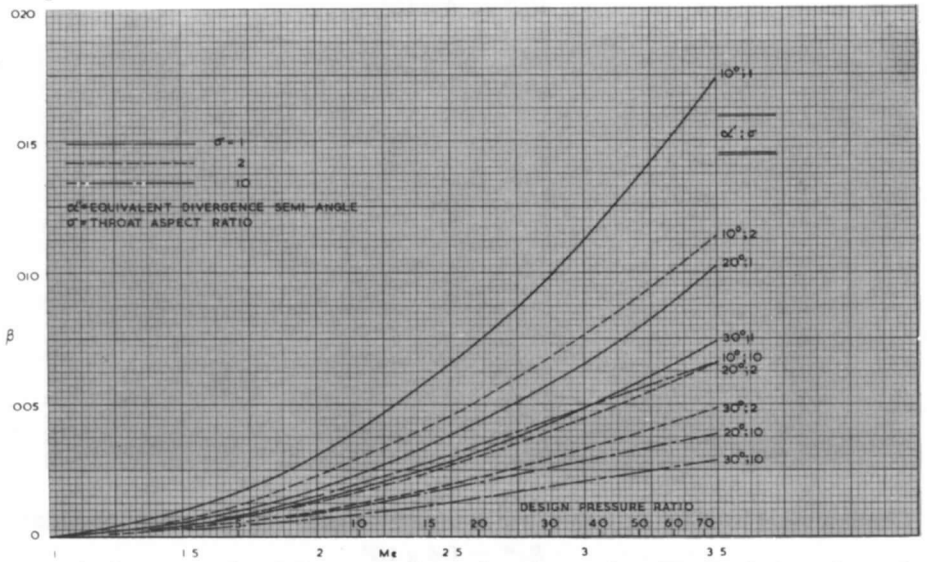

FIG. 67. 'Displacement loss' for two-dimensional nozzles – II. Turbulent boundary layer: $Re^* = 0{\cdot}6 \times 10^6$.

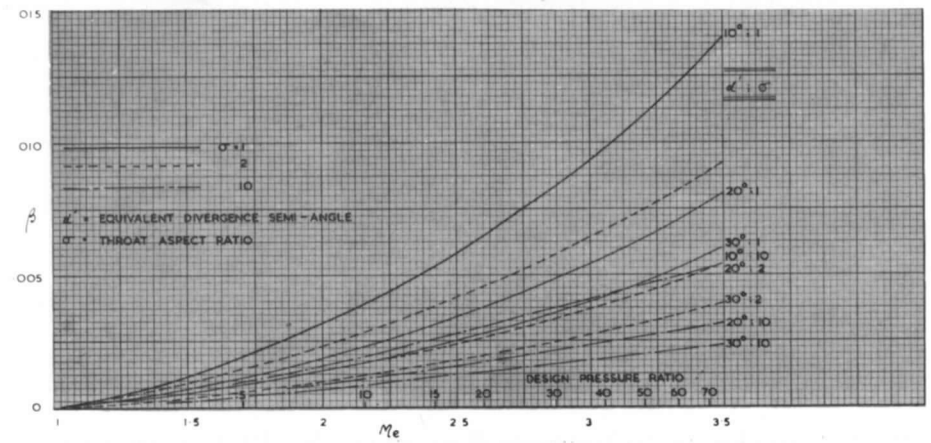

FIG. 68. 'Displacement loss' for two-dimensional nozzles – III. Laminar boundary layer: $Re^* = 0{\cdot}6 \times 10^6$.

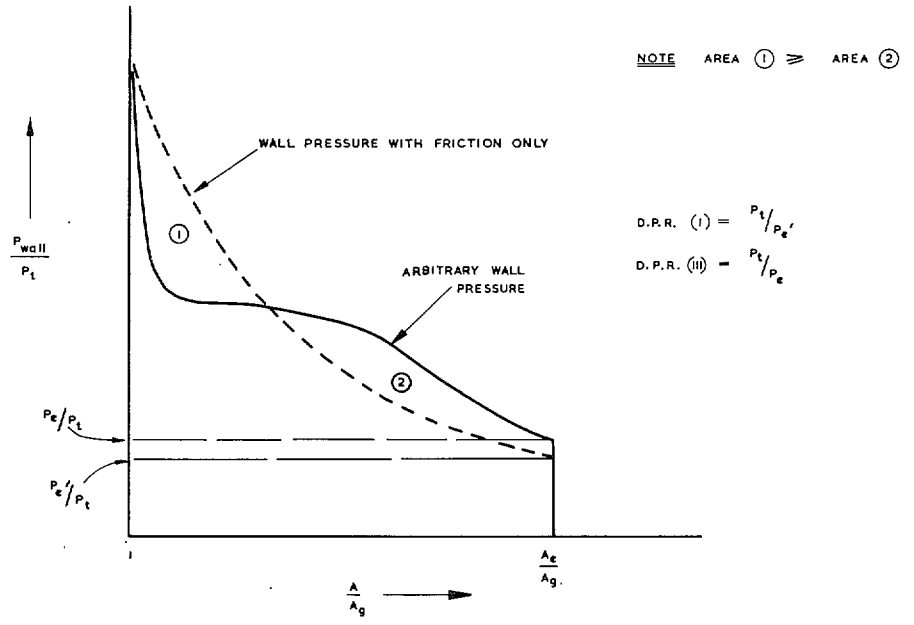

FIG. 69. Diagram to describe definitions of design pressure ratio.

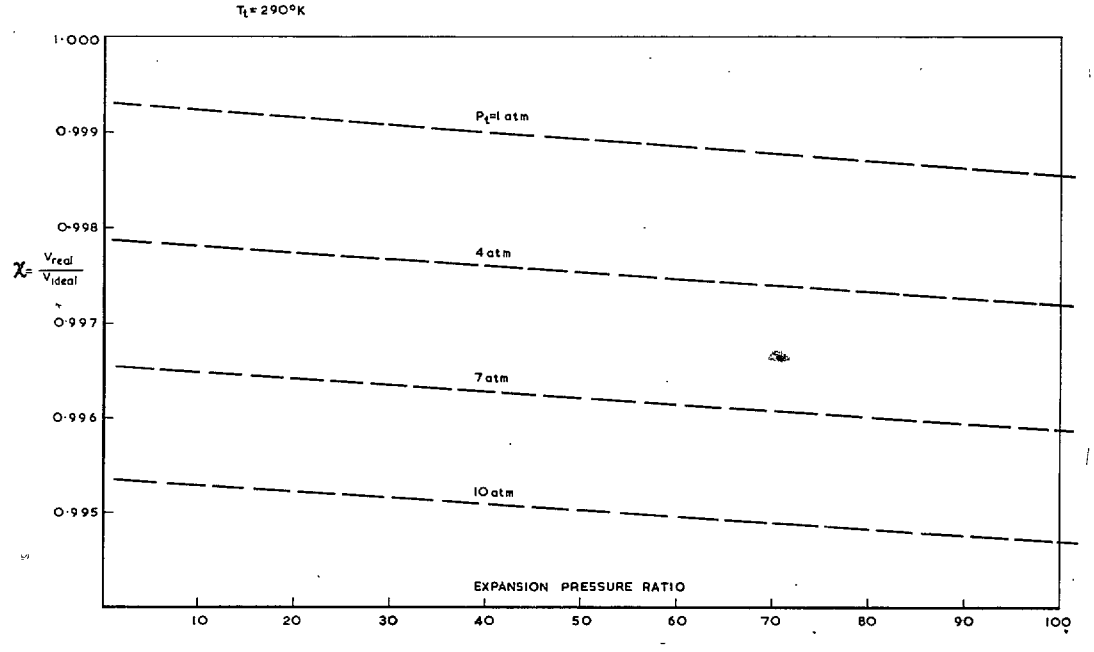

FIG. 70. Correction factor to isentropic thrust.

Dd. 125874 K5

Printed in Wales for Her Majesty's Stationery Office
by Allen Printers (Wales) Limited

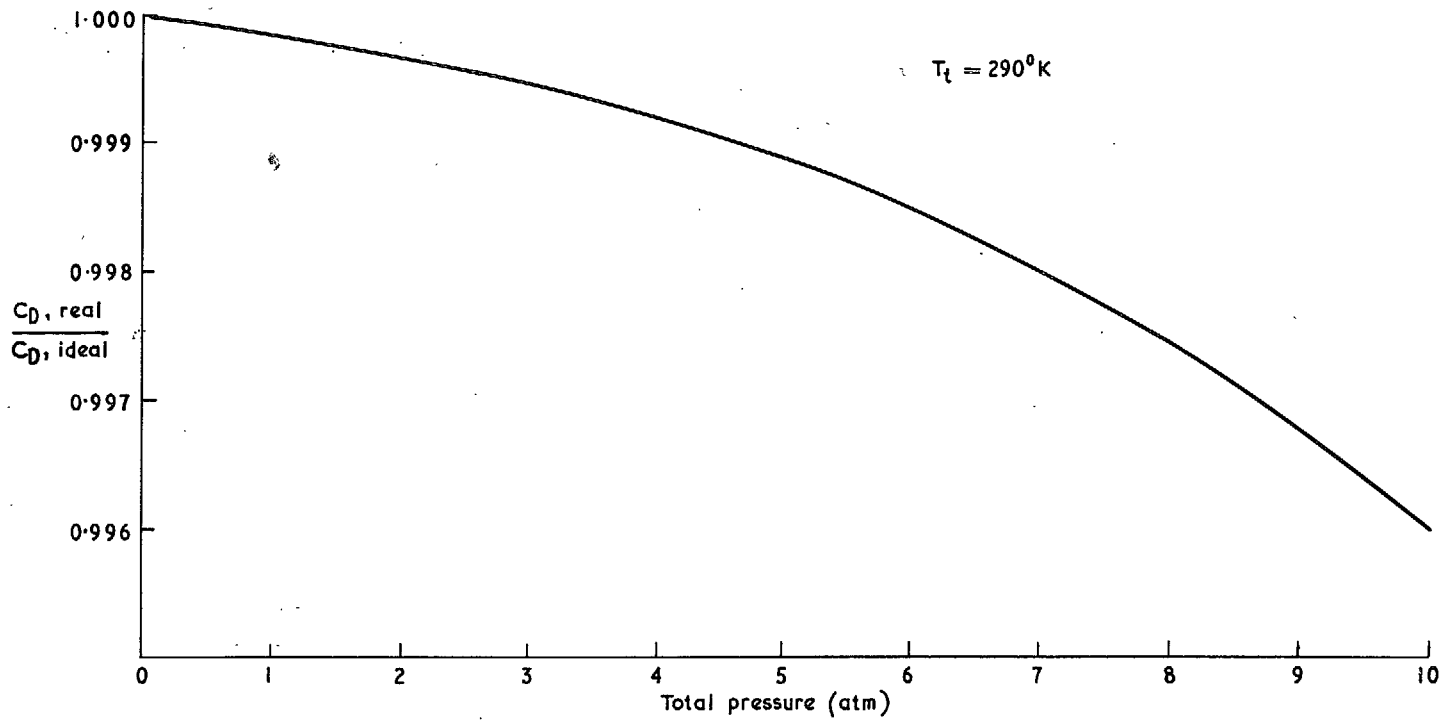

FIG. 71. Correction factor to discharge coefficient.

Published by
HER MAJESTY'S STATIONERY OFFICE

To be purchased from
49 High Holborn, London W.C.1
423 Oxford Street, London W.1
13A Castle Street, Edinburgh 2
109 St. Mary Street, Cardiff
Brazennose Street, Manchester 2
50 Fairfax Street, Bristol 1
35 Smallbrook,Ringway, Birmingham 5
7–11 Linenhall Street, Belfast 2
or through any bookseller

R. & M. No. 3477

S.O. Code No. 23–3477